Many-body phenomena in a Bose-Einstein condensate of light

Cover: The cover shows an artist's impression of Bose-Einstein condensation of light in a dye-filled optical microcavity. This is inspired by a similar illustration in Physics **7**, 7 (2014) (Credit: APS/Alan Stonebraker)

ISBN: 978-90-393-6569-4
Printed by Ipskamp Printing

Many-body phenomena in a Bose-Einstein condensate of light

Veeldeeltjesverschijnselen in een Bose-Einstein condensaat van licht

(met een samenvatting in het Nederlands)

Proefschrift

ter verkrijging van de graad van doctor aan de Universiteit Utrecht op gezag van de rector magnificus, prof. dr. G.J. van der Zwaan, ingevolge het besluit van het college voor promoties in het openbaar te verdedigen op woensdag 22 juni 2016 des middags te 4.15 uur

door

Arie-Willem de Leeuw

geboren op 9 mei 1989 te Leerdam

Promotoren: Prof. dr. ir. H.T.C. Stoof
Prof. dr. R.A. Duine

Contents

Publications

The main Chapters of this thesis are based on the following papers:

- A.-W. de Leeuw, H.T.C. Stoof, and R.A. Duine, *Schwinger-Keldysh Theory for Bose-Einstein Condensation of Photons in a Dye-Filled Optical Microcavity*, Phys. Rev. A **88**, 033829 (2013).

- A.-W. de Leeuw, H.T.C. Stoof, and R.A. Duine, *Phase Fluctuations and First-Order Correlation Functions of Dissipative Bose-Einstein Condensates*, Phys. Rev. A **89**, 053627 (2014).

- E.C.I. van der Wurff, A.-W. de Leeuw, R.A. Duine, and H.T.C. Stoof, *Interaction Effects on Number Fluctuations in a Bose-Einstein Condensate of Light*, Phys. Rev. Lett. **113**, 135301 (2014).

- A.-W. de Leeuw, E.C.I. van der Wurff, R.A. Duine, and H.T.C. Stoof, *Phase Diffusion in a Bose-Einstein Condensate of Light*, Phys. Rev. A **90**, 043627 (2014).

- A.-W. de Leeuw, O. Onishchenko, R.A. Duine, and H.T.C. Stoof, *Effects of dissipation on the superfluid-Mott-insulator transition of photons*, Phys. Rev. A **91**, 033609 (2015).

- A.-W. de Leeuw, E.C.I. van der Wurff, R.A. Duine, D. van Oosten, and H.T.C. Stoof, *Theory for Bose-Einstein condensation of light in nano-fabricated semiconductor microcavities*, submitted for publication in Phys. Rev. A, arXiv:1505.01732.

Chapter 1

Introduction

In many cases the behavior of objects can be explained by theories within a classical framework. The most famous example is probably the motion of macroscopic masses that is described by Newton's laws. However, it turns out that the behavior of particles at the microscopic level cannot be explained within the same framework. This is a consequence of the different set of rules that must be obeyed on each scale. Namely, at the microscopic level the laws of quantum mechanics apply, which are quite different from the rules of classical mechanics.

To distinguish whether quantum mechanics is important or not, we need to compare the average distance between the particles in the system of interest with the thermal de Broglie wavelength of the particles. Here, the latter is defined as

$$\Lambda_{\mathrm{th}} = \sqrt{\frac{2\pi\hbar^2}{mk_{\mathrm{B}}T}}, \tag{1.1}$$

with $\hbar$ Planck's constant, m the mass of the particle, k_{B} Boltzmann's constant, and T the temperature of the collection of particles in the system. In the regime where this wavelength is smaller than the average distance between the particles, the behavior is classical and the quantum mechanical nature of the particles can be ignored. However, if the de Broglie wavelength becomes larger than the interparticle spacing, or if both quantities are comparable, the effects of the laws of quantum mechanics set in.

A prominent example of a many-body phenomenon that is purely quantum mechanical is Bose-Einstein condensation (BEC) [1,2]. Based on work of the Indian physicist Bose, Einstein concluded that a nonzero fraction of the number of particles in a gas of bosons occupies the ground state, if the de Broglie wavelength is comparable to the interparticle distance. For the macroscopic occupation of the ground state, the bosonic nature of the particle is crucial, since fermions are not allowed to occupy the

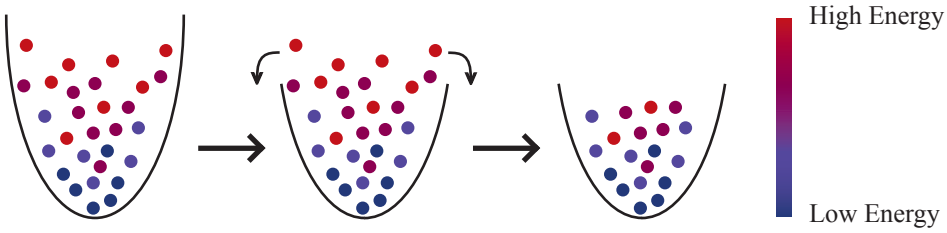

Figure 1.1: Schematic picture of evaporative cooling. By reducing the height of the external potential the most energetic atoms are removed from the trap, thereby reducing the average temperature of the trapped atomic gas.

same state. At first instance an experimental realization of BEC seemed unrealistic. Namely, for the most convenient bosonic gases, such as rubidium and sodium, the maximal densities in experiments are in the range of $10^{13} - 10^{15}\,\mathrm{cm}^{-3}$. Therefore, these gases must be cooled to temperatures in the nanokelvin regime to observe BEC.

1.1 Bose-Einstein condensation of atoms

The key insight for achieving these ultracold temperatures was the notion of the equivalence between the temperature of a gas and the average velocity of the particles of which this gas consists. Namely, reducing the velocity of the particles is equivalent to lowering the temperature of the gas. This is the basic principle behind laser cooling. By shining a red-detuned laser in the direction opposite to the motion of a particle, the particle can absorb a photon. This reduces the velocity of the particle due to momentum conservation. Hereafter, the photon is emitted in an arbitrary direction and therefore on average the velocity of the particle is reduced. By using this principle, temperatures of the order of $10\,\mu\mathrm{K}$ are achievable. Since this is still not low enough for achieving BEC, laser cooling is followed by evaporative cooling. Evaporative cooling is a process where the most energetic particles are removed from the system. By simply reducing the height of the trapping potential, the particles with the highest energy escape. This process is illustrated in Fig. 1.1. This reduces the average temperatures of the gas to the nanokelvin regime, which was sufficient for the first observation of BEC in atomic vapors [3–5].

There are several experiments that can be performed to distinguish whether a Bose gas is in the Bose-Einstein condensed phase or not. The most obvious experiment is measuring the density of particles and therefrom extracting the number of particles in the ground state. Another possibility

is performing correlation measurements and in particular investigating the one-particle density matrix $n(\mathbf{x}, \mathbf{x}')$. In the language of second quantization, it is given by

$$n(\mathbf{x}, \mathbf{x}') = \langle \hat{\psi}^\dagger(\mathbf{x}) \hat{\psi}(\mathbf{x}') \rangle, \tag{1.2}$$

where $\hat{\psi}^\dagger(\mathbf{x})$ and $\hat{\psi}(\mathbf{x}')$ are the creation and annihilation operator of the atoms. In an ordinary gas or liquid, the density matrix typically decays exponentially as a function of the separation $|\mathbf{x} - \mathbf{x}'|$. On the other hand, for a macroscopic occupation of the ground state there is an additional contribution. Since this contribution is independent of the separation, we find that in the Bose-Einstein condensed phase the density matrix does not vanish at large separations. This so-called off-diagonal long-range order is another characteristic for BEC.

True off-diagonal long-range order is only present in three dimensions. In lower dimensions, interaction effects will lead to fluctuations that affect the behavior of the single-particle density matrix. This is particularly important in atomic vapors, since in these systems it is possible to manipulate the degrees of freedom of the particles. By changing the configuration of the external trapping potential, the motion of the atoms in one or two directions can be frozen out. In this case the gas is equivalent to a two-dimensional or one-dimensional gas, respectively. For a Bose-Einstein condensate in lower dimensions, it is important to distinguish between fluctuations of the density and the phase. Since phase fluctuations cost less energy, for most practical purposes the density fluctuations are strongly surpressed and the phase fluctuations are most important. In fact, it is due to these phase fluctuations that in one-dimensional systems, the one-particle density matrix decays algebraically and therefore in this case true BEC is no longer possible. In two dimensions, one finds algebraic decay with an exponent that is proportional to the temperature. Hence, it is only possible to undergo BEC at zero temperature. However, this does not affect some of the properties of the gas at low temperatures. Specifically, superfluidity, which is arguably the most important feature of interacting Bose-Einstein condensates, is still present in these low-dimensional systems.

The transition from atoms in the normal state to the Bose-Einstein condensed state where the atoms are superfluid, is a typical example of a phase transition that is driven by changing the temperature. Phase transitions are usually characterized by an order parameter that changes from zero to a nonzero value. We call a phase transition first order if this change is discontinuous. If the change in the value of the order parameter is continuous, the phase transition is of second or higher order. The order parameter

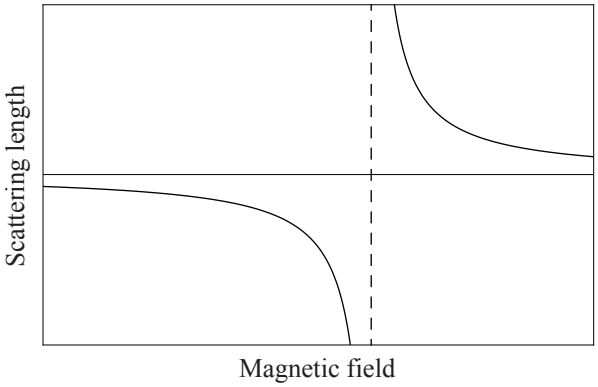

Figure 1.2: Illustration of a Feshbach resonance. By changing the value of the magnetic field, the scattering length can be tuned to arbitrary values. This allows for studying cold atomic gases with any kind of interaction strength.

for BEC is the expectation value of the annihilation operator. During the phase transition, the value of this order parameter changes continuously and therefore BEC is a second-order phase transition.

Another important concept in the context of phase transitions is spontaneous symmetry breaking. The principle is that after undergoing the phase transition, the state of the system no longer obeys the symmetry of the underlying microscopic Hamiltonian. For BEC the $U(1)$-symmetry is spontaneously broken. In the normal state all the atoms have an arbitrary phase, whereas in the Bose-Einstein condensed state all the condensed atoms have the same global phase. However, the description of a Bose-Einstein condensate with a fixed phase is only valid in the thermodynamic limit. For finite-sized Bose-Einstein condensates, quantum fluctuations give rise to non-trivial dynamics of the global phase. This is known as phase diffusion [6]. Intuitively, this phenomenon is more clear in the case of ferromagnetism. Below a critical temperature, all spins allign and the nonzero expectation value of the magnetization spontaneously breaks the $SO(3)$-symmetry. For a finite number of spins, even at zero temperature, quantum fluctuations can provide enough energy for all spins to make a rotation to a magnetization with the same absolute value but a different direction. Only in the thermodynamic limit would this rotation of all spins require an infinite amount of energy. In this case the magnetization remains fixed once the temperature is below the critical temperature.

One of the main advantages of ultracold alkali atoms is the possibility to tune the interactions to arbitrary values by using a Feshbach resonance [7]. This not only allows for studying the regime where the previously

mentioned phase fluctuations are small, but it also opens up an avenue to study systems with both weak and strong interactions. Moreover, it is even possible to change between attractive and repulsive interactions. Since the Bose-Einstein condensate is not stable for attractive interactions [8, 9], the case of repulsive interaction is most relevant for experiments with ultracold Bose gases. Theoretically, the interatomic interactions can be treated by using a relatively simple contact interaction, with a proportionality constant that is completely determined by the s-wave scattering length. Therefore, we can incorporate the interactions via an interaction potential that is given by

$$V(\mathbf{x} - \mathbf{x}') = V_0 \delta(\mathbf{x} - \mathbf{x}'), \tag{1.3}$$

where $V_0 = 4\pi\hbar^2 a/m$ is the interaction strength, with a the s-wave scattering length. As can be seen in Fig. 1.2, the value of this scattering length can be changed by varying the strength of the magnetic field. We have a so-called Feshbach resonance if a magnetic field tunes the energy of a bound state into resonance with the energy of the scattering atoms.

To validate the correctness of this contact interaction, it is important to make comparisons with experiments on many-body phenomena in ultracold alkali gases. The collective modes of ultracold atoms are well-known examples of many-body phenomena where this comparison is possible. In very good approximation, we can calculate the frequency of the collective motion of the condensed particles as a consequence of an external perturbation. Without an external trapping potential this result into a sound mode with a speed that is given by $\sqrt{V_0 n_0/m}$, with n_0 the condensate density. In the presence of a harmonic trapping potential, the so-called breathing oscillation frequencies of the condensate are related to the trap frequency via $\omega = \sqrt{l}\omega_\rho$, where ω_ρ is the trapping frequency and l only takes integer values. Since every different value of l corresponds to a different angular momentum mode of the condensate, several modes can be excited depending on the precise perturbation of the trap. The excellent agreement between theory and experiment is an important verification for the many-body theory of BEC [10–15]. Apart from these collective modes, there are of course more many-body phenomena that are nowadays well-understood both experimentally and theoretically. An overview of some important examples can be found in Ref. [16].

The large tunability in experiments with ultracold Bose gases is important for making a comparison between theory and experiment. Moreover, this large freedom also opens up the possibility to investigate models that are important in many areas in condensed-matter physics, such as Hubbard models [18]. In particular, the Bose-Hubbard model describes an ultracold

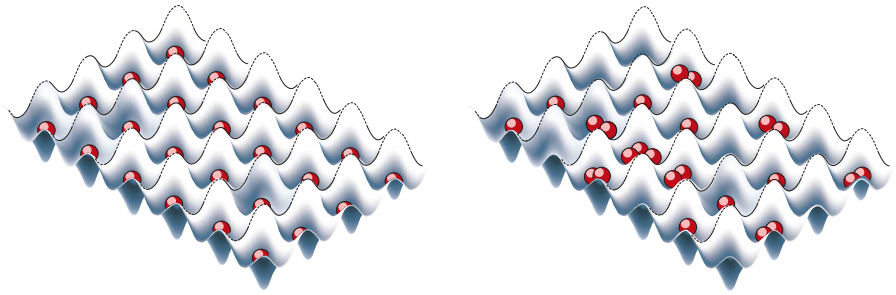

(a) **(b)**

Figure 1.3: The two different phases of ultracold atoms in a periodic potential with (a) the mott-insulating phase and (b) the superfluid phase, respectively. The figures are taken from Ref. [17].

Bose gas in a periodic potential. The two important parameters in this model are the nearest-neighbour hopping amplitude t and the on-site interaction strength U. Here, t characterizes the probability for an atom to move to a neighbouring well. In the case of repulsive interactions, U indicates the energy cost for two atoms to occupy the same site. Hopping to sites that are not nearest neighbours is usually neglected as for deep lattices these processes are exponentially surpressed.

The Bose-Hubbard model has two different regimes. For strong repulsive interaction $t \ll U$, it is energetically unfavourable for an atom to move to a site with another atom. Hence, we expect that particles are equally distributed over the lattice sites. This is called the Mott-insulator phase due to the band gap in the excitation spectrum in this state. However, in the opposite limit, $t \gg U$, the energy is minimal if the atoms continuously hop between lattice sites. This is the superfluid phase, where the particles delocalize over the lattice and form a Bose-Einstein condensate with a well-defined global phase. The two different phases are shown in Fig. 1.3. In experiments, we can switch between both phases by tuning the values of both parameters. For example, the intensity of the external lasers that are used to create the periodic potential influences the hopping parameter t and the interaction strength U. Therefore, in experiments the so-called quantum phase transition from the superfluid to the Mott-insulator phase has been observed [19]. In cold atomic gases many other models have been investigated [20] and also other quantum phase transitions were explored [21].

Although up to now we focused on ultracold bosonic atoms, BEC is not only restricted to those particles. An intriguing example is a Fermi gas in

the presence of attractive interactions. Without the attractive interactions the particles cannot form a Bose-Einstein condensate because occupying the same state is forbidden by Pauli's exclusion principle. However, due to the attractive interactions it is energetically favourable to form bound pairs of fermions with opposite spin. If the attraction is weak, the particles are weakly bound and the size of these so-called Cooper pairs is much larger than the average interparticle distance. For very strong attraction, the pairs become more tightly bound and their size is smaller than the avarage distance between the particles. In this case the pairs are analogous to point particles that obey Bose-Einstein statistics. Therefore, in this regime the ground state of the Fermi gas is a Bose-Einstein condensate that consist of diatomic molecules. This transition from weakly bound Cooper pairs to strongly bound molecules that can condense is known as the BEC-BCS crossover. It has been studied extensively over the past years, see for example Refs. [22–28].

1.2 Driven-dissipative Bose-Einstein condensates

From the last example it is clear that BEC is not restricted to alkali atoms. In principle all particles that obey Bose-Einstein statistics can undergo the transition to a Bose-Einstein condensate. Therefore, it is also possible to form Bose-Einstein condensates of photons and quasiparticles such as magnons and exciton-polaritons. Magnons are the quanta of collective spin-wave excitations and exciton-polaritons are photons that are strongly coupled to electronic excitations. However, a priori there are certain problems that could prevent these particles from undergoing BEC. Firstly, the particles have no bare mass and their number can change due to thermal fluctuations. Moreover, another important issue is the short finite lifetime of these quasiparticles. As a fixed, average number of particles is a prerequisite for BEC, these are major obstacles for achieving BEC.

Recently, new methods were developed to circumvent these problems. Since in these three different systems the problems preventing BEC are quite similar, there are many similarities between the manner in which these issues are resolved. First of all, inside the system of interest the energy-dispersion relation of the quasiparticle is made quadratic. Therefore, the second derivative in the minimum of the dispersion relation defines an effective mass and the quasiparticles behave similar to massive bosons. Moreover, the minimal energy of the quasiparticles is larger than the thermal energy and therefore the number of particles is not affected by thermal fluctuations. To compensate for the finite lifetime, there is external pump-

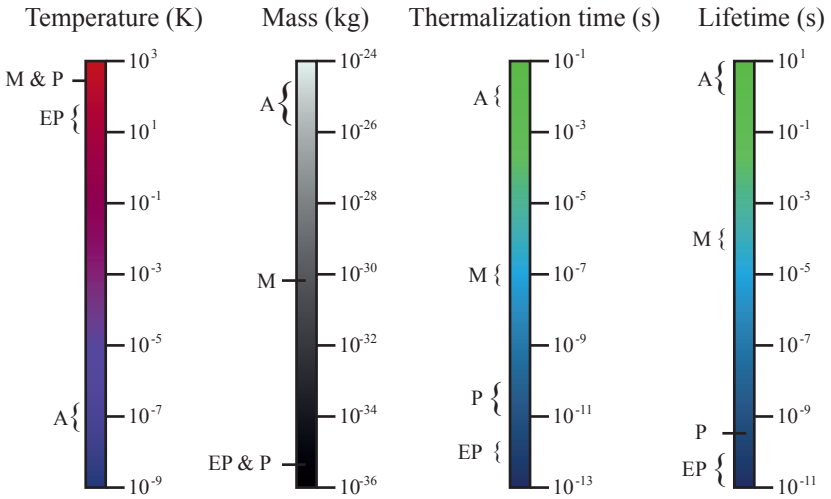

Figure 1.4: Overview of some charateristics of a Bose-Einstein condensate of atoms (A), exciton-polaritons (EP), dipolar magnons (M), and photons (P).

ing to keep the average number of particles in the system fixed. Thus, these systems are in a quasi-equilibrium state that is a dynamical balance between external pumping and particle losses through dissipation. Moreover, it is possible to make the lifetime of the quasiparticles a few orders of magnitude larger than the thermalization time. In this situation the steady state is equivalent to the equilibrium state of a thermalized massive Bose gas with a constant average number of particles. Therefore, it is possible to achieve BEC of magnons [29], exciton-polaritons [30, 31] and photons [32].

However, there are still several differences with respect to BEC of ultracold alkali atoms. First of all, the effective mass of the quasiparticles is several orders of magnitude smaller than the typical mass of alkali atoms. Therefore, as can be understood from Eq. (1.1), these systems undergo BEC at much higher temperatures. Second, Bose-Einstein condensates of ultracold atoms are usually very clean and isolated systems, which is quite different from these systems because of the dissipation and external pumping. Finally, another big difference is the manner in which BEC is achieved. Contrary to atomic Bose-Einstein condensates, the temperature remains unchanged throughout the process of condensation. In these systems the condition for BEC is satisfied by enlarging the total number of particles in the system through increasing the external pumping. Because of the differences these systems form a new class of Bose-Einstein condensates, i.e., the so-called driven-dissipative Bose-Einstein condensates. To get an idea of the appropriate regimes in the different Bose-Einstein condensates,

we display an overview of some characteristic feautures in Fig. 1.4.

1.3 Bose-Einstein condensation of light

In this thesis we consider one of these driven-dissipative Bose-Einstein condensates in more detail, namely a Bose-Einstein condensate of photons. For a long time it was an open question whether it is possible to make a Bose-Einstein condensate of light. The main reason for this is that whenever light is trapped and in contact with walls, it obeys Stefan-Boltzmann's law. Therefore the number of photons decreases if the temperature is lowered, whereas for BEC an independent tuning of the average number of photons and the temperature is necessary. Moreover, as already mentioned before, the second problem is that the number of photons is not conserved. Namely, a free photon is massless and therefore has zero energy for zero momentum. Therefore, photons can be created as a consequence of thermal fluctuations or simply disappear into the walls.

These problems can be solved by confining light in a cavity that is filled with a dye solution. In this case the photons interact with the dye via absorption and emission processes. The absorption and emission profiles of the dye determine how many photons of a certain frequency are absorbed and emitted. The photon gas thermalizes to the temperature of the dye via multiple cycles of absorption and emission. Since the photons are trapped between two mirrors, we obtain that the longitudinal momentum satisfies $k_z(r) = q\pi/D(r)$, where q is an integer that determines the wave number and

$$D(r) = D_0 - 2\left(R - \sqrt{R^2 - r^2}\right), \tag{1.4}$$

is the distance between the two mirrors with D_0 the distance at the optical axis, R the radius of curvature of the mirrors and r the distance from the optical axis. It is clear that the difference between the two distinct longitudinal momenta increases if the distance between the mirrors decreases. As can be seen in Fig. 1.5, we observe that for distances that are small enough, in very good approximation only photons with a certain longitudinal wave number are absorped and emitted. In the example given in Fig. 1.5, this implies that inside the cavity only photons with longitudinal wavenumber $q = 7$ are present. In the paraxial approximation we use that the transversal momentum k_r is small compared to k_z and also that $r \ll R$. This is an accurate description, because in the experiments R is large and most of the light is close to the optical axis. In this approximation, we obtain for

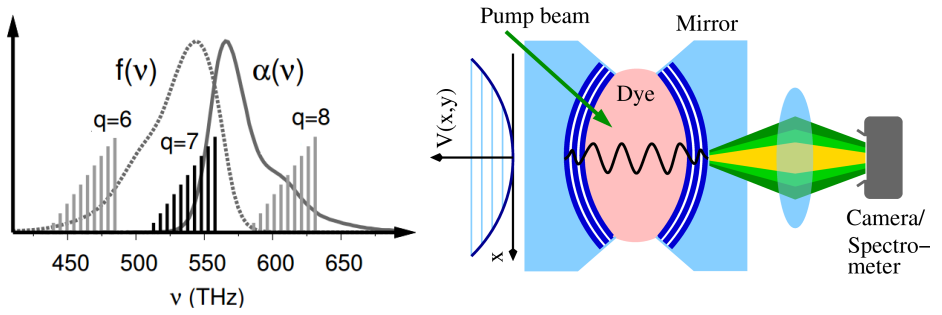

(a) (b)

Figure 1.5: (a) Spectrum of cavity modes and fluorescence and absorption spectra of Rhodamine 6G dye as function of the frequency ν. The wavenumber q determines the longitudinal momentum of the photons and the height of the bars denotes the degeneracy of the transverse modes arising from the harmonic trapping potential. In good approximation only photons with longitudinal momentum $q = 7$ are absorped and emitted by the dye, generating an effective mass and making the photons two dimensional. (b) Scheme of the set-up of the experiment for BEC of photons. The harmonic potential is imposed by the curvature of the cavity mirrors. The photons with zero transversal momentum are emitted in the longitudinal direction and higher energetic photons are emitted at a larger angle with respect to the optical axis. The figures are adapted from Ref. [32].

the energy of the photons inside the cavity

$$E_{\mathrm{ph}}(r,k_r) = \frac{\hbar c}{n_0}\sqrt{k_r^2 + k_z^2(r)} \simeq \frac{m_{\mathrm{ph}}^2 c^2}{n_0^2} + \frac{(\hbar k_r)^2}{2m_{\mathrm{ph}}} + \frac{1}{2}m_{\mathrm{ph}}\Omega^2 r^2, \qquad (1.5)$$

where c is the speed of light and n_0 is the index of refraction of the dye solution.

To cast this energy into this more familiar form, we defined an effective photon mass m_{ph} and trapping frequency Ω that depend on the experimental parameters, such as D_0 and q [32]. In this expression we recognize the energy of a two-dimensional massive particle that is confined in a harmonic trapping potential. Since these particles can undergo BEC at nonzero temperature, the photons inside the dye-filled cavity are able to undergo BEC as well.

However, we still need to check explicitly whether the fixed longitudinal momentum solves the orignal problems that prevented light from undergoing BEC. First, we observe that for typical experimental parameters the minimal energy of the photons $\hbar\omega_{\mathrm{cutoff}} = m_{\mathrm{ph}}^2 c^2/n_0^2 \simeq 80\, k_{\mathrm{B}}T$. Therefore, thermal fluctuations do not influence the average particle number and the

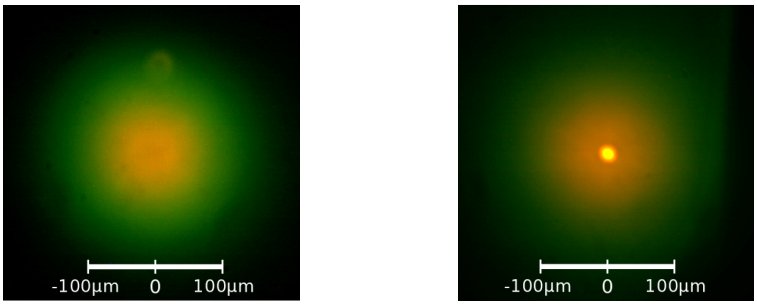

(a) **(b)**

Figure 1.6: Image of the spatial intensity profile leaking through the cavity mirrors. (a) Below criticality the photons have an ordinary Bose-Einstein distribution at room temperature. (b) Above the critical power of the pump beam the bright spot in the center signals the a macroscopic occupation of the ground state. The figures are taken from Ref. [32].

average number of photons is fixed during the thermalization. As a consequence, the temperature is decoupled from the average number of particles; the average number of photons is determined by the power of the external pump laser and the temperature is equal to the temperature of the dye. Therefore, BEC should be possible by increasing the number of photons in the cavity. Indeed, as can be seen in Fig. 1.6, above a critical value of the power of the external pump beam a macroscopic occupation of the ground state has been observed.

By looking at the expression for the energy of the photons inside the cavity as given by Eq. (1.5), we expect that the size of the condensate remains the same if the number of condensed photons is increased; the width of the ground state wave function of a two-dimensional harmonic oscillator is determind by the harmonic oscillator length $l = \sqrt{\hbar/m_{\mathrm{ph}}\Omega}$ that is independent of the number of condensed photons. However, in the experiment different behavior has been observed. For increasing pumping powers and therefore for larger condensate fractions, the diameter of the condensate increases. This signals the presence of repulsive interactions, which makes it energetically more favourable to increase the interparticle distance in the photon gas for larger condensate fractions. Although the origin of these interactions is still an open question, it turns out that they can be modeled by a contact interaction [32].

Since the expression for the energy of the photons inside the cavity is

similar as for trapped ultracold alkali atoms, we want to apply the description that is used for atomic Bose-Einstein condensates to describe BEC of light. Therefore, we work in second quantization and use a theory for the photon creation and annihilation operators, which are defined via the electric field. Hence, we introduce $\hat{a}^{\dagger}_{\mathbf{k},\nu}$ and $\hat{a}_{\mathbf{k},\nu}$ with $\mathbf{k}$ the momentum of the different modes and ν indicates the different polarizations. In this thesis the possible difference in polarization of the photons is ignored and whenever appropriate we included an additional factor of 2 to account for the two-fold polarization degeneracy. Hence, the Bose-Einstein condensate of light is described by the famous Gross-Pitaevskii equation

$$\left(-\frac{\hbar^2\nabla^2}{2m_{\mathrm{ph}}}+\frac{1}{2}m_{\mathrm{ph}}\Omega^2r^2+\tilde{g}|\phi_0(r)|^2\right)\phi_0(r)=\mu\phi_0(r), \tag{1.6}$$

where $\phi_0(r)$ is the wave function of the condensate, $\tilde{g}$ is the dimensionless interaction parameter and μ is the chemical potential of the photons.

As mentioned before, an important issue in the driven-dissipative Bose-Einstein condensates is thermalization. In fact, thermalization is a prerequisite for calling the macroscopic occupation of the ground state a true Bose-Einstein condensate. In Ref. [33] it is shown that depending on the lifetime of the photons inside the cavity, this system can operate both as a laser and a Bose-Einstein condensate. If the lifetime is short, the photons cannot thermalize and the system operates as a laser. However, if the thermalization timescale is shorter than the lifetime, the photon gas thermalizes and macroscopic occupation of the ground state is really a consequence of the Bose-Einstein statistics. The same conclusions are found in theoretical studies of Kirton and Keeling [34,35]. Therefore, this confirms the previous remarks that BEC in the driven-dissipative systems is only possible when the lifetime of the quasiparticles is larger than the thermalization lifetime.

This pioneering experiment also inspired other groups to realize this Bose-Einstein condensate of light. Currently, there are other realizations of the experiment at Imperial college [36] in London and in Utrecht. Moreover, the different circumstances in comparison with Bose-Einstein condensates of ultracold alkali atoms, also made it interesting to investigate BEC of light from a theoretical perspective [37–42].

1.4 Outline

In this thesis we focus on many-body phenomena in a Bose-Einstein condensate of light. The many-body phenomena that we study in this thesis can be divided into two different categories. On the one hand, we are interested in the effect of dissipation on many-body phenomena that have

already been investigated in the context of Bose-Einstein condensates of ultracold alkali atoms. On the other hand, we use the properties of light to study many-body phenomena that have not yet been observed in atomic Bose-Einstein condensates. The precise content of the Chapters of this thesis is as follows.

In Chapter 2 we use the Schwinger-Keldysh formalism to develop a theory for BEC of light. In particular, we derive Langevin field equations that describe the complete dynamics of the photons gas and we demonstrate that the dissipation can, at low energies, be characterized by a single dimensionless parameter. As an example we also calculate the effects of the dissipation on the Bogoliubov dispersion relation. The results of this Chapter will frequently be used in the subsequent Chapters.

Hereafter, in Chapter 3 we address the question whether the Bose-Einstein condensate of light is a true condensate. Since the photons are two dimensional, we investigate if the phase fluctuations destroy the phase coherence. Moreover, we study the effects of dissipation on the temporal and spatial first-order correlation functions in both the normal and Bose-Einstein condensed state. In particular, we examine the effect of the damping parameter that was introduced in Chapter 2.

Subsequently, in Chapter 4 we set up the theory for describing number fluctuations in Bose-Einstein condensates. In this model the number fluctuations only depend on the value of the strength of the interactions. As the number fluctuations have been measured in the Bose-Einstein condensate of photons, we apply our model to this case. In addition, to make a connection with experiments we further investigate several possible photon-photon interaction mechanisms.

In Chapter 5 we investigate phase diffusion. Since this phenomenon has not yet been observed in atomic Bose-Einstein condensate, photons offers a new oppertunity to investigate this intriguing phenomenon. Because the phase of light can be determined from an interference experiment, we propose to use interference measurements to investigate phase diffusion. Moreover, we predict the outcome of possible measurements.

Next, in Chapter 6 we study the Superfluid-Mott-Insulator transition in a Bose-Einstein condensate of light. Motivated by experimental ideas in the direction of combining this system with an periodic potential by locally changing the index of refraction, we construct a theory for the photon system in this periodic structure. We investigate the effects of interaction with the dye and show that this prevents the true Mott-Insulator phase from occuring.

Finally, in Chapter 7 we address the superfluidity of light. Since the

origin of the photon-photon interactions in the dye-filled optical microresonator is unknown and these interactions are crucial for superfluidity, we investigate a different system where BEC of light is possible. We develop a model for BEC of light in semiconductor microcavities and again investigate the effects of dissipation in this system. Moreover, we propose to probe the superfluidity of light via the excitation of so-called scissors modes and calculate the decay of these modes.

Chapter 2

Schwinger-Keldysh theory

We consider BEC of photons in an optical cavity filled with dye molecules that are excited by laser light. By using the Schwinger-Keldysh formalism we derive a Langevin field equation that describes the dynamics of the photon gas, and, in particular, its equilibrium properties and relaxation towards equilibrium. Furthermore we show that the finite-lifetime effects of the photons are captured in a single dimensionless damping parameter, that depends on the power of the external laser pumping the dye. Finally, as applications of our theory we determine spectral functions and collective modes of the photon gas in both the normal and the Bose-Einstein condensed phases.[1]

2.1 Introduction

After the theoretical prediction of Bose-Einstein condensation (BEC) in 1925 [1, 2], it took until 1995 for the first direct experimental observation of this phenomenon in weakly interacting atomic vapors [3–5]. In addition to these atomic gases, BEC of bosonic quasiparticles such as magnons [29], exciton-polaritons [30, 31], and photons [32] is now also observed. The Bose-Einstein condensates of these quasiparticles form a different class of condensates as they are not in true thermal equilibrium.

These non-equilibrium Bose-Einstein condensates are driven by external pumping to compensate for the particle losses and thereby to keep the average number of particles in the system at a constant level. In these systems the steady state of the Bose gas is therefore determined by interparticle interactions that lead to quasi-equilibration and by the balance between

[1] This Chapter is directly based on *Schwinger-Keldysh Theory for Bose-Einstein Condensation of Photons in a Dye-Filled Optical Microcavity*, A.-W. de Leeuw, H.T.C. Stoof, and R.A. Duine, Phys. Rev. A **88**, 033829 (2013).

pumping and particle losses. Furthermore, contrary to dilute atomic gases, the temperature is typically constant in these experiments. Instead, one varies the strength of the external pumping power while keeping the system at a constant temperature. Above some critical value of the pumping power, the density of particles in the system is above the critical density, and the system undergoes BEC.

Another special feature of these pumped systems is the temperature at which BEC occurs. Since BEC happens when the phase-space density is of the order of unity [43], the temperature at which the magnons, exciton-polaritons, and photons condense is inversely related to their mass to the power 3/2. Although these particles do not even always have a bare mass, they are all formally equivalent to bosons with an effective mass that is several orders of magnitude smaller than that of alkali atoms. Therefore, these systems undergo BEC at temperatures in the range of 10 to 300 K instead of in the nK regime relevant for the atomic Bose-Einstein condensates.

In order to get a detailed understanding of these non-equilibrium Bose-Einstein condensates, we from now onwards focus on the photon experiment of Klaers *et al.* [32]. This experiment is concerned with a photon gas in a dye-filled optical resonator. The distance between the cavity mirrors is chosen such that the emission and absorption of photons with a certain momentum in the longitudinal direction dominates over that of other momenta. Thus, this component of the momentum of the photons is fixed, and the photon gas becomes equivalent to a Bose gas with a small effective mass. Furthermore, the gas becomes effectively two-dimensional. In general this prohibits observing BEC at nonzero temperature, since a homogeneous two-dimensional Bose gas can only condense at zero temperature [43]. However, due to the curvature of the cavity mirrors there is a harmonic potential for the photons. Therefore, BEC of photons is observed above some critical pumping power, since a harmonically trapped two-dimensional Bose gas can exhibit BEC at a nonzero temperature [44, 45].

Theoretically, a lot of progress has been made for BEC of magnons and exciton-polaritons [46–52]. Although the observation of Bose-Einstein condensation of photons is more recent, it has also motivated theoretical studies: Klaers *et al.* predicted a regime of large fluctuations of the condensate number [53]. Furthermore, the authors of Ref. [34] found that the photons cannot reach thermal equilibrium for small absorption and emission rates. The modification of the Stark shift of an atom in a Bose-Einstein condensate of photons was investigated in Ref. [54], and conditions for BEC of photons that are in thermal equilibrium with atoms of dilute gases were

derived in Ref. [38].

In this Chapter we develop a theory for the photon experiment performed by Klaers *et al.* [32]. We describe this photon system by using the Schwinger-Keldysh formalism, which is commonly used in the quantum optics community, see, for example, Ref. [55]. In Sec. 2.2 we derive an effective action for the photons. In Sec. 2.3 we use this effective action to derive a Langevin field equation for the photons including Gaussian noise, which incorporates the effect of thermal and quantum fluctuations. The main advantage of this approach is that it simultaneously treats coherent and incoherent effects. In particular, it enables us to describe the complete time evolution of the photons, including the relaxation towards equilibrium; thus equilibrium properties can also be obtained. Subsequently, we show that the finite-lifetime effects of the photons can be captured in a single dimensionless parameter α, that depends on the power of the external laser pumping the dye. In Sec. 2.4 we calculate equilibrium properties of the homogeneous photon gas in the normal and Bose-Einstein condensed phase, such as spectral functions, collective modes, and damping. We end with conclusions and outlook in Sec. 2.5.

2.2 Model

In this section we derive an effective action for the photons by using the Schwinger-Keldysh formalism developed in Ref. [56]. In particular, the photons are coupled to a reservoir of dye molecules. The energy of the photons is given by

$$\epsilon_\gamma(\mathbf{k}) = \hbar c\sqrt{k_x^2 + k_y^2 + k_\gamma^2}, \tag{2.1}$$

where $\hbar$ is Planck's constant, c is the speed of light in the medium, and $\mathbf{k}$ is the transverse momentum of the photon. In agreement with the experiment k_z is $\pm k_\gamma$, since the frequency of the pump laser is such that in the longitudinal direction the absorption of photons with mode number $q = 7$ dominates over other absorption processes [32]. For the molecules we take an ideal gas in a box with volume V. Since this gas is at equilibrium and at room temperature, we describe the translational motion of the molecules by a classical Maxwell-Boltzmann distribution. Furthermore, we model these molecules as a two-level system with energy difference $\Delta > 0$ between the excited and ground states. This is a simplification since these molecules have a rovibrational structure. Therefore, the dye molecules have more than two levels as the rovibrational structure divides the ground and excited levels into several sublevels. However, in this section we will show

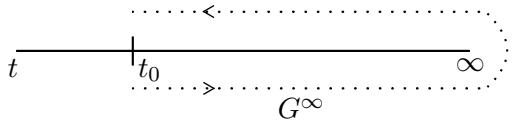

Figure 2.1: The Schwinger-Keldysh contour G^∞. The integration is first from t_0 to ∞ and then back from ∞ to t_0.

that we can model this multi-level system by introducing an effective mass for the molecules in our two-level model.

At time t_0 the photons are coupled to the molecules with a momentum-independent coupling constant g. To study the dynamics of the coupled system at times larger than t_0 we consider the action

$$
\begin{aligned}
S[a_{\mathbf{k}}, a^*_{\mathbf{k}}, b_{\mathbf{k}}, b^*_{\mathbf{k}}] = &\sum_{\mathbf{k}} \int_{G^\infty} dt\, a^*_{\mathbf{k}}(t) \left\{ i\hbar \frac{\partial}{\partial t} - \epsilon_\gamma(\mathbf{k}) + \mu_\gamma \right\} a_{\mathbf{k}}(t) \qquad (2.2)\\
&+ \sum_{\mathbf{p},\rho} \int_{G^\infty} dt\, b^*_{\mathbf{p},\rho}(t) \left\{ i\hbar \frac{\partial}{\partial t} - \epsilon(\mathbf{p}) + \mu_\rho - K_\rho \right\} b_{\mathbf{p},\rho}(t)\\
&- \frac{i}{\sqrt{2V}} \sum_{\mathbf{k},\mathbf{p}} \int_{G^\infty} dt\, g a_{\mathbf{k}}(t) b_{\mathbf{p},\downarrow}(t) b^*_{\mathbf{p}+\mathbf{k}_+,\uparrow}(t) + \text{h.c.}\\
&+ \frac{i}{\sqrt{2V}} \sum_{\mathbf{k},\mathbf{p}} \int_{G^\infty} dt\, g a_{\mathbf{k}}(t) b_{\mathbf{p},\downarrow}(t) b^*_{\mathbf{p}+\mathbf{k}_-,\uparrow}(t) + \text{h.c.}.
\end{aligned}
$$

Here time is integrated along the Schwinger-Keldysh contour G^∞, which is depicted in Fig. 2.1. The photons are described by the fields $a_{\mathbf{k}}(t)$ and $a^*_{\mathbf{k}}(t)$. Furthermore, $\epsilon_\gamma(\mathbf{k})$ is given by Eq. (2.1), and μ_γ is the chemical potential of the photons. For now we neglect the harmonic potential for the photons, since this term is not important for the coupling between molecules and photons. The fields $b_{\mathbf{p},\rho}(t)$ and $b^*_{\mathbf{p},\rho}(t)$ describe the dye molecules, with ρ being equal to $\downarrow$ or $\uparrow$, corresponding to the ground and excited states, respectively. Also, $\epsilon(\mathbf{p}) = \hbar^2\mathbf{p}^2/2m_{\text{d}}$ with m_{d} being the mass of the Rhodamine 6G molecule. Moreover, K_ρ accounts for the energy difference between the molecular states, and we take $K_\downarrow = 0$ and $K_\uparrow = \Delta$. The last two terms describe the processes of the absorption and emission of a photon, respectively. Here g is the coupling strength between the photons and molecules, $\mathbf{k}_+ = (k_{\text{x}}, k_{\text{y}}, k_\gamma)$ and $\mathbf{k}_- = (k_{\text{x}}, k_{\text{y}}, -k_\gamma)$. Note that the structure of the interaction terms is a consequence of the expansion of the photon field in terms of a standing wave, instead of a plane wave, in the z-direction. Furthermore, the summation over $\mathbf{k}$ is two-dimensional, whereas

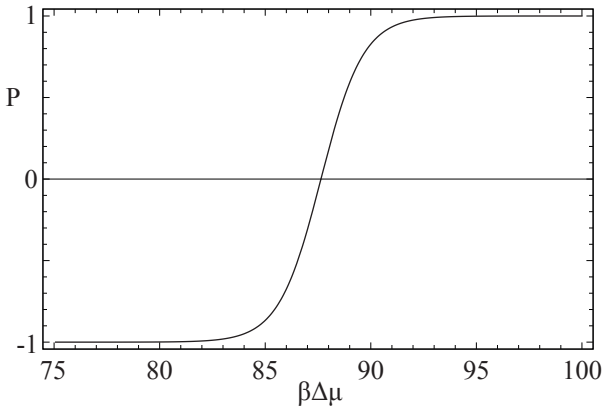

Figure 2.2: Polarization of the molecules P at room temperature $T = 300\,\mathrm{K}$ as a function of $\beta\Delta\mu$ for a density of molecules $n_\mathrm{m} = 9 \cdot 10^{23}\,\mathrm{m}^{-3}$, $\Delta = 3.63 \cdot 10^{-19}\,\mathrm{J}$. The polarization is exactly zero if $\Delta\mu$ is equal to the energy difference between the excited and ground states of the molecules.

the summations over $\mathbf{p}$ are three-dimensional. The latter convention will be used throughout the Chapter.

In this system one of the two molecular chemical potentials determines the density of molecules. The experiment of Klaers *et al.* one used Rhodamine 6G dye solved in methanol with a of concentration $1.5 \cdot 10^{-3}\,\mathrm{mol} \cdot \mathrm{L}^{-1}$. Therefore, we use a typical value of $n_\mathrm{m} = 9 \cdot 10^{23}\,\mathrm{m}^{-3}$ for the density of molecules. Furthermore the value of $\Delta\mu = \mu_\uparrow - \mu_\downarrow$ determines the polarization of the molecules. This polarization is defined as

$$P(\Delta\mu) := \frac{N_\uparrow - N_\downarrow}{N_\uparrow + N_\downarrow} = \frac{e^{\beta(\Delta\mu-\Delta)} - 1}{e^{\beta(\Delta\mu-\Delta)} + 1}, \tag{2.3}$$

where β is the inverse of the thermal energy $k_\mathrm{B}T$, and $N_\uparrow$ and $N_\downarrow$ are, respectively, the total number of excited-state and ground-state molecules. For small $\Delta\mu$ all molecules are in the ground state. By increasing the value of $\Delta\mu$, the number of molecules in the excited state increases. Since the total number of molecules is constant, the number of ground-state molecules thereby decreases. Thus for increasing $\Delta\mu$ the polarization increases. Moreover, the polarization is exactly zero for $\Delta\mu = \Delta$. A plot of the polarization as a function of $\Delta\mu$ is given in Fig. 2.2. The parameter $\Delta\mu$ is also important for making a connection with the experiment, since the number of excited molecules and thereby the polarization are determined by the pumping power of the external laser.

In our non-equilibrium theory the chemical potential of the photons μ_γ becomes only well defined after the photon gas equilibrates by cou-

pling to the dye molecules. Since both the sum of the number of ground-state molecules and excited-state molecules, and the sum of the number of excited-state molecules and photons are constant, we have in equilibrium

$$\Delta\mu \quad = \quad \mu_\gamma. \tag{2.4}$$

To derive an effective action for the photons, we first integrate out the molecules. Next, we use perturbation theory up to second order in g to obtain

$$\begin{aligned} S^{\text{eff}}[a_{\mathbf{k}}, a^*_{\mathbf{k}}] = \sum_{\mathbf{k}} \int_{G^\infty} dt' \int_{G^\infty} dt\, a^*_{\mathbf{k}}(t) \\ \times \left[\left\{ i\hbar \frac{\partial}{\partial t} - \epsilon_\gamma(\mathbf{k}) + \mu_\gamma \right\} \delta(t,t') - \hbar\Sigma(\mathbf{k},t,t') \right] a_{\mathbf{k}}(t'), \end{aligned} \tag{2.5}$$

where the photon self-energy due to coupling with the dye is given by

$$\begin{aligned} \Sigma(\mathbf{k},t,t') = \frac{-i|g|^2}{2\hbar^2 V} \sum_{\mathbf{p}} G_\downarrow(\mathbf{p},t',t) \\ \times \left\{ G_\uparrow(\mathbf{k}_+ + \mathbf{p},t,t') + G_\uparrow(\mathbf{k}_- + \mathbf{p},t,t') \right\}. \end{aligned} \tag{2.6}$$

It turns out that both terms on the right-hand side are equal, and therefore we can write

$$\Sigma(\mathbf{k},t,t') = \frac{-i|g|^2}{\hbar^2 V} \sum_{\mathbf{p}} G_\downarrow(\mathbf{p},t',t) G_\uparrow(\mathbf{k}_+ + \mathbf{p},t,t'). \tag{2.7}$$

Here the Keldysh Green's function for the dye molecules is given by

$$\begin{aligned} G_\rho(\mathbf{p},t,t') = ie^{-i(\epsilon(\mathbf{p})-\mu_\rho+K_\rho)(t-t')/\hbar} \\ \times \{\Theta(t,t')(N_\rho(\mathbf{p})-1) + \Theta(t',t)N_\rho(\mathbf{p})\}, \end{aligned} \tag{2.8}$$

where $\Theta(t,t')$ and $\Theta(t',t)$ are the corresponding Heaviside functions on the Schwinger-Keldysh contour. Furthermore, the occupation numbers for the dye molecules are

$$N_\rho(\mathbf{p}) = e^{-\beta(\epsilon(\mathbf{p})-\mu_\rho+K_\rho)}, \tag{2.9}$$

with $\rho \in \{\uparrow,\downarrow\}$. Since this action is defined on the Schwinger-Keldysh contour, we can only use this action to calculate quantities on the Schwinger-Keldysh contour. However, the relevant physical quantities should be calculated on the real-time axis. Therefore, we need to transform this action into an action that is defined on this real-time axis. As is shown in Ref. [56],

this boils down to determining the retarded, advanced, and Keldysh self-energies. Roughly speaking, the advanced and retarded self-energies determine the dynamics of the single-particle wave function in the gas, i.e., the coherent dynamics, and the Keldysh component accounts for the dynamics of their occupation numbers, i.e., the incoherent dynamics.

In the continuum limit the retarded self-energy becomes

$$\hbar\Sigma^{(+)}(\mathbf{k}, t-t') = \frac{i}{\hbar}\Theta(t-t')|g|^2 \int \frac{d\mathbf{p}}{(2\pi)^3} e^{i(\epsilon(\mathbf{k}_+,\mathbf{p})+\Delta\mu)(t-t')/\hbar} \left\{N_\uparrow(\mathbf{k}_+ + \mathbf{p}) - N_\downarrow(\mathbf{p})\right\}. \tag{2.10}$$

Here we used Eqs. (2.6) and (2.8) and we defined $\epsilon(\mathbf{k}_+, \mathbf{p}) = \epsilon(\mathbf{p}) - \epsilon(\mathbf{k}_+ + \mathbf{p}) - \Delta$. In Fourier space this self-energy reads

$$\begin{aligned}\hbar\Sigma^{(+)}(\mathbf{k},\omega) &:= S(\mathbf{k},\omega) - iR(\mathbf{k},\omega) \\ &:= \int d(t-t')\, \hbar\Sigma^{(+)}(\mathbf{k}, t-t') e^{i\omega(t-t')}.\end{aligned} \tag{2.11}$$

Since the molecules behave as a Maxwell-Boltzmann gas at room temperature, we can find an analytical expression for $R(\mathbf{k},\omega)$. We obtain

$$R(\mathbf{k},\omega) = A(\mathbf{k},\omega)\frac{|g|^2 m_\mathrm{d}^2}{2|\mathbf{k}_+|\pi\beta\hbar^4} \sinh\left\{\frac{\beta\hbar\omega}{2}\right\}, \tag{2.12}$$

with

$$\begin{aligned}A(\mathbf{k},\omega) &= \exp\left\{\beta\left(\mu_\downarrow + \mu_\uparrow - \Delta\right)/2\right\} \\ &\quad \times \exp\left\{-\frac{\beta}{4}\left[\epsilon(\mathbf{k}_+) + \frac{(\Delta - \Delta\mu - \hbar\omega)^2}{\epsilon(\mathbf{k}_+)}\right]\right\}.\end{aligned} \tag{2.13}$$

Furthermore, in Fourier space the Keldysh self-energy is given by

$$\begin{aligned}\hbar\Sigma^K(\mathbf{k},\omega) &= i|g|^2 \int \frac{d\mathbf{p}}{(2\pi)^2}\, \delta(\hbar\omega + \epsilon(\mathbf{k}_+,\mathbf{p}) + \Delta\mu) \\ &\quad \times \{2N_\downarrow(\mathbf{p})N_\uparrow(\mathbf{k}_+ + \mathbf{p}) - N_\downarrow(\mathbf{p}) - N_\uparrow(\mathbf{k}_+ + \mathbf{p})\}.\end{aligned} \tag{2.14}$$

Since the dye is in quasi-equilibrium, this Keldysh self-energy can be related to the imaginary part of the retarded self-energy. We find

$$\hbar\Sigma^K(\mathbf{k},\omega) = -2i(1 + 2N_\mathrm{BE}(\omega))R(\mathbf{k},\omega), \tag{2.15}$$

where

$$N_\mathrm{BE}(\omega) = \frac{1}{e^{\beta\hbar\omega} - 1}. \tag{2.16}$$

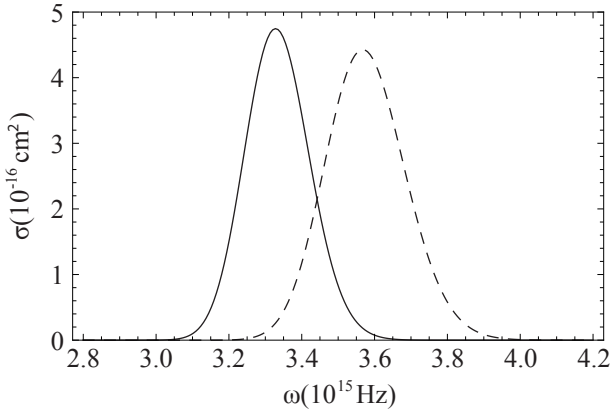

Figure 2.3: Absorption and emission cross sections of the photons obtained from the imaginary part of the retarded self-energy for $m_{\mathrm{d}} = 9.3 \cdot 10^{-35}$ kg, $\Delta = 3.63 \cdot 10^{-19}\,\mathrm{J}$ and $g = 6.08 \cdot 10^{-26}\,\mathrm{J} \cdot \mathrm{m}^{3/2}$. The solid curve corresponds to the emission and the dashed curve denotes the absorption of photons. The absorption cross section is given by Eq. (2.19), and the plotted emission cross section is obtained from the same equation by replacing $R_{\mathrm{abs}}(\omega)$ with $R_{\mathrm{emis}}(\omega)$.

This result is known as the fluctuation-dissipation theorem. As we show in the next section, this result guarantees that the photon gas relaxes towards thermal equilibrium in the limit of $t \to \infty$.

To make further progress, we have to determine typical numerical values for Δ and g appropriate for the experiment of Klaers *et al.*. These values can be obtained by looking at the physical meaning of the self-energy. Consider a system of molecules that can be in either a ground state or excited state. If we apply a laser to this system, we can measure, for instance, the total number of molecules in the excited state. This number depends on the rate of photon absorption and emission, and therefore on the lifetime of the photons. Since the imaginary part of the retarded self-energy is related to the lifetime of the photon, we can determine the emission and absorption spectra of the molecules with the help of our expression for $R(\mathbf{k}, \omega)$.

In order to obtain the absorption and emission spectrum separately, we take a closer look at the retarded self-energy given by Eq. (2.10). In this expression the factor with the Maxwell-Boltzmann distribution can be rewritten as $N_{\downarrow}(\mathbf{p})(N_{\uparrow}(\mathbf{k}_+ + \mathbf{p}) \pm 1) - N_{\uparrow}(\mathbf{k}_+ + \mathbf{p})(N_{\downarrow}(\mathbf{p}) \pm 1)$. The first term can be understood as the absorption of a photon, since this statistical factor accounts for the process where a ground-state molecule scatters into an excited state. The factor $N_{\downarrow}(\mathbf{p})$ simply is the number of molecules that can undergo the collision, and $(N_{\uparrow}(\mathbf{k}_+ + \mathbf{p}) \pm 1)$ denotes the Bose enhancement factor or Pauli blocking factor depending on the quantum statistics

of the dye molecules. By using a similar reasoning the second term can be understood as the emission of a photon. Hence, the part of the self-energy proportional to $N_\downarrow(\mathbf{p})$ is related to the absorption spectrum, and the part proportional to $N_\uparrow(\mathbf{k}_+ + \mathbf{p})$ is related to the emission spectrum.

The absorption and emission spectra are usually obtained in experiments where the number of photons is not conserved. So, in these systems the photons have no chemical potential. To make a comparison, we therefore have to set $\mu_\downarrow = \mu_\uparrow$. Furthermore, contrary to the experiment of Klaers *et al.*, there is no restriction on the momentum of the photons. This implies that the photon field should be expanded into plane waves instead of standing waves. Therefore, the fourth term on the right-hand side of the action in Eq. (2.2) is absent, and the prefactor of the third term is changed into $1/\sqrt{V}$. However, this modification leaves the expressions for the self-energies unchanged.

In order to get more insight into the role of the parameters of our model in the absorption and emission spectra, we first consider the experiment of Klaers *et al.* and we keep $\mathbf{k}$ fixed. Then, the spectra have a maximum at

$$\hbar\omega_\pm = \Delta \pm \frac{\hbar^2 \mathbf{k}_+^2}{2m_\mathrm{d}}, \tag{2.17}$$

where we used $\Delta\mu = 0$. Here the plus sign is the maximum of the absorption spectrum and the minus sign corresponds to the position of the maximum of the emission spectrum. So we obtain a difference in frequency between the maximum of the absorption and emission spectra. This difference is also obtained experimentally and is known as the Stokes shift. From this expression we find that the value of m_d determines the value of the Stokes shift. Furthermore we can see from Eq. (2.17), that we can change the position of the peaks by varying Δ.

Now we turn to more conventional experiments, where the absorption of laser light by the medium is measured as a function of frequency. To obtain the absorption and emission spectra only as a function of frequency, we have to consider the self-energy on shell and thus replace $\mathbf{k}_+$ with ω/c. For the physical mass of the Rhodamine 6G molecule, we obtain peaks that are too narrow and a Stoke shift that is too small. This is because we neglected the rovibrational structure of the molecules. Due to this rovibrational structure there are many possible transitions, since the excited and ground levels are split into several sublevels. Therefore there is a whole range of photon energies which can be absorbed or emitted by the molecule. This causes a considerable broadening of the spectra. As mentioned before, we model this rovibrational structure by choosing an effective mass for the molecules. We can also see explicitly from Eqs. (2.12) and (2.13), that de-

creasing the value of m_{d} will indeed broaden the peaks. For $\Delta = 3.63 \cdot 10^{-19}$ J and $m_{\mathrm{d}} = 9.3 \cdot 10^{-35}$ kg we recover in good approximation the normalized absorption and emission spectra given in Ref. [32].

Up to now, we have considered the relative absorption and emission spectra. To obtain the correct height of these spectra, we have to find an appropriate value for g. By using Ref. [57], we can actually compare our results to the experimentally obtained absorption and emission spectra. However, to calculate the emission spectrum for this particular experiment within our formalism, we have to take into account that the emission of a photon can be in an arbitrary direction. Thus to obtain the emission spectrum we have to perform an integral which averages over all possible emission directions. However, the absorption spectrum can be obtained without performing additional integrals, and therefore we focus on this spectrum to obtain a numerical value for g. Then, as a consequence of our formalism, for our purposes the correct emission spectrum is also incorporated.

Before we can fit g, we have to relate our calculated decay rates to the measured absorption cross sections. We have

$$\frac{dN}{dx} = -n_{\downarrow}\sigma_{\mathrm{abs}}(\omega), \tag{2.18}$$

where the left hand-side is the number of absorbed photons dN after a distance dx along the path of a beam. Furthermore, $n_{\downarrow}$ is the density of ground-state molecules and σ_{abs} is the absorption cross section. By using Fermi's golden rule, we obtain that dN/dt is equal to $-2R_{\mathrm{abs}}(\omega)/\hbar$. Here $R_{\mathrm{abs}}(\omega)$ denotes the absorption term in the imaginary part of the self-energy. Hence

$$\sigma_{\mathrm{abs}}(\omega) = \frac{2R_{\mathrm{abs}}(\omega)}{c\hbar n_{\downarrow}}. \tag{2.19}$$

Since the molecules behave as a classical Maxwell-Boltzmann gas,

$$n_{\downarrow} = \left(\frac{m_{\mathrm{d,real}}}{2\pi\hbar^2\beta}\right)^{3/2} e^{\beta\mu_{\downarrow}}. \tag{2.20}$$

Note that contrary to the mass of the dye molecules used in the self-energies, we here use the real mass of the dye molecules to obtain the correct densities. Thus m_{d} is the effective mass to model the rovibrational structure of the molecules, and $m_{\mathrm{d,real}} \simeq 7.95 \cdot 10^{-25}$ kg is the physical mass of a Rhodamine 6G molecule. By using our expression for $R(\mathbf{k}, \omega)$ we observe that the absorption cross section is independent of $\mu_{\downarrow}$. Therefore we do not need

to specify the number of molecules to obtain a numerical estimate for g. Furthermore, we can relate the absorption cross section given by Eq. (2.19) to the molecular extinction coefficient obtained in Ref. [57]. According to Ref. [58],

$$\sigma = (3.82 \cdot 10^{-21} \cdot \epsilon)\,\mathrm{cm}^3 \cdot \mathrm{mol} \cdot \mathrm{L}^{-1}, \tag{2.21}$$

where $\epsilon = 1.16 \cdot 10^5\,\mathrm{L} \cdot \mathrm{mol}^{-1} \cdot \mathrm{cm}^{-1}$ is the molar extinction coefficient. This results in $g \simeq 6.08 \cdot 10^{-26}\,\mathrm{J} \cdot \mathrm{m}^{3/2}$. A plot of the absorption and emission cross sections for the obtained numerical values for Δ, m_d and g is given in Fig. 2.3. The shown emission cross section is obtained from Eq. (2.19) by replacing $R_\mathrm{abs}(\omega)$ with $R_\mathrm{emis}(\omega)$. As mentioned before, this is not the physical emission cross section since that can only be obtained by integrating over all directions of emission.

2.3 Non-equilibrium physics

We introduce a complex field $\phi(\mathbf{x}, t)$ for the photons such that

$$\langle |\phi(\mathbf{k}, t)|^2 \rangle = N(\mathbf{k}, t) + \frac{1}{2}, \tag{2.22}$$

where $N(\mathbf{k}, t)$ corresponds to the average occupation number of the single-particle state with momentum $\mathbf{k}$ at time t. As is shown in Ref. [56], $\phi(\mathbf{x}, t)$ obeys a Langevin field equation for describing the dynamics of the photon gas. This equation ultimately reads

$$\begin{aligned} i\hbar \frac{\partial}{\partial t}\phi(\mathbf{x}, t) &= \left(H(\mathbf{x}) + T^{2\mathrm{B}}|\phi(\mathbf{x}, t)|^2\right)\phi(\mathbf{x}, t) \\ &+ \int d\mathbf{x}' dt' \hbar\Sigma^{(+)}(\mathbf{x} - \mathbf{x}', t - t')\phi(\mathbf{x}', t') + \eta(\mathbf{x}, t), \end{aligned} \tag{2.23}$$

where the Hamiltonian

$$H(\mathbf{x}) = -\frac{\hbar^2\nabla^2}{2m_\mathrm{ph}} - \mu_\gamma + \hbar c k_\gamma + \frac{1}{2} m_\mathrm{ph}\Omega^2 |\mathbf{x}|^2. \tag{2.24}$$

Here $\mathbf{x} = (x, y)$ and the field $\phi^*(\mathbf{x}, t)$ satisfies the complex conjugate equation. Furthermore, to obtain this equation, we expanded Eq. (2.1) for small transverse momenta, using that $k_\gamma(\mathbf{x})$ is position dependent due to the curvature of the cavity mirrors. In this equation $m_\mathrm{ph} \simeq 6.7 \cdot 10^{-36}\,\mathrm{kg}$ is the effective mass of the photons, and $\Omega \simeq 2.6 \cdot 10^{11}\,\mathrm{Hz}$ is the trapping frequency of the harmonic potential. We also introduced a self-interaction

term with strength $T^{2\mathrm{B}} \simeq 1.2{\cdot}10^{-36}\,\mathrm{J}\cdot\mathrm{m}^2$. According to Ref. [32], this self-interaction of the photons arises from Kerr nonlinearity or thermal lensing in the dye. This self-interaction is an effective interaction, and therefore also incorporates renormalization from interactions at high momenta and energies. Finally, the Gaussian noise $\eta(\mathbf{x},t)$ satisfies

$$\langle \eta(\mathbf{x},t)\eta^*(\mathbf{x}',t')\rangle = \frac{i\hbar}{2}\hbar\Sigma^K(\mathbf{x}-\mathbf{x}',t-t'). \tag{2.25}$$

Here, the brackets denote averaging over different realizations of the noise. In general it is difficult to determine correlation functions from these equations, especially because of the non-locality of the retarded self-energy. However, since we are interested in Bose-Einstein condensation of photons we focus on the low-energy behavior of this self-energy. In the low-energy regime we are interested in $k\xi$ of the order of unity and ω around $\omega_{\mathrm{B}}(\mathbf{k})$, where

$$\hbar\omega_{\mathrm{B}}(\mathbf{k}) = \sqrt{\left(\frac{\hbar^2\mathbf{k}^2}{2m_{\mathrm{ph}}}\right)^2 + 2n_0T^{2\mathrm{B}}\left(\frac{\hbar^2\mathbf{k}^2}{2m_{\mathrm{ph}}}\right)}, \tag{2.26}$$

is the Bogoliubov dispersion and

$$\xi = \frac{\hbar}{2\sqrt{m_{\mathrm{ph}}n_0T^{2\mathrm{B}}}}, \tag{2.27}$$

is the coherence length, with n_0 being the density of condensed photons. Note that k is the norm of the two-dimensional momentum vector $\mathbf{k} = (k_{\mathrm{x}}, k_{\mathrm{y}})$. Since for the experiment of Ref. [32] the critical number of photons $N_{\mathrm{c}} \simeq 77000$ and the diameter of the condensate is measured as a function of the condensate fraction, we can make an estimate of n_0. We obtain condensate densities in the range of at least $10^{12} - 10^{13}\,\mathrm{m}^{-2}$.

We make a low-energy approximation to the imaginary part of the retarded self-energy. As we see in Fig. 2.4, this is a good approximation in the low-energy regime. Furthermore, the real part of the retarded self-energy is small, and as a zeroth-order approximation we neglect this contribution. Thus we approximate

$$\hbar\Sigma^{(+)}(\mathbf{k},\omega) = -i\alpha\hbar\omega, \tag{2.28}$$

and we can write for the Langevin field equation that

$$i\hbar(1+i\alpha)\frac{\partial}{\partial t}\phi(\mathbf{x},t) = (H(\mathbf{x}) + T^{2\mathrm{B}}|\phi(\mathbf{x},t)|^2)\phi(\mathbf{x},t) + \eta(\mathbf{x},t). \tag{2.29}$$

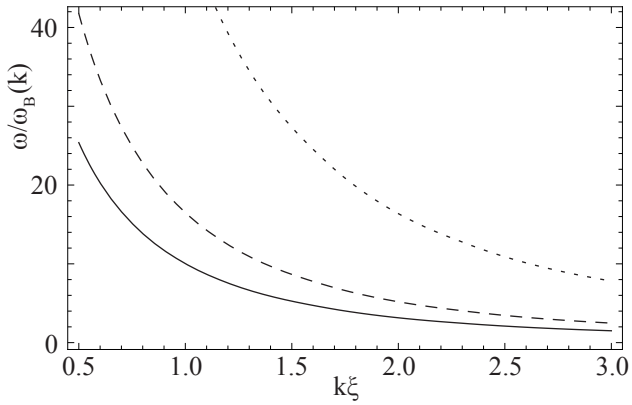

Figure 2.4: Validity of the linear approximation of the retarded self-energy for $n_0 = 10^{12}\,\mathrm{m}^{-2}$ and certain values of ω and k. The dashed, dotted and solid curves are for, respectively, $\Delta\mu$ equal to $3.4\cdot10^{-19}$ J, $3.7\cdot10^{-19}$ J, and $4.0\cdot10^{-19}$ J. Below the curves is the region where the linear approximation is within 1% of the actual value of the self-energy.

This is the equation which determines the complete dynamics of the photon gas. The finite-lifetime effects are captured by the single dimensionless parameter α, which depends on the difference between the chemical potentials of the excited-state and ground-state molecules. Furthermore, the noise $\eta(\mathbf{x}, t)$ is related to the Keldysh self-energy via Eq. (2.25) and in this approximation

$$\Sigma^K(\mathbf{x}' - \mathbf{x}, t' - t) = -2i\alpha\delta(\mathbf{x} - \mathbf{x}') \int \frac{d\omega}{2\pi} \left(1 + 2N(\omega)\right) \omega e^{-i\omega(t'-t)}. \quad (2.30)$$

The explicit dependence of α on $\Delta\mu$ is given by

$$\alpha = \alpha_{\max} n_{\mathrm{m}} \frac{e^{-C(\Delta\mu - \Delta)^2}}{\cosh\left\{\frac{1}{2}\beta(\Delta\mu - \Delta)\right\}}, \quad (2.31)$$

where n_{m} is the density of dye molecules,

$$C = \frac{\beta m_{\mathrm{d}}}{2\hbar^2 |k_\gamma|^2}, \quad (2.32)$$

and

$$\alpha_{\max} = \sqrt{\frac{\pi m_{\mathrm{d,real}}}{8\beta\hbar^2 k_\gamma^2}} \left(\frac{\beta|g|m_{\mathrm{d}}}{m_{\mathrm{d,real}}}\right)^2 e^{-\beta\hbar^2 k_\gamma^2/8m_{\mathrm{d}}}. \quad (2.33)$$

The damping parameter α is inversely proportional to the photon lifetime, and accounts for the decay of photons due to the interaction with the dye

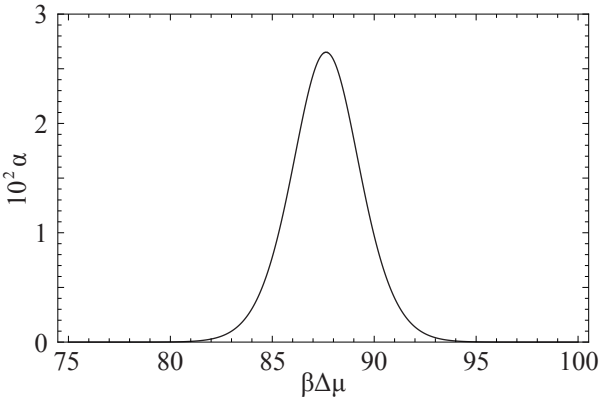

Figure 2.5: Plot of the dimensionless damping parameter α as a function of $\beta\Delta\mu$. For this plot we used $n_{\rm m} = 9 \cdot 10^{23}{\rm m}^{-3}$. The parameter α has a maximum value of about $2.65 \cdot 10^{-2}$ at $\Delta\mu$ equal to Δ.

molecules. The emission and absorption of photons are equally important for the photon equilibration. Therefore, α has a maximum when there is an equal amount of excited-state and ground-state molecules, i.e., for $\Delta\mu = \Delta$ where $P = 0$. This also explains the symmetric form of α around $\Delta\mu = \Delta$. Namely, α should be symmetric while changing the sign of the polarization as this only switches the excited-state and ground-state molecule densities. A plot of α as a function of $\Delta\mu$ is shown in Fig. 2.5.

The Langevin field equation given by Eq. (2.29) incorporates the complete dynamics of the photons. However, we still need to check that for large times the photon distribution function relaxes to the correct equilibrium. For this it suffices to consider the homogeneous case and to neglect the self-interaction of the photons. For purposes of generality, we do not make a low-energy approximation to the self-energy, and we Fourier transform the Langevin field equation into

$$i\hbar\frac{\partial}{\partial t}\phi(\mathbf{k},t) = (\epsilon_\gamma(\mathbf{k}) - \mu_\gamma)\phi(\mathbf{k},t) + \eta(\mathbf{k},t) + \int_{t_0}^{\infty} dt'\, \hbar\Sigma^{(+)}(\mathbf{k}, t-t')\phi(\mathbf{k},t'). \tag{2.34}$$

As mentioned in the previous section, the fluctuation-dissipation theorem given by Eq. (2.15) should ensure that the gas relaxes towards thermal equilibrium. To check that this formalism contains this correct equilibrium, we assume that $\langle\phi(\mathbf{k},t)\phi^*(\mathbf{k},t')\rangle$ only depends on the difference $t - t'$ and

write,

$$\langle \phi(\mathbf{k},t)\phi^*(\mathbf{k},t')\rangle = \int \frac{d\omega}{2\pi} G(\mathbf{k},\omega) e^{-i\omega(t-t')}. \tag{2.35}$$

Then

$$i\hbar \frac{d}{d(t+t')} \langle \phi(\mathbf{k},t)\phi^*(\mathbf{k},t')\rangle = 0, \tag{2.36}$$

and for $t' = t$ we obtain the equilibrium value for $\langle \phi(\mathbf{k},t)\phi^*(\mathbf{k},t)\rangle$. Since we are interested in the equilibrium, we consider times much larger than t_0. Therefore we are allowed to take the limit of $t_0 \to -\infty$. Now Eq. (2.36) can be rewritten as

$$\begin{aligned} &\langle \eta(\mathbf{k},t)\phi^*(\mathbf{k},t')\rangle - \int_{-\infty}^{\infty} dt''\, \langle \phi(\mathbf{k},t)\phi^*(\mathbf{k},t'')\rangle \hbar\Sigma^{(-)}(\mathbf{k},t''-t') = \\ &\langle \phi(\mathbf{k},t)\eta^*(\mathbf{k},t')\rangle - \int_{-\infty}^{\infty} dt''\, \hbar\Sigma^{(+)}(\mathbf{k},t-t'')\langle \phi(\mathbf{k},t'')\phi^*(\mathbf{k},t')\rangle. \end{aligned} \tag{2.37}$$

Here we used that $\hbar\Sigma^{(-)}(\mathbf{k},t'-t) = (\hbar\Sigma^{(+)}(\mathbf{k},t'-t))^*$. Furthermore, since the field $\phi(\mathbf{k},t)$ and its complex conjugate depend on the noise, we have a nonzero value for $\langle \eta(\mathbf{k},t)\phi^*(\mathbf{k},t')\rangle$, which can be determined by formally integrating Eq. (2.34) and using Eq. (2.25). In Fourier space Eq. (2.37) is given by

$$-\frac{1}{2i}\Sigma^K(\mathbf{k},\omega)G^{(+)}(\mathbf{k},\omega)G^{(-)}(\mathbf{k},\omega) = G(\mathbf{k},\omega), \tag{2.38}$$

where the retarded (+) and advanced (-) photon Green's functions are determined by

$$\hbar G^{(\pm),-1}(\mathbf{k},\omega) = \hbar\omega^{\pm} - \epsilon_\gamma(\mathbf{k}) + \mu_\gamma - \hbar\Sigma^{(\pm)}(\mathbf{k},\omega). \tag{2.39}$$

To make further progress, we introduce the spectral function

$$\begin{aligned} \rho(\mathbf{k},\omega) &= -\frac{1}{\pi\hbar}\mathrm{Im}\left[G^{(+)}(\mathbf{k},\omega)\right] \\ &= \frac{1}{\pi}\frac{R(\mathbf{k},\omega)}{[\hbar\omega - \epsilon_\gamma(\mathbf{k}) + \mu_\gamma - S(\mathbf{k},\omega)]^2 + [R(\mathbf{k},\omega)]^2} \\ &= \frac{1}{\pi\hbar^2} R(\mathbf{k},\omega)G^{(+)}(\mathbf{k},\omega)G^{(-)}(\mathbf{k},\omega). \end{aligned} \tag{2.40}$$

This spectral function $\rho(\mathbf{k},\omega)$ can be interpreted as a single-particle density of states. Therefore we can calculate densities in equilibrium by multiplying

this spectral function with the Bose-distribution function $N_{\rm BE}(\omega)$ and then integrating over $\hbar\omega$. Hence,

$$N(\mathbf{k}) = \int d(\hbar\omega)\, N_{\rm BE}(\omega)\rho(\mathbf{k},\omega), \tag{2.41}$$

where $N(\mathbf{k})$ is the number of photons in a state with momentum $\mathbf{k}$. Thus, in equilibrium

$$G(\mathbf{k},\omega) = 2\pi\hbar \left[\frac{1}{2} + N_{\rm BE}(\omega)\right] \rho(\mathbf{k},\omega), \tag{2.42}$$

where we used the fluctuation-dissipation theorem in Eq. (2.15). Hence,

$$\langle \phi(\mathbf{k},t)\phi^*(\mathbf{k},t)\rangle = N(\mathbf{k}) + \frac{1}{2}. \tag{2.43}$$

By comparing this result to Eq. (2.22), we find that the average occupation numbers $N(\mathbf{k},t)$ relax to $N(\mathbf{k})$. During this calculation we did not use an approximation for the imaginary part of the retarded self-energy. However, we can do the same calculation for $R(\mathbf{k},\omega)$ given by $\alpha\hbar\omega$. This approximation will directly manifest itself in the fluctuation-dissipation theorem and ultimately in the spectral function. Therefore, in this approximation the equilibrium occupation numbers are also given by Bose-Einstein distribution functions.

2.4 Equilibrium physics

In the previous section we have shown that the complete dynamics of the photon gas can be obtained from a Langevin field equation for a complex field $\phi(\mathbf{x},t)$. On top of this non-equilibrium physics, we have demonstrated that the relaxation of the photons towards the correct equilibrium. In this section we discuss equilibrium properties of the photon gas, and we therefore set $\Delta\mu = \mu_\gamma$ according to Eq. (2.4). We perform calculations in both the normal and in the Bose-Einstein condensed states.

2.4.1 Normal state

We first consider the spectral function of the photons defined in Eq. (2.40). The spectral function should satisfy two conditions. First of all, because we are dealing with bosons, the spectral function should be positive (negative) for positive (negative) frequencies. From Eq. (2.12) it is clear that $R(\mathbf{k},\omega)$ has this property, and therefore this condition is indeed satisfied by the

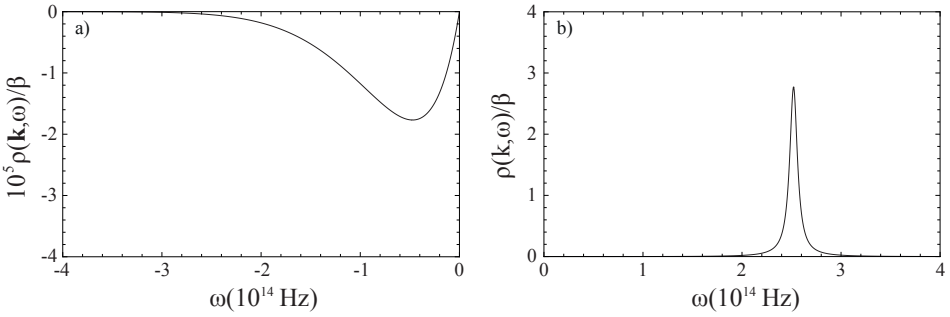

Figure 2.6: a) Negative frequency and b) positive frequency parts of the spectral function of the photons in the normal state as a function of the frequency ω for $k_y = k_x = 0$, $n_m = 9 \cdot 10^{23}\,\mathrm{m}^{-3}$, and $\mu_\gamma = 3.5 \cdot 10^{-19}\mathrm{J}$.

spectral function. Second, the spectral function should satisfy the zeroth-frequency sum rule

$$\int d(\hbar\omega)\rho(\mathbf{k},\omega) = 1. \tag{2.44}$$

By numerically integrating this spectral function, we check that we satisfy the sum rule for all chemical potentials smaller than the lowest energy of the photons.

As we can see from Figs. 2.6, the spectral function consists of a Lorentzian-like peak for positive frequencies and a continuum for negative frequencies. The latter is roughly five orders of magnitude smaller than the positive contribution. Since the positive contribution is approximately a Lorentzian, we can determine the lifetime of the photons by looking at the width of these peaks [59]. This lifetime is defined as the time for which a photon in a certain momentum state $\mathbf{k}$ goes into another state with momentum $\mathbf{k}'$ due to absorption and re-emission by the molecules.

Numerically, we obtained for small momenta and $\beta\mu_\gamma$ up to roughly 87, a lifetime of the order of 10^{-13} s. If we increase μ_γ even further, the lifetime of the photons increases rapidly. Because for larger values of μ_γ the peaks of the spectral function are at smaller frequencies, we can also show this fact analytically. Since we know that the lifetime of the photon is related to the imaginary part of this pole, we need to determine the poles of Eq. (2.39).

In the previous section we found that for small frequencies we can use an approximation for the imaginary part of the self-energy in which it is linear in frequency. Within this approximation, the Green's function given

by Eq. (2.39) has a pole at

$$\hbar\omega^{\mathrm{pole}}(\mathbf{k}) = \frac{1-i\alpha}{1+\alpha^2}\left(\epsilon_\gamma(\mathbf{k}) - \mu_\gamma\right). \tag{2.45}$$

Since $\alpha^2 \ll 1$, a typical lifetime of the photons in the normal state is given by

$$\tau(\mathbf{k}) = \frac{\hbar}{2\alpha\left(\epsilon_\gamma(\mathbf{k}) - \mu_\gamma\right)} \sim \frac{1}{\alpha\Omega}. \tag{2.46}$$

where α is given by Eq. (2.31), $\Delta\mu$ is sufficiently large, and Ω is the trap frequency of the photons. In the last step we used the fact that the photons are trapped in a harmonic potential and therefore the typical energy of the photons is proportional to $\hbar\Omega$. From Fig. 2.5 we know that for the relevant values of μ_γ, α is in the range of $10^{-3} - 10^{-2}$. Therefore, the lifetime of the photons is in the nanosecond regime, which agrees with Ref. [32]. We also note that the smallness of α implies that the collective-mode dynamics of the gas is underdamped as the ratio between the damping and frequency of the collective modes is precisely α.

2.4.2 Condensed state

In this section we consider the homogeneous two-dimensional photon gas below the critical temperature for Bose-Einstein condensation. To describe the condensate of photons we start from the following two-dimensional action

$$\begin{aligned} S^{\mathrm{eff}}[a^*, a] = &\sum_{\mathbf{k},n} \hbar G^{-1}(\mathbf{k}, i\omega_n) a^*_{\mathbf{k},n} a_{\mathbf{k},n} \\ &+ \frac{T^{2\mathrm{B}}}{2} \sum_{\mathbf{K},\mathbf{k},\mathbf{q},n,m,l} a^*_{\mathbf{K}-\mathbf{k},n-m} a^*_{\mathbf{k},m} a_{\mathbf{K}-\mathbf{q},n-l} a_{\mathbf{q},l}. \end{aligned} \tag{2.47}$$

Here

$$\hbar G^{-1}(\mathbf{k}, i\omega_n) = i\hbar\omega_n - \epsilon_\gamma(\mathbf{k}) + \mu_\gamma - \hbar\Sigma(\mathbf{k}, i\omega_n), \tag{2.48}$$

and $\hbar\Sigma(\mathbf{k}, i\omega_n)$ follows from the retarded self-energy by Wick rotation of the real frequency to Matsubara frequencies $i\omega_n$. This action describes the same equilibrium physics as coming from the Langevin field equation in Eq. (2.34), since after a Wick rotation the equations of motion for the field $a_{\mathbf{k},n}$ are determined by the average of the Langevin equations. Substituting

$a_{\mathbf{0},0} \to a_{\mathbf{0},0}+\phi$ and requiring that the terms linear in the fluctuations vanish leads to the equation

$$\mu_\gamma = \hbar c k_\gamma + S(\mathbf{0},0) + T^{2\mathrm{B}} n_0, \tag{2.49}$$

where n_0 is the density of condensed photons. This equation determines the chemical potential of the Bose-Einstein condensate of photons. We obtain $\beta\mu_\gamma \simeq 90.9$, and according to Eq. (2.3), we have a corresponding polarization of roughly 0.93. Therefore, almost all molecules are in the excited state.

To determine the collective excitations of the condensate over the ground state we consider the action up to second order in the fluctuations. This is the so-called Bogoliubov approximation. So

$$S^{\mathrm{Bog}}[a^*, a] = -\frac{1}{2}\sum_{\mathbf{k},n} u^\dagger_{\mathbf{k},n} \cdot \hbar G^{-1}_{\mathrm{B}}(\mathbf{k}, i\omega_n) \cdot u_{\mathbf{k},n}, \tag{2.50}$$

where

$$u_{\mathbf{k},n} := \begin{bmatrix} a_{\mathbf{k},n} \\ a^*_{-\mathbf{k},-n} \end{bmatrix}, \tag{2.51}$$

and

$$\hbar G^{-1}_{\mathrm{B}}(\mathbf{k}, i\omega_n) = \hbar G^{-1}(\mathbf{k}, i\omega_n) \begin{bmatrix} 1 & 0 \\ 0 & 1 \end{bmatrix} - T^{2\mathrm{B}} n_0 \begin{bmatrix} 2 & 1 \\ 1 & 2 \end{bmatrix}. \tag{2.52}$$

Since μ_γ is given by Eq. (2.49), we obtain that $\mathrm{Det}[G^{-1}_{\mathrm{B}}(0,0)] = 0$. Therefore we have a gapless excitation, which agrees with Goldstone's theorem. By Wick rotating and solving for which ω the determinant of this matrix vanishes, we can determine the dispersions. Since we are interested in the low-energy behavior, we can use Eq. (2.28) for the self-energy. In this approximation the dispersions are given by

$$\begin{aligned}(1+\alpha^2)\hbar\omega(\mathbf{k}) = &-i\alpha(\tilde{\epsilon}_\gamma(\mathbf{k}) + T^{2\mathrm{B}} n_0) \\ &\pm \sqrt{-(\alpha T^{2\mathrm{B}} n_0)^2 + \tilde{\epsilon}_\gamma(\mathbf{k})(\tilde{\epsilon}_\gamma(\mathbf{k}) + 2T^{2\mathrm{B}} n_0)},\end{aligned} \tag{2.53}$$

with $\tilde{\epsilon}_\gamma(\mathbf{k}) = \epsilon_\gamma(\mathbf{k}) - \hbar c k_\gamma$. The imaginary part of the dispersion relations is always negative and we find a lifetime in the nanosecond regime for n_0 in the range of $10^{12} - 10^{13}\,\mathrm{m}^2$ and excitations for which $k\xi < 0.2$, with $k = |(k_\mathrm{x}, k_\mathrm{y})|$. For excitations with larger momentum the lifetime decreases, until it approaches zero in the limit of $k \to \infty$.

Furthermore, we have the same behavior as was first shown in Ref. [60] for a non-equilibrium Bose-Einstein condensate of exciton-polaritons. Also

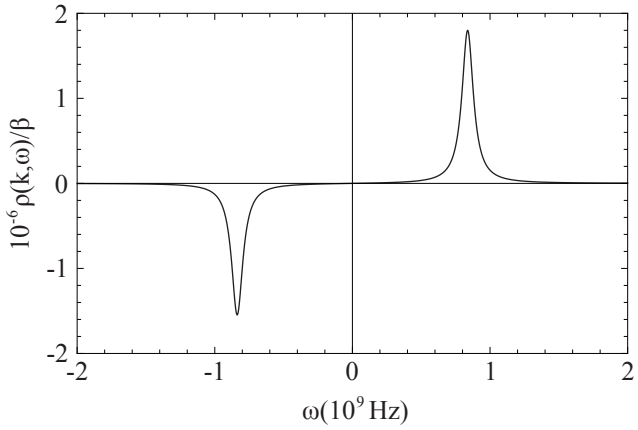

Figure 2.7: The spectral function as a function of ω for $n_{\mathrm{m}} = 9 \cdot 10^{23}\,\mathrm{m}^{-3}$ and $n_0 = 10^{12}\,\mathrm{m}^{-2}$. In this plot $k\xi \simeq 3.8 \cdot 10^{-2}$.

in this case the dispersions become purely imaginary for small momenta. For the numerical values of the experiment and $n_0 = 10^{12}\,\mathrm{m}^2$, we have purely imaginary dispersions for $k\xi < 2.2 \cdot 10^{-3}$. However, this does not imply that for small momenta there are only decaying quasiparticles at zero energy. This can be seen in the spectral function, which in this case corresponds to the imaginary part of $G_{\mathrm{B};11}(\mathbf{k}, \omega^+)$. In Figs. 2.7 and 2.8 we can see the two qualitatively different forms of the spectral function. For relatively large momenta, we have two peaks at the real part of the dispersions, and the width of the peaks is determined by the imaginary part of the dispersions. In the small-momenta region where both dispersions are purely imaginary, we have a continuum for both negative and positive frequencies. Still, the spectral function has a maximum and a minimum. Therefore, in agreement with the large-momentum case we can also define the position of these extrema as the dispersion. So, contrary to what the analytical dispersion given by Eq. (2.53) suggests, for small momenta the spectral function also has a maximum and minimum at nonzero energy.

Finally, we check if the spectral function satisfies the sum rule given by Eq. (2.44). In the low-frequency approximation for the retarded self-energy we can integrate the spectral function analytically, and we obtain

$$\int d(\hbar\omega)\, \rho(\mathbf{k}, \omega) = \frac{1}{1 + \alpha^2}. \tag{2.54}$$

Since we are in the Bose-Einstein condensed phase $\alpha \simeq 4.5 \cdot 10^{-3}$, and we satisfy in very good approximation the sum rule. Note that this small deviation from the sum rule is a consequence of making the low-energy

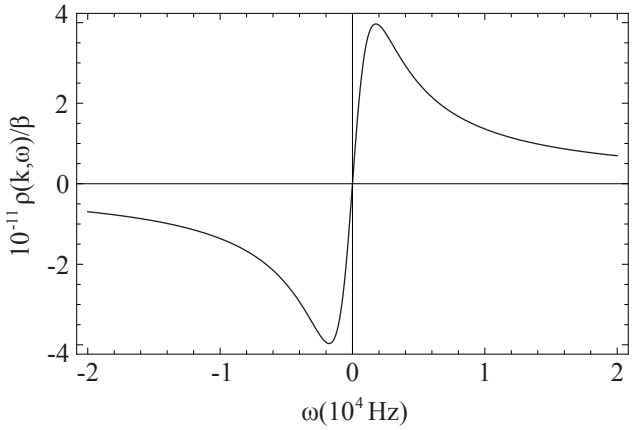

Figure 2.8: The spectral function as a function of ω for $n_{\rm m} = 9 \cdot 10^{23}\,{\rm m}^{-3}$ and $n_0 = 10^{12}\,{\rm m}^{-2}$. In this plot $k\xi \simeq 1.9 \cdot 10^{-5}$.

approximation to the self-energy. Namely, this approximation for the self-energy is only valid for small energies, and therefore the high-frequency behavior is not incorporated correctly. However, without this low-energy approximation the self-energy has the correct low-energy and high-energy limits, and we indeed find that the spectral function with the full self-energy satisfies the sum rule.

2.5 Conclusion and outlook

In this Chapter we constructed a theory for BEC of photons in a dye-filled cavity. By using the Schwinger-Keldysh formalism, we obtained a Langevin field equation that describes the complete dynamics of the photons. In particular, it incorporates both the coherent and incoherent dynamics of the gas. Furthermore we found that the finite lifetime of the photons can be captured in a single parameter α, which depends on the external laser pumping the dye. In addition, we also found an analytic expression for this parameter. In the homogeneous case we have shown that our theory incorporates the correct equilibrium properties of the gas.

Subsequently, we calculated the collective modes and spectral functions of the homogeneous photon gas in the normal and Bose-Einstein condensed state. In both phases we found that the lifetime of the photons in the cavity is in the nanosecond regime, which is the same regime as found experimentally in Ref. [32]. Moreover, we obtained that the dynamics of the collective modes is underdamped. Furthermore, in agreement with the results of Ref. [60] for exciton-polaritons, we found in the Bose-Einstein condensed

phase that dispersions become formally purely imaginary for small momentum. Nevertheless, for small momentum the spectral function also has qualitatively a maximum and minimum at nonzero energy. Finally, in both phases the spectral function is well-behaved and satisfies the sum rule.

In future research we will consider in detail the fluctuations, in particular the phase fluctuations, of the photon Bose-Einstein condensate. For a condensate density of $n_0 \simeq 10^{12}\,\mathrm{m}^{-2}$, the trap length $l = \sqrt{\hbar/m_{\mathrm{ph}}\Omega} \simeq 7.8 \cdot 10^{-6}\,\mathrm{m}$ is about 2 times smaller than the coherence length ξ. However, a condensate density of $n_0 \simeq 10^{13}\,\mathrm{m}^{-2}$ results in a trap length l that is about 2 times larger than the coherence length ξ. Both condensate densities are accessible experimentally [32], and therefore we intend to explore both the regime of Bose-Einstein condensation and the quasi-condensate regime.

Chapter 3

First-order correlation functions

We investigate the finite-lifetime effects on first-order correlation functions of dissipative Bose-Einstein condensates. By taking into account the phase fluctuations up to all orders, we show that the finite-lifetime effects are negligible for the spatial first-order correlation functions, but have an important effect on the temporal correlations. As an application, we calculate the one-particle density matrix of a quasi-condensate of photons. Finally, we also consider the photons in the normal state and we demonstrate that the finite-lifetime effects decrease both the spatial and temporal first-order correlation functions.[1]

3.1 Introduction

Bose-Einstein condensation (BEC) was first directly observed by cooling atomic vapors to temperatures in the nK regime [3–5]. These vapors were confined in three-dimensional traps, of which the shape could be altered by changing certain experimental parameters, e.g., the magnetic field. For sufficiently tight confinement in two or one directions, the dynamics in these dimensions can be frozen out and the atoms behave as a quasi one-dimensional or two-dimensional gas. This manipulation opened up the possibility of exploring Bose-Einstein condensates in lower dimensions [61–64].

From a theoretical point of view these low-dimensional Bose-Einstein condensates are particulary interesting because their physics is fundamentally different from three-dimensional condensates. Namely, in two dimensions a homogeneous Bose gas can only undergo BEC at zero temperature, and in one dimension BEC in a homogeneous Bose gas cannot take place at all [65,66]. In the presence of an external potential the situation drastically

[1] This Chapter is directly based on *Phase Fluctuations and First-Order Correlation Functions of Dissipative Bose-Einstein Condensates*, A.-W. de Leeuw, H.T.C. Stoof, and R.A. Duine, Phys. Rev. A **89**, 053627 (2014).

changes. In particular, harmonically trapped bosons can undergo BEC at nonzero temperatures in both one and two dimensions [44, 45, 67].

For homogeneous two-dimensional Bose gases, theoretical studies show that even though the Bose-Einstein condensate does not exist at nonzero temperatures, there still exists a critical temperature in the system. Below the so-called Kosterlitz-Thouless temperature the gas is superfluid, and above this temperature the bosons lose their superfluid property [68]. This is known as the Kosterlitz-Thouless transition, and it implies that superfluidity only requires the presence of a quasi-condensate [69] with phase coherence over a distance much less than the system size. This quasi-condensate can be roughly interpreted as a system consisting of several patches, each with a fixed phase, whereas the phases of these different patches in the system are uncorrelated.

In addition to atomic gases, there are presently also other low-dimensional systems in which BEC is observed, such as systems consisting of exciton-polaritons [30, 31] or photons [32]. Together with BEC of magnons [29], these systems form a class of condensates that is different from the atomic Bose-Einstein condensates. In particular, the bosonic quasiparticles have a small effective mass resulting in BEC at temperatures in the range of 10 to 300 K instead of in the nK regime relevant to the atomic Bose-Einstein condensates. Furthermore, these condensates are not in true thermal equilibrium, and the steady state is a dynamical balance between particle losses and external pumping. Therefore, the particles have a finite lifetime, which can be characterized by a single dimensionless damping parameter.

In the context of exciton-polariton condensates the first-order correlation functions are extensively studied theoretically. In Refs. [70, 71] the temporal and spatial first-order correlation functions are calculated, by introducing a cutoff to handle the ultra-violet divergence at zero temperature. Furthermore, a more general discussion on spatial correlation functions of non-equilibrium condensates in reduced dimension is given in Ref. [72]. In that work, the main results are obtained for a frequency-independent damping, and a first attempt is made to incorporate frequency-dependent damping. Moreover, in Refs. [73, 74] the spatial correlations of one-dimensional driven-dissipative non-equilibrium condensates are investigated by studying a stochastic equation for the phase fluctuations.

In this Chapter we study the effect of the appropriate frequency-dependent damping parameter on the first-order correlation functions of low-dimensional Bose-Einstein condensates. In particular, we focus on a Bose-Einstein condensate of photons for which this damping parameter is explicitly calculated in Ref. [75]. First, we derive a general expression for the first-order

correlation function for a homogeneous Bose gas in the condensed phase in Sec. 3.2. Thereafter, we use this general expression for the first-order correlation functions to determine the effect of the finite lifetime on the spatial and temporal correlations in Sec. 3.3. In Sec. 3.4 we consider BEC of photons, taking their interaction with the dye molecules into account, and determine the off-diagonal long-range behavior of the one-particle density matrix in the Bose-Einstein condensed phase. We show that for the relevant parameters used in the experiment the photons form a true condensate and Kosterlitz-Thouless physics is not observable. Subsequently, we determine the first-order correlation functions of photons in the normal state, and we end with conclusions and an outlook in Sec. 3.5.

3.2 Phase fluctuations

In this section we derive a general expression for the first-order correlation functions for a homogeneous Bose gas consisting of N bosons in a box of volume V. We start from the Euclidean action

$$S[\phi^*,\phi] = \int_0^{\hbar\beta} d\tau\, d\tau' \int d\mathbf{x}\, d\mathbf{x}'\, \phi^*(\mathbf{x},\tau)\hbar\Sigma(\mathbf{x}-\mathbf{x}',\tau-\tau')\phi(\mathbf{x}',\tau') \quad (3.1)$$
$$+ \int_0^{\hbar\beta} d\tau \int d\mathbf{x}\, \phi^*(\mathbf{x},\tau)\left[\hbar\frac{\partial}{\partial\tau} - \frac{\hbar^2\nabla^2}{2m} - \mu + \frac{T^{2\mathrm{B}}}{2}|\phi(\mathbf{x},\tau)|^2\right]\phi(\mathbf{x},\tau),$$

where τ and τ' denote imaginary times, $\beta = 1/k_{\mathrm{B}}T$ with T the temperature, μ is the chemical potential and $T^{2\mathrm{B}}$ is the strength of the self-interaction. Furthermore, we included a self-energy $\hbar\Sigma(\mathbf{x}-\mathbf{x}',\tau-\tau')$ describing additional interaction effects, e.g., in the photon experiment of Klaers *et al.*, the interaction of the photons with the dye molecules [32].

To obtain an expression for the first-order correlation functions in the superfluid phase, we split the density and phase fluctuations and substitute $\phi(\mathbf{x},\tau) = \sqrt{n+\delta n(\mathbf{x},\tau)}e^{i\theta(\mathbf{x},\tau)}$. Here n is the average density of the gas, $\delta n(\mathbf{x},\tau)$ denotes the density fluctuations, and $\theta(\mathbf{x},\tau)$ represents the phase. We expand up to second order in θ and δn, and define

$$\theta(\mathbf{x},\tau) = \frac{1}{\sqrt{\hbar\beta V}}\sum_{\mathbf{k},m}\theta_{\mathbf{k},m}e^{i(\mathbf{k}\cdot\mathbf{x}-\omega_m\tau)}, \quad (3.2)$$
$$\delta n(\mathbf{x},\tau) = \frac{1}{\sqrt{\hbar\beta V}}\sum_{\mathbf{k},m}\delta n_{\mathbf{k},m}e^{i(\mathbf{k}\cdot\mathbf{x}-\omega_m\tau)},$$

to obtain

$$S[\delta n,\theta]=\frac{n}{2}\sum_{\mathbf{k},m}\left\{\hbar\Sigma^{\mathrm{s}}(\mathbf{k},i\omega_m)+2\epsilon(\mathbf{k})\right\}\theta_{\mathbf{k},m}\theta_{-\mathbf{k},-m} \tag{3.3}$$
$$+\frac{1}{8n}\sum_{\mathbf{k},m}\left\{\hbar\Sigma^{\mathrm{s}}(\mathbf{k},i\omega_m)+4n\chi^{-1}(\mathbf{k})\right\}\delta n_{\mathbf{k},m}\delta n_{-\mathbf{k},-m}$$
$$+\sum_{\mathbf{k},m}\left\{\hbar\omega_m+\frac{i}{2}\hbar\Sigma^{\mathrm{a}}(\mathbf{k},i\omega_m)\right\}\delta n_{-\mathbf{k},-m}\theta_{\mathbf{k},m}$$

with the inverse of the static density-density correlation function $\chi^{-1}(\mathbf{k})=\epsilon(\mathbf{k})/2n+T^{2\mathrm{B}}$, the single-particle dispersion $\epsilon(\mathbf{k})=\hbar^2\mathbf{k}^2/2m$ and the antisymmetric and symmetric parts of the self-energy obeying

$$\hbar\Sigma^{\mathrm{a}}(\mathbf{k},i\omega_m)=\hbar\Sigma(\mathbf{k},i\omega_m)-\hbar\Sigma(-\mathbf{k},-i\omega_m), \tag{3.4}$$
$$\hbar\Sigma^{\mathrm{s}}(\mathbf{k},i\omega_m)=\hbar\Sigma(\mathbf{k},i\omega_m)+\hbar\Sigma(-\mathbf{k},-i\omega_m).$$

Here $\hbar\Sigma(\mathbf{k},i\omega_m)$ is defined in a similar way as the Fourier transform of the phase and density fluctuations in Eq. (3.2) except for the normalization factor, which is $1/\hbar\beta V$ in this case. Furthermore, in Fourier space we take without loss of generality $\hbar\Sigma(\mathbf{0},0)=0$. For bosons this assumption is automatically satisfied for the imaginary part, and the constant real part results in a energy shift of the poles of the Green's function and can be absorbed in the chemical potential. Note that in Eq. (3.3) we substituted the zero-loop result for the chemical potential $\mu=nT^{2\mathrm{B}}$.

By using the classical equations of motion, we can now eliminate the phase $\theta_{\mathbf{k},m}$ and find an action for the density fluctuations $\delta n_{\mathbf{k},m}$ alone. From this action we obtain

$$\langle\delta n(\mathbf{x},\tau)\delta n(\mathbf{x}',\tau')\rangle= \tag{3.5}$$
$$\frac{n}{\beta V}\sum_{\mathbf{k},m}\frac{\hbar\Sigma^{\mathrm{s}}(\mathbf{k},i\omega_m)+2\epsilon(\mathbf{k})}{\mathrm{Det}[\hbar\mathbf{G}_{\mathrm{B}}^{-1}(\mathbf{k},i\omega_m)]}e^{i(\mathbf{k}\cdot(\mathbf{x}-\mathbf{x}')-\omega_m(\tau-\tau'))},$$

where the Green's function of the density and phase fluctuations has the matrix structure

$$\hbar\mathbf{G}_{\mathrm{B}}^{-1}(\mathbf{k},i\omega_m)= \tag{3.6}$$
$$\begin{bmatrix}\hbar G^{-1}(\mathbf{k},i\omega_m)-nT^{2\mathrm{B}} & -nT^{2\mathrm{B}}\\ -nT^{2\mathrm{B}} & \hbar G^{-1}(-\mathbf{k},-i\omega_m)-nT^{2\mathrm{B}}\end{bmatrix},$$

in terms of the single-particle Green's function

$$\hbar G^{-1}(\mathbf{k},i\omega_m)=i\hbar\omega_m-\epsilon(\mathbf{k})-\hbar\Sigma(\mathbf{k},i\omega_m). \tag{3.7}$$

Similarly we use the equation of motion for $\delta n_{\mathbf{k},m}$ to eliminate the density fluctuations, and we find

$$\langle\theta(\mathbf{x},\tau)\theta(\mathbf{x}',\tau')\rangle = \frac{1}{4n\beta V}\sum_{\mathbf{k},m}\frac{\hbar\Sigma^{\rm s}(\mathbf{k},i\omega_m)+2\epsilon(\mathbf{k})+4nT^{\rm 2B}}{{\rm Det}[\hbar\mathbf{G}_{\rm B}^{-1}(\mathbf{k},i\omega_m)]}e^{i(\mathbf{k}\cdot(\mathbf{x}-\mathbf{x}')-\omega_m(\tau-\tau'))}. \tag{3.8}$$

However, from Ref. [76] we know that the contribution of the phase fluctuations is proportional to the density. The first two terms are not proportional to n and they are an artifact of making an expansion up to second order in $\theta(\mathbf{x},\tau)$, and of neglecting the interaction terms between the density and phase fluctuations. A more accurate approach that takes into account higher-order terms in $\theta(\mathbf{x},\tau)$ would not contain these high-momentum contributions. Therefore, the correct expression for the phase fluctuations is given by

$$\langle\theta(\mathbf{x},\tau)\theta(\mathbf{x}',\tau')\rangle = \frac{1}{n\beta V}\sum_{\mathbf{k},m}\frac{nT^{\rm 2B}}{{\rm Det}[\hbar\mathbf{G}_{\rm B}^{-1}(\mathbf{k},i\omega_m)]}e^{i(\mathbf{k}\cdot(\mathbf{x}-\mathbf{x}')-\omega_m(\tau-\tau'))}. \tag{3.9}$$

In certain cases the self-energy is only known for real frequencies. Therefore, we define

$$\rho_\theta(\mathbf{k},\omega) = -\frac{nT^{\rm 2B}}{2\hbar}\rho_{\rm B}(\mathbf{k},\omega) := -\frac{nT^{\rm 2B}}{\pi\hbar}{\rm Im}\left[\frac{1}{{\rm Det}[\hbar\mathbf{G}_{\rm B}^{-1}(\mathbf{k},\omega^+)]}\right], \tag{3.10}$$

and we write for the phase correlation function

$$\begin{aligned}
&\langle\theta(\mathbf{x},\tau)\theta(\mathbf{x}',\tau')\rangle \\
&= \frac{\hbar}{n\hbar\beta V}\sum_{\mathbf{k},m}\int_{-\infty}^{\infty}d(\hbar\omega)\,\frac{\rho_\theta(\mathbf{k},\omega)}{i\omega_m-\omega}e^{-i\omega_m(\tau-\tau')}e^{i\mathbf{k}\cdot(\mathbf{x}-\mathbf{x}')} \\
&= -\frac{\hbar}{nV}\sum_{\mathbf{k}}\int_{-\infty}^{\infty}d(\hbar\omega)\,\rho_\theta(\mathbf{k},\omega)e^{-\omega(\tau-\tau')}e^{i\mathbf{k}\cdot(\mathbf{x}-\mathbf{x}')} \\
&\times\left\{\Theta(\tau'-\tau)N_{\rm BE}(\hbar\omega)+\Theta(\tau-\tau')(N_{\rm BE}(\hbar\omega)+1)\right\},
\end{aligned} \tag{3.11}$$

where

$$N_{\rm BE}(\hbar\omega) = \frac{1}{e^{\beta\hbar\omega}-1}, \tag{3.12}$$

is the Bose-Einstein distribution function. For simplicity we take $\tau'>\tau$, and the case $\tau'<\tau$ is treated analogously. In principle we have to consider

both the density and phase fluctuations, in order to calculate the first-order correlation functions. However, here we consider relatively high condensate fractions for which the density fluctuations are strongly suppressed and the phase fluctuations are most important, especially for the description of the long-range order which is of most interest to us here [77–80]. Hence, we have

$$\langle \phi^*(\mathbf{x},t)\phi(\mathbf{x}',t')\rangle \simeq n_0 \langle e^{-i(\theta(\mathbf{x},t)-\theta(\mathbf{x}',t'))}\rangle = n_0 e^{-\frac{1}{2}\langle[\theta(\mathbf{x},t)-\theta(\mathbf{x}',t')]^2\rangle}, \quad (3.13)$$

with n_0 the quasi-condensate density. Note that for the Gaussian approach used here, the second line of Eq. (3.13) is exact. However, in principle there are corrections to this result which can be incorporated by treating the phase of the condensate as a stochastic variable. As is shown in Ref. [74], these corrections are rather small and therefore we neglect these corrections throughout the remainder of this Chapter.

By using Eq. (3.11) and performing the analytical continuation to real time $\tau = it$, we obtain for the exponent of this expression

$$\langle[\theta(\mathbf{x},t)-\theta(\mathbf{x}',t')]^2\rangle = -\frac{T^{2\mathrm{B}}}{V}\sum_{\mathbf{k}}\int_{-\infty}^{\infty} d(\hbar\omega)\rho_{\mathrm{B}}(\mathbf{k},\omega)N_{\mathrm{BE}}(\hbar\omega) \quad (3.14)$$
$$\times\left\{1-\cos(\mathbf{k}\cdot(\mathbf{x}-\mathbf{x}'))\cos(\omega(t-t'))\right\},$$

where we used $\hbar\Sigma(\mathbf{k},\omega) = \hbar\Sigma(-\mathbf{k},\omega)$ for an isotropic system.

To make further progress, we perform a long-wavelength approximation to the self-energy. As mentioned before, the real part of the self-energy can effectively be absorbed in the chemical potential and therefore we neglect this part. The imaginary part is zero for $\mathbf{k} = \mathbf{0}$ and $\omega = 0$, and therefore for small frequencies the imaginary part is linear in ω. Since the result of Eq. (3.14) is dominated by the contributions for small frequencies, the large frequency behavior is not visible in the final result. Therefore we can safely assume that the self-energy obeys $\hbar\Sigma(\mathbf{k},\omega) = \hbar\Sigma^*(\mathbf{k},-\omega)$ for the imaginary part of both the retarded and advanced self-energy. This allows us to rewrite

$$\langle[\theta(\mathbf{x},t)-\theta(\mathbf{x}',t')]^2\rangle = -\frac{T^{2\mathrm{B}}}{V}\sum_{\mathbf{k}}\int_{0}^{\infty} d(\hbar\omega)\rho_{\mathrm{B}}(\mathbf{k},\omega) \quad (3.15)$$
$$\times\left\{1+2N_{\mathrm{BE}}(\hbar\omega)\right\}\left\{1-\cos(\mathbf{k}\cdot(\mathbf{x}-\mathbf{x}'))\cos(\omega(t-t'))\right\}.$$

This expression for the phase fluctuations contains an ultraviolet divergence. This divergence is a consequence of not taking into account the proper energy dependence of the self-interaction of the bosons. For atoms

this problem was already encountered in Ref. [76], and in that case the divergence was handled by appropriate renormalization of the interactions. In our case the form of the divergence is the same, since the self-energy must vanish for large momenta. However, we do not know the exact energy dependence of $T^{2\mathrm{B}}$. Therefore, the cancellation of the ultra-violet divergence requires us to introduce another energy scale $\gamma n T^{2\mathrm{B}}$ that models the correct energy dependence of the self-interaction of the bosons. We come back to the precise determination of γ in the next section. We thus write,

$$\langle[\theta(\mathbf{x},t)-\theta(\mathbf{x}',t')]^2\rangle = -\frac{T^{2\mathrm{B}}}{V}\sum_{\mathbf{k}}\int_0^\infty d(\hbar\omega)\rho_{\mathrm{B}}(\mathbf{k},\omega) \tag{3.16}$$
$$\times\left\{1+2N_{\mathrm{BE}}(\hbar\omega)-\frac{\hbar\omega_{\mathrm{B}}(\mathbf{k})}{\epsilon(\mathbf{k})+\gamma n T^{2\mathrm{B}}}\right\}\left\{1-\cos(\mathbf{k}\cdot(\mathbf{x}-\mathbf{x}'))\cos(\omega(t-t'))\right\},$$

with $\hbar\omega_{\mathrm{B}}(\mathbf{k})=\sqrt{\epsilon(\mathbf{k})[\epsilon(\mathbf{k})+2n_0T^{2\mathrm{B}}]}$ the Bogoliubov dispersion. The integrant in Eq. (3.16) must be positive for all $\mathbf{k}$ and all temperatures, because this term corresponds to the expectation value of $|\theta_{\mathbf{k},n}|^2$. Therefore, we have the restriction that $\gamma\geq 1$. Finally, note that this result is consistent with the expressions found in Ref. [76].

3.3 Correlation functions in the condensed phase

In the previous section we found an expression for the first-order correlation function by taking into account the phase fluctuations up to all orders. As mentioned before, the phase fluctuations are dominated by the small-frequency contributions and for bosons the imaginary part of the self-energy is linear in ω for small frequencies. Therefore, in this section we take the retarded self-energy equal to $\hbar\Sigma^+(\mathbf{k},\omega)=-i\alpha\hbar\omega$ and we investigate the effect of α on the first-order correlation functions.

3.3.1 Spatial correlations

From Eq. (3.16) we obtain that the phase fluctuations contain a contribution that is temperature dependent, and a zero-temperature part. For the equal-time phase fluctuations at zero temperature, we have

$$\langle[\theta(\mathbf{x},0)-\theta(\mathbf{0},0)]^2\rangle = -\frac{T^{2\mathrm{B}}}{V}\sum_{\mathbf{k}}\int_0^\infty d(\hbar\omega)\rho_{\mathrm{B}}(\mathbf{k},\omega) \tag{3.17}$$
$$\times\left\{1-\frac{\hbar\omega_{\mathrm{B}}(\mathbf{k})}{\epsilon(\mathbf{k})+\gamma n T^{2\mathrm{B}}}\right\}\left\{1-\cos(\mathbf{k}\cdot\mathbf{x})\right\}.$$

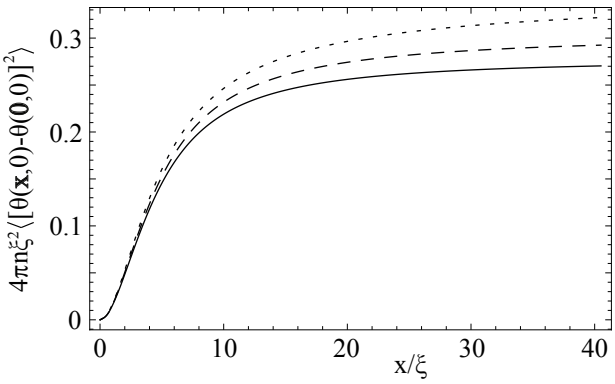

Figure 3.1: Zero-temperature part of the phase fluctuations in two dimensions for a condensate density $n \simeq 5 \cdot 10^{13}\mathrm{m}^{-2}$ and correlation length $\xi \simeq 2.8 \cdot 10^{-6}\,\mathrm{m}$. The dotted, dashed and solid curves correspond to, respectively, $\alpha = 0$, $\alpha = 5 \cdot 10^{-2}$, and $\alpha = 10^{-1}$.

Without loss of generality we have set $\mathbf{x}' = 0$ and we have put t equal to zero. Before we consider the effect of the self-energy on the spatial correlations, we investigate the effect of γ. We first consider the case without a self-energy. By writing the sum over $\mathbf{k}$ as an integral, we find in two dimensions

$$\langle[\theta(\mathbf{x},0) - \theta(\mathbf{0},0)]^2 = \int_0^\infty dk\, \frac{1 - J_0(kx)}{4\pi n\xi^2} \left\{ \frac{1}{\sqrt{k^2+1}} - \frac{2k}{2k^2+\gamma} \right\}, \quad (3.18)$$

where $J_0(kx)$ is the Bessel function of the first kind, $\xi = \hbar/[4mn_0T^{2\mathrm{B}}]^{1/2}$ is the correlation length and $x = |\mathbf{x}|$. In the limit $x \to \infty$, the Bessel function vanishes and we obtain

$$\langle[\theta(\mathbf{x},0) - \theta(\mathbf{0},0)]^2\rangle \to \frac{\log(2\gamma)}{2\pi} \frac{mT^{2\mathrm{B}}}{\hbar^2}. \quad (3.19)$$

Thus, the condensate density is given by the right-hand side of the following equation

$$\langle\phi^*(\mathbf{x},0)\phi(\mathbf{0},0)\rangle \to n_0 \exp\left\{ -\frac{\log(2\gamma)}{4\pi} \frac{mT^{2\mathrm{B}}}{\hbar^2} \right\}, \quad (3.20)$$

where we again considered the limit $\mathbf{x} \to \infty$. Therefore, by increasing γ we effectively increase the interaction strength and, thereby decrease the condensate density of the gas. This dependence can in principle be used to determine the value of γ from experiment. To determine the effect of the self-energy we here just fix γ and set it equal to 1. In Fig. 3.1 we show the

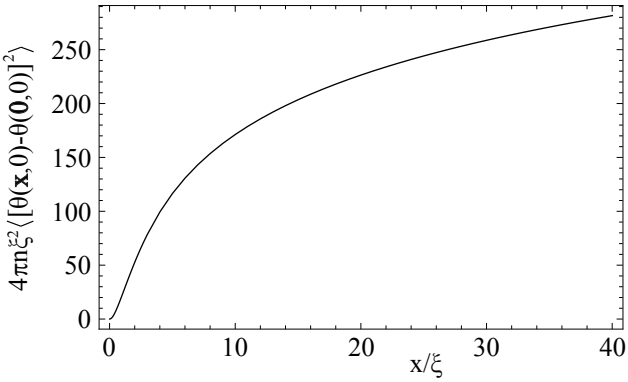

Figure 3.2: Nonzero-temperature part of the phase fluctuations in two dimensions for a condensate density $n \simeq 5 \cdot 10^{13}\mathrm{m}^{-2}$, correlation length $\xi \simeq 2.8 \cdot 10^{-6}\,\mathrm{m}$ and $\beta n_0 T^{2\mathrm{B}} \simeq 1.3 \cdot 10^{-2}$.

result for the zero-temperature part of the phase fluctuations for different values of α. If α increases, the contribution of the phase fluctuations decreases. Therefore, for increasing α we obtain that the quantum depletion of the condensate decreases.

For systems at low temperatures this is the dominating contribution. However, here we are interested in BEC at higher temperatures such as BEC of photons. For these condensates the temperature-dependent part is the most relevant contribution. The temperature-dependent part of the phase fluctuations is free of ultra-violet divergences and given by

$$\langle[\theta(\mathbf{x},0)-\theta(\mathbf{0},0)]^2\rangle = \\ -\frac{2T^{2\mathrm{B}}}{\pi}\int_0^\infty dk\,k\int_0^\infty d(\hbar\omega)\rho_{\mathrm{B}}(k,\omega)N_{\mathrm{BE}}(\hbar\omega)\left\{1-J_0(kx)\right\}. \tag{3.21}$$

We evaluate this quantity for $\beta n_0 T^{2\mathrm{B}} \simeq 1.3 \cdot 10^{-2}$. This corresponds to a typical value for BEC of photons in the regime where the density fluctuations are suppressed and we can focus on the phase fluctuations [83]. By looking at Fig. 3.2, we observe that the temperature-dependent contribution is indeed several orders of magnitude larger than the zero-temperature part. Furthermore, it turns out that the α dependence of the nonzero-temperature part is negligible.

To understand this feature, we distinguish between two different frequency regimes. Namely, $\beta\hbar\omega < 1$ and $\beta\hbar\omega > 1$. Since we are at room temperature, the latter corresponds to relatively high values of the momentum k. In the Bose-Einstein condensed phase the contributions for small momenta are dominant. Therefore, the contributions coming from $\beta\hbar\omega > 1$

are suppressed, and we can focus on the first regime.

To make analytical progress, we use $2N_{\mathrm{BE}}(\hbar\omega) \simeq 2/\beta\hbar\omega - 1$ for $\beta\hbar\omega < 1$. Furthermore, we can neglect the -1 since this is a contribution of the same order as the zero-temperature part and is therefore negligible compared to the temperature-dependent part. Hence, we obtain for the nonzero-temperature part of the phase fluctuations

$$\langle[\theta(\mathbf{x},0)-\theta(\mathbf{0},0)]^2\rangle = \\ -\frac{2T^{2\mathrm{B}}}{\pi\beta}\int_0^\infty dk\,k\int_0^\infty d(\hbar\omega)\frac{\rho_{\mathrm{B}}(k,\omega)}{\hbar\omega}\left\{1-J_0(kx)\right\}. \tag{3.22}$$

We can perform the integral over ω analytically, and we obtain

$$\langle[\theta(\mathbf{x},0)-\theta(\mathbf{0},0)]^2\rangle = \frac{T^{2\mathrm{B}}}{\pi\beta}\int_0^\infty dk\,k\frac{1-J_0(kx)}{(\hbar\omega_{\mathrm{B}}(k))^2}. \tag{3.23}$$

This expression is indeed independent of α, and this explains why the α dependence of the spatial phase fluctuations is negligible. Note that this argument is independent of the number of dimensions, and therefore also in one dimension the α dependence of the spatial correlations is negligible. For a frequency-independent damping, this independence of the spatial correlations is also encountered in exciton-polariton condensates [81].

3.3.2 Temporal correlations

To study the temporal correlation function, we define the first-order correlation function $g^{(1)}(\mathbf{x},t)$ as

$$g^{(1)}(\mathbf{x},t) := \frac{\langle\phi^*(\mathbf{x},t)\phi(\mathbf{0},0)\rangle}{\langle|\phi(\mathbf{0},0)|^2\rangle}, \tag{3.24}$$

with the temporal correlations defined as $g^{(1)}(t) = g^{(1)}(\mathbf{0},t)$. Similar to the spatial correlations, we consider the regime in which the phase fluctuations are dominant. Therefore, we can directly calculate $g^{(1)}(t)$ by using Eqs. (3.13) and (3.16), where we again consider $\beta n_0 T^{2\mathrm{B}} \simeq 1.3\cdot 10^{-2}$. In Fig. 3.3 we show $g^{(1)}(t)$ in two dimensions for several values of α. As can be seen from the figure, $g^{(1)}(t)$ increases for increasing α. Furthermore, we find the same qualitative behavior in one dimension. Thus as opposed to the spatial correlations, the finite-lifetime effects are important for the temporal correlations.

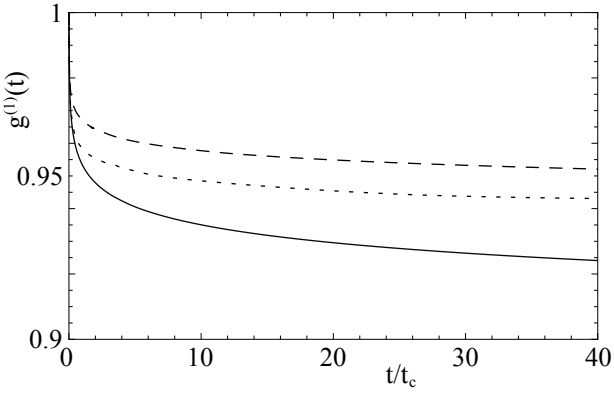

Figure 3.3: Normalized first-order correlation function $g^{(1)}(t)$ for a two-dimensional Bose-Einstein condensate as a function of t/t_c, with $t_c = \hbar(n_0 T^{2B}\sqrt{\beta})^{-2} \simeq 1.5 \cdot 10^{-10}$ s. Here $\beta n_0 T^{2B} \simeq 1.3 \cdot 10^{-2}$ and the dashed, dotted, and solid curves are for, respectively, $\alpha = 10^{-1}$, $\alpha = 10^{-2}$, and $\alpha = 0$.

3.4 Photons

In the previous section we gave a general discussion on finite-lifetime effects on correlation functions of bosons in the Bose-Einstein condensed phase. In this section we will focus on a specific example of such a system, namely, BEC of photons [32]. Since this system is two-dimensional and of finite size due to the presence of a trap for the photons, we first investigate whether the photons form a quasi-condensate or a true condensate.

3.4.1 One-particle density matrix

To determine whether the photons form a quasi-condensate or a true condensate, we need to calculate the off-diagonal long-range behavior of the one-particle density matrix, and compare the size of the condensate with the distance over which the one-particle density matrix falls off. In particular, if the size of the condensate is smaller than the distance over which the one-particle density matrix reduces to, say, half of the maximum value, we have a true condensate. Otherwise, we are in the quasi-condensate regime. Furthermore, we consider the regime where the density fluctuations are suppressed and therefore we have large condensate fractions. Therefore we are allowed to use the Thomas-Fermi approximation, and we obtain for the number of condensed photons

$$N_0 = \frac{2\pi}{T^{2B}} \int_0^{R_{TF}} dr\, r \left(\mu - \frac{1}{2} m\Omega^2 r^2 \right), \tag{3.25}$$

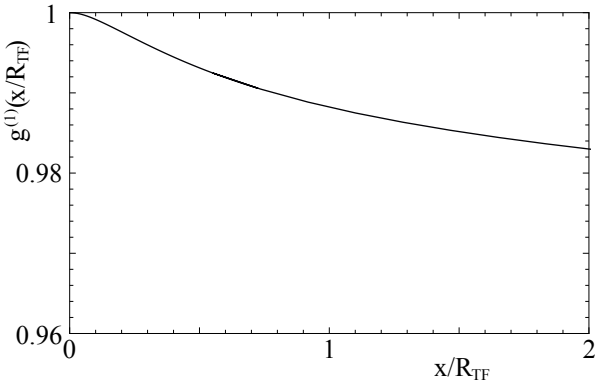

Figure 3.4: Normalized first-order correlation function $g^{(1)}(x/R_{\mathrm{TF}})$ for the Bose-Einstein condensate of photons for the condensate fraction $N_0/N = 0.2$.

where the Thomas-Fermi radius $R_{\mathrm{TF}} = \sqrt{2\mu/m\Omega^2}$ is the size of the condensate and Ω is the frequency of the isotropic harmonic trap. Note that the constant energy mc^2, with c the speed of the photons in the medium, is absorbed in the definition of the chemical potential μ. Furthermore, N_0 can be related to the total number of photons N according to [43]

$$N_0 = N - \frac{\pi^2}{3}\left(\frac{k_{\mathrm{B}}T}{\hbar\Omega}\right)^2. \tag{3.26}$$

By performing the integral in Eq. (3.25), we can relate the chemical potential to the total number of photons in our system. This then implies

$$R_{\mathrm{TF}} = \left(\frac{4T^{2\mathrm{B}}N_0}{\pi m\Omega^2}\right)^{1/4}. \tag{3.27}$$

Furthermore, for the density of condensed photons n_0 we take the density in the center of the trap. Hence,

$$n_0 = \sqrt{\frac{m\Omega^2 N_0}{\pi T^{2\mathrm{B}}}}. \tag{3.28}$$

Experimentally, the relevant parameter is the condensate fraction N_0/N. Therefore given a condensate fraction, we use Eq. (3.26) to determine N_0 and with this value we obtain the size and density of the condensate via Eqs. (3.27) and (3.28). Furthermore, we use Ref. [32] to obtain numerical values for the parameters m, Ω and $T^{2\mathrm{B}}$.

In Fig. 3.4 we show a plot of the normalized first-order spatial correlation function $g^{(1)}(x/R_{\mathrm{TF}}) = g^{(1)}(x/R_{\mathrm{TF}}, 0)$ as defined in Eq. (3.24) for

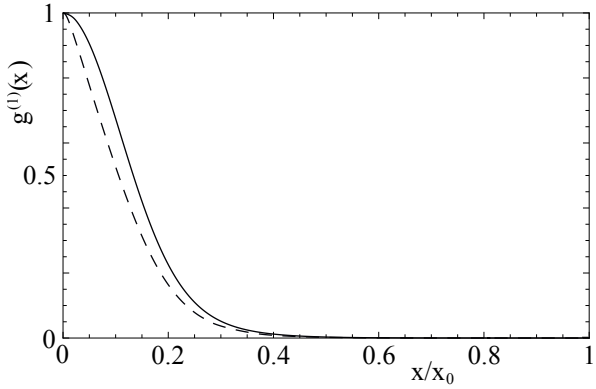

Figure 3.5: Normalized first-order correlation function $g^{(1)}(x)$ of the photons in the normal state for $\mu = 0.99\mu_c$ as a function of x/x_0, where $x_0 = \hbar\beta c \simeq 6{\cdot}10^{-6}$ m. The solid curve is the result without taking into account the molecules, and the dashed curve corresponds to a molecular density $n_m = 4.5 \cdot 10^{24}\,\mathrm{m}^{-3}$.

a condensate fraction of 20 %. From this plot it is clear that the phase correlation function $g^{(1)}(\mathbf{x})$ hardly drops over the condensate size, and that the photons form a true condensate. Note that this conclusion is also valid for a homogeneous system with the same central density and confined to a square with size R_{TF}. Furthermore, in Ref. [82] it is shown that at large length scales, in the regime of Kosterlitz-Thouless physics, isotropic systems undergo a Kardar-Parisi-Zhang (KPZ) crossover. Since these length scales are even larger than the length scales for Kosterlitz-Thouless physics, this KPZ regime is not accessible with the present set up.

In principle we should also include the harmonic trap in the calculation for $g^{(1)}(x/R_{TF})$. As shown in Ref. [76], in this case the phase fluctuations correlation function can also be found by solving the Bogoliubov-de Gennes equations. However, the thermal energy $k_B T$ is roughly two orders of magnitude larger than the energy splitting $\hbar\Omega$ of the harmonic potential $V^{ex}(\mathbf{x})$. Therefore, incorporation of the harmonic potential is only a small correction and since for the homogeneous calculation we are already far in the true condensate regime, this correction will not influence our conclusion.

3.4.2 Normal state

Apart from the Bose-Einstein condensed phase, the photons can also be in the normal state. Since in this case not only the small frequency behavior of the self-energy is important, the details of the system of interest should also be included and we need the exact expression for the self-energy. Therefore, we use the explicit expression for the self-energy as given in Ref. [75]. In

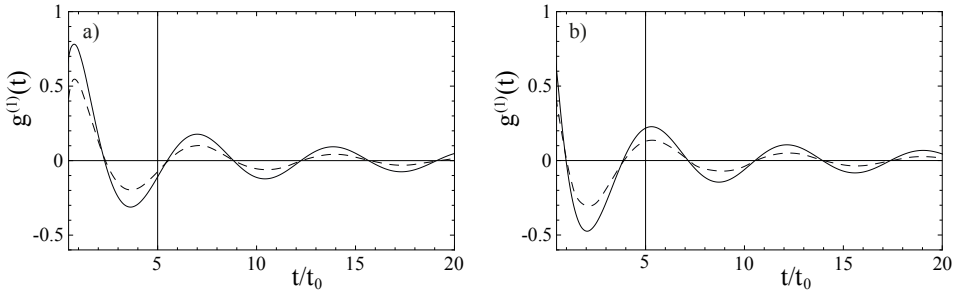

Figure 3.6: a) Real and b) imaginary parts of the normalized first-order temporal correlation function $g^{(1)}(t)$ for the photons in the normal state for $\mu = 0.99\mu_{\rm c}$ as a function of t/t_0 with $t_0 = \beta\hbar \simeq 2.5 \cdot 10^{-14}\,{\rm s}$. For the solid curve we omitted the effect of the molecules and the dashed curve corresponds to the molecular density $n_{\rm m} = 4.5 \cdot 10^{24}\,{\rm m}^{-3}$.

the normal state we write for the first-order correlation function

$$\langle \phi^*(\mathbf{x},\tau)\phi(\mathbf{0},0)\rangle = \frac{1}{\hbar\beta V}\sum_{\mathbf{k},n} G(\mathbf{k},i\omega_n)e^{i(\omega_n\tau-\mathbf{k}\cdot\mathbf{x})}, \tag{3.29}$$

where

$$G(\mathbf{k},i\omega_n) = \frac{-\hbar}{-i\hbar\omega_n + \epsilon(\mathbf{k}) - \mu + \hbar\Sigma(\mathbf{k},i\omega_n)}. \tag{3.30}$$

Note that in this calculation we neglect the self-interaction of the photons, since we are primarily interested in the effect of the imaginary part of the self-energy. Furthermore, for the same reasons as mentioned before, we neglect the harmonic potential $V^{\rm ex}(\mathbf{x})$ which in the local-density approximation can be incorporated by the replacement $\mu(\mathbf{x}) = \mu - V^{\rm ex}(\mathbf{x})$. By defining

$$\rho(\mathbf{k},\omega) := \frac{1}{\pi\hbar}{\rm Im}\left[G(\mathbf{k},\omega^+)\right], \tag{3.31}$$

we write

$$\langle \phi^*(\mathbf{x},t)\phi(\mathbf{0},0)\rangle = \frac{1}{2\pi}\int dk \int d(\hbar\omega)\, k\, \rho(\mathbf{k},\omega)N_{\rm BE}(\hbar\omega)J_0(kx)e^{i\omega t}, \tag{3.32}$$

where $J_0(kx)$ is the Bessel function of the first kind, $N_{\rm BE}(\hbar\omega)$ is the Bose-Einstein distribution function as defined in Eq. (3.12) and $x = |\mathbf{x}|$.

We study the spatial and temporal correlation functions $g^{(1)}(t)$ and $g^{(1)}(x)$ separately. In general we are interested in the regime where we are close to condensation, and therefore we take $\mu \simeq 0.99\mu_{\rm c}$. Furthermore, we

take the parameters as in the experiment of Ref. [32]. It turns out that for the densities used in these experiments the effect of the molecules is small. To demonstrate the effect of the dye molecules we take $n_{\mathrm{m}} = 4.5 \cdot 10^{24}\,\mathrm{m}^{-3}$. In general high molecular densities can spoil the thermalization of the photons, but this value should be within the regime in which the photons can still thermalize.

As can be seen in Fig. 3.5, the normalized spatial correlation function $g^{(1)}(x)$ is lowered by the effect of the molecules. The normalized first-order temporal correlation $g^{(1)}(t)$ consists of an imaginary and a real part, which we show separately in Figs. 3.6. For both parts the amplitude of the oscillations are decreased by the interaction with the molecules. Here, we used correlation functions in terms of creation and annihilation operators. In experiments one measures the correlation between the electric field at different times and positions, and therefore experimentally only the real part is relevant.

3.5 Conclusion and outlook

In this Chapter we investigated energy-dependent finite-lifetime effects, characterized by the dimensionless parameter α, on the first-order correlation functions. By taking into account the phase fluctuations up to all orders, we derived an explicit expression for the first-order correlation functions in the Bose-Einstein condensed phase for high condensate fractions. We showed that the value of α does not influence the spatial correlations, but it enhances the temporal correlation function.

Subsequently, we focused on BEC of photons under the relevant experimental conditions and we showed that the phase of the condensate is coherent over length scales larger than the size of the condensate. Therefore, the photons form a true condensate. Finally, we calculated the normalized first-order correlation functions of the photons in the normal state and we showed that the spatial and temporal correlations are both suppressed by the interaction with the dye molecules.

For future research it would be interesting to investigate the regime with smaller condensate fractions. Here the density fluctuations are important and they also have to be incorporated in the formalism. For BEC of photons this regime is also accessible experimentally [83], and in this case the effect of the interaction with the dye molecules can be different from the case with high condensate fractions.

Chapter 4

Number fluctuations

We investigate the effect of interactions on condensate-number fluctuations in Bose-Einstein condensates. For a contact interaction we variationally obtain the equilibrium probability distribution for the number of particles in the condensate. To facilitate comparison with experiment, we also calculate the zero-time delay autocorrelation function $g^{(2)}(0)$ for different strengths of the interaction. Thereafter, we focus on the case of a Bose-Einstein condensate of photons and find good agreement with recent experiments. Finally, we discuss possible photon-photon interaction in the Bose-Einstein condensate of light.[1]

4.1 Introduction

Fluctuations are ubiquitous in physics: from the primordial quantum fluctuations in the early universe that reveal themselves as fluctuations in the cosmic microwave background, to current fluctuations in every-day conductors. For large voltages, the latter fluctuations give rise to shot noise, that is due to the discrete nature of charge [84]. As a consequence, shot noise can be used to determine the quanta of the electric charge of the current carriers in conducting materials [85]. Indeed, it has been used to characterize the nature of Cooper pairs in superconductors [86] and the fractional charge of the quasiparticles of the quantum Hall effect [87]. For low voltages, the noise in the current is thermal and is called Johnson-Nyquist noise [88, 89]. Contrary to shot noise, this thermal noise is always present in electrical circuits, even if no externally applied voltage is present, since it is due to

[1] This Chapter is directly based on *Interaction Effects on Number Fluctuations in a Bose-Einstein Condensate of Light*, E.C.I. van der Wurff, A.-W. de Leeuw, R.A. Duine, and H.T.C. Stoof, Phys. Rev. Lett. **113**, 135301 (2014). The content of this Chapter is also part of the Master's thesis of E.C.I. van der Wurff, who was supervised by A.-W. de Leeuw, R.A. Duine and H.T.C. Stoof.

thermal agitation of charge carriers, that leads to fluctuating electromotive forces in the material.

Theoretically, fluctuations in equilibrium are described by the fluctuation-dissipation theorem, as formulated by Nyquist in 1928 and proven decades later [90]. This theorem relates the response of a system to an external perturbation to the fluctuations in the system in the absence of that perturbation. Given a certain fluctuation spectrum we can reconstruct the response of the system. Therefore, this theorem is very powerful, as was fervently argued by the Japanese physicist Kubo [91].

Having stressed the importance of fluctuations in physics and the information they contain, we now zoom in on condensate-number fluctuations as our main point of interest. Traditionally, weakly interacting Bose-Einstein condensates were first observed in dilute atomic vapors [3]. For these systems, it is very difficult to measure number fluctuations because typically number measurements are destructive. Therefore, theoretical work has focused more on density-density correlation functions [92, 93].

In recent years, Bose-Einstein condensates of quasiparticles have also been created, such as exciton-polariton condensates [30], magnon condensates [29] and condensates of photons [32, 94]. These condensates of quasiparticles are realized under different circumstances compared to the atomic condensates. For instance, these condensates are created at higher temperatures than the condensates of dilute atomic gases: from several kelvin for the exciton-polariton condensate to room temperature for the photonic condensate. Additionally, the condensates of quasiparticles are not in true equilibrium, since the steady state is a dynamical balance between particle losses and particle gain by external pumping with a laser. Due to these differences, new experimental possibilities have opened up. For example, large number fluctuations of the order of the total particle number have been observed in a condensate of photons [83].

In this Chapter we investigate number fluctuations in Bose-Einstein condensates. We start by introducing an effective contact interaction into the grand-canonical Hamiltonian of a Bose gas and derive an equilibrium probability distribution for the number of particles in the condensate. Subsequently, we investigate these distributions for different condensate fractions and interaction strengths. We also calculate the zero-time delay autocorrelation function $g^{(2)}(0)$ to quantify the number fluctuations. In this manner we are able to reproduce all experimental curves of Schmitt *et al.* [83] by using the interaction strength as a single fitting parameter. Having provided this interpretation of the experimental results, we finally discuss possible mechanisms for the interactions in a condensate of light.

4.2 Probability distribution

We consider a harmonically trapped Bose gas with a fixed number of particles. Because the condensates of quasiparticles are typically confined in one direction, we specialize to the case of two dimensions. However, the following treatment is completely general and can easily be generalized to higher or lower dimensions.

To investigate the number fluctuations, we first calculate the average number of particles $\langle N_0 \rangle$ in the condensate. Because the condensates of quasiparticles allow for a free exchange of bosons with an external medium we treat the system in the grand-canonical ensemble: the probability distribution $P(N_0)$ for the number of condensed particles is of the form $P(N_0) \propto \exp\{-\beta\Omega(N_0)\}$, with $\Omega(N_0)$ the grand potential of the gas of bosons.

To find the grand potential we use a variational wave function approach. We note that the bosons in the condensate typically interact with each other. A reasonable first approximation for the form of this interaction is a contact interaction, as essentially every interaction is renormalized to a contact interaction at long length and time scales, independent of the precise origin of the interactions. Therefore, we consider the following energy functional for the macroscopic wave function $\phi_0(\mathbf{x})$ of the Bose-Einstein condensate [59]

$$\Omega[\phi_0] = \int d\mathbf{x} \left[\frac{\hbar^2}{2m} |\nabla\phi_0(\mathbf{x})|^2 + \left(V(\mathbf{x}) - \mu + \frac{g}{2} |\phi_0(\mathbf{x})|^2 \right) |\phi_0(\mathbf{x})|^2 \right], \quad (4.1)$$

where $\mathbf{x}$ is the two-dimensional position, the first term represents the kinetic energy of the condensate, $V(\mathbf{x}) = m\omega^2|\mathbf{x}|^2/2$ is the harmonic trapping potential, μ is the chemical potential for the particles and g is the coupling constant of the effective pointlike interaction between the particles.

We use the Bogoliubov substitution $\phi_0(\mathbf{x}) = \sqrt{N_0}\psi_q(\mathbf{x})$, with the normalized variational wave function $\psi_q(\mathbf{x})$, such that $\int d\mathbf{x}\, |\phi_0(\mathbf{x})|^2 = N_0$. Subsequently, we minimize the energy as a function of the variational parameter q, which describes the width of the condensate. As a variational ansatz we take the wave function to be the Gaussian

$$\psi_q(\mathbf{x}) = (\sqrt{\pi}q)^{-1} \exp\{-|\mathbf{x}|^2/2q^2\}. \quad (4.2)$$

Substituting this into the energy given by Eq. (4.1) and minimizing with respect to the variational parameter, we obtain

$$q_{\min} = \sqrt[4]{\frac{2\pi\hbar^2 + mN_0g}{2\pi\omega^2m^2}} = q_{\mathrm{ho}} \sqrt[4]{1 + \frac{\tilde{g}N_0}{2\pi}}, \quad (4.3)$$

where we introduced the dimensionless coupling constant $\tilde{g} := mg/\hbar^2$ and the harmonic oscillator length $q_{\rm ho} = \sqrt{\hbar/m\omega}$. Note that for a sufficiently small number of condensate particles $q_{\rm min}$ reduces to $q_{\rm ho}$. For a large number of condensate particles the Thomas-Fermi ansatz for the wave function is in principle more appropriate. However, it is well known from the atomic condensates that even in this case the Gaussian approach is rather accurate [95].

We now substitute the minimal value for the variational parameter q into the energy functional, yielding the probability distribution

$$P(N_0) \propto \exp\left\{\beta N_0 \left(\mu - \hbar\omega\sqrt{1+\frac{\tilde{g}N_0}{2\pi}}\right)\right\}, \tag{4.4}$$

where the normalization is $\int_0^\infty dN_0\, P(N_0) = 1$.

Experimentally, the relevant parameter is the condensate fraction $x := \langle N_0\rangle/\langle N\rangle$, with N the total number of particles. Thus, to relate our results to the experiments we need a relation between $\langle N_0\rangle$ and the average total number of particles. For temperatures T below the critical temperature for Bose-Einstein condensation, the average number of particles in excited states can in a good approximation be determined from the ideal-gas result. We obtain

$$\langle N_{\rm ex}(T)\rangle = \int_0^\infty \frac{g(\epsilon)d\epsilon}{\exp\{\epsilon/k_BT\}-1} = \frac{N_s}{6}\left(\frac{\pi k_BT}{\hbar\omega}\right)^2, \tag{4.5}$$

where we used the density of states $g(\epsilon) = N_s\epsilon/(\hbar\omega)^2$ for a two-dimensional harmonic trapping potential [43]. The integer N_s denotes the number of spin components of the boson. The critical temperature T_c is defined by $\langle N\rangle = \langle N_{\rm ex}(T_c)\rangle$. With this criterion, we find

$$\langle N_0\rangle = \frac{xN_s}{6(1-x)}\left(\frac{\pi k_BT}{\hbar\omega}\right)^2. \tag{4.6}$$

4.3 Results

Given an interaction strength $\tilde{g}$, we use the normalized probability distribution in Eq. (4.4) to calculate the chemical potential as a function of $\langle N_0\rangle$, i.e. $\mu = \mu(\langle N_0\rangle)$. Given a condensate fraction x, we then use Eq. (4.6) to calculate $\langle N_0\rangle$ and the corresponding μ. As an example we take $N_s = 2$, which is appropriate for the Bose-Einstein condensate of photons [32,83,94]. Finally, we use the obtained chemical potential to plot the probability distribution at fixed x and $\tilde{g}$. Typical plots of the probability distribution for different

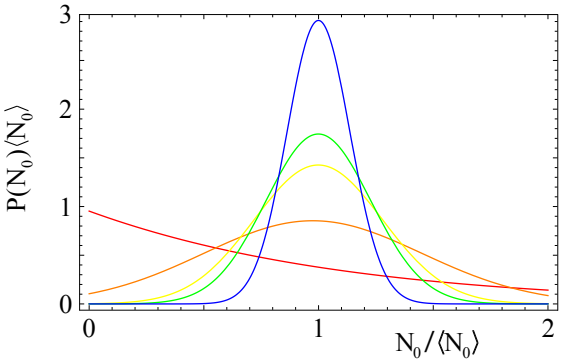

Figure 4.1: Probability distribution for two-component bosons for a fixed interaction strength $\tilde{g} = 5 \cdot 10^{-6}$ and different condensate fractions $x_{\text{red}} = 0.04$, $x_{\text{orange}} = 0.28$, $x_{\text{yellow}} = 0.40$, $x_{\text{green}} = 0.45$, and $x_{\text{blue}} = 0.58$.

condensate fractions are displayed in Fig. 4.1. Clearly, we have exponential behavior due to a Poissonian process for small condensate fractions and Gaussian behavior for larger condensate fractions. Physically, this shows that the effect of repulsive interactions is to reduce number fluctuations, as the interactions give fluctuations an energy penalty. Increasing the interaction strength yields Gaussian behavior for even smaller condensate fractions. These Gaussians are also more strongly peaked around $\langle N_0 \rangle$ for higher interaction strengths, which is expected since stronger interactions between the bosons leads to the supression of fluctuations.

Next, we obtain the second moment $\langle N_0^2 \rangle$ from the probability distribution $P(N_0)$. This gives us all the information needed to quantify the number fluctuations of the condensate. The time-averaged second-order correlation function of the light intensity is given by

$$g^{(2)}(\tau) := \langle I(t)I(t+\tau)\rangle / \langle I(t)\rangle\langle I(t+\tau)\rangle, \tag{4.7}$$

where τ is the time difference in the arrival of two beams of photons on the detectors in a Hanbury-Brown and Twiss experiment and $I(t)$ represents the intensity of those beams at time t. In fact, the corresponding zero-time delay autocorrelation function is given by

$$g^{(2)}(0) = \frac{\langle N_0^2 \rangle}{\langle N_0 \rangle^2}. \tag{4.8}$$

A plot of $g^{(2)}(0)$ against the condensate fraction is displayed in Fig. 4.2 for different interaction strengths $\tilde{g}$. We note that bunching of bosons takes place for all interactions at small condensate fractions. Theoretically, we

know that for thermal photons $g^{(2)}(0) = 2$ [96], which is exactly what we observe in our plots for the corresponding case $x = 0$. For larger condensate fractions $g^{(2)}(0) \to 1$. The interpretation is as follows. Suppose we fix the condensate fraction x. At small interactions the quartic term in the energy in Eq. (4.1) is small and the minima of the energy are small and broad, yielding large number fluctuations. If we increase the interaction, the minima become deeper and more narrow, effectively reducing the fluctuations. The same reasoning holds for a fixed interaction strength and increasing condensate fractions, as we can also see in Fig. 4.1.

4.4 Comparison with experiment

The results in the previous sections were quite generic for a two-dimensional, harmonically trapped gas of bosons with two possible polarizations. In fact, measurements of $g^{(2)}(0)$ have been performed recently [83] in a Bose-Einstein condensate of photons, enabling us to compare our theory with experiments. In this experiment photons are confined in a dye-filled cavity, providing a harmonic potential and giving the photons an effective mass m by fixing their longitudinal momentum k_z [32]. The photons thermalize to the temperature of the dye solution by scattering of the dye molecules. Additionally, photon losses from the cavity are compensated by external pumping, yielding a constant average number of photons.

In Fig. 4.2 we plot the experimental data points of Ref. [83]. We are able to reproduce all data sets by tuning the interaction parameter $\tilde{g}$. Unfortunately, only one experimental value for $\tilde{g}$ is known. By measuring the size of the condensate for different condensate fractions, it was experimentally found that $\tilde{g} = (7 \pm 3) \cdot 10^{-4}$ [32], which only differs a factor of two with our result for the purple curve $g_{\text{purple}} = 2 \cdot 10^{-4}$. However, we note that the trapping potential, concentration of dye molecules and effective photon mass were somewhat different for the purple data points and the measurement of the interaction strength. We expect the interaction strength to vary smoothly with variations in the experimental parameters. Hence the agreement is remarkable and points to the important role of interactions on number fluctuations in these experiments.

The data points in Fig. 4.2 were obtained for different dye molecule densities n_{mol} and detunings δ, which is roughly the difference between the cavity frequency and a dye specific frequency related to the effective absorption threshold of the dye molecules. Within our theory, the dependence of number fluctuations on these parameters can be incorporated via their influence on the interactions. Therefore, it would be useful to perform

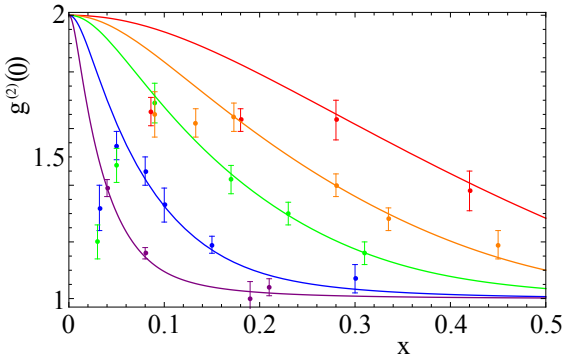

Figure 4.2: Zero-time delay autocorrelation function $g^{(2)}(0)$ against the condensate fraction x for $\omega = 8\pi \cdot 10^{10}$ Hz and $T = 300$ K. The different curves correspond to different interaction strengths: $\tilde{g}_{\text{red}} = 5 \cdot 10^{-7}$, $\tilde{g}_{\text{orange}} = 2 \cdot 10^{-6}$, $\tilde{g}_{\text{green}} = 5 \cdot 10^{-6}$, $\tilde{g}_{\text{blue}} = 3 \cdot 10^{-5}$, $\tilde{g}_{\text{purple}} = 2 \cdot 10^{-4}$. All curves are compared to the included experimental points from Schmitt *et al.* [83]. The experimental results for small condensate fraction x are unreliable due to systematic measurement errors. Indeed, theoretically we have $\lim_{x \to 0} g^{(2)}(0) = 2$.

systematic measurements of $\tilde{g}$ for different detunings and molecule concentrations, as is also proposed in Ref. [40]. With this information, we would be able to directly compare all experimental results with our theoretical predictions for the number fluctuations.

4.5 Photon-photon interaction

The question remains what mechanism can cause an interaction that depends on both n_{mol} and the detuning δ. It has been suggested that the interaction is caused by slight changes in the refractive index of the solution as a function of either temperature or the intensity of the photons [40]. The former phenomenon is known as thermal lensing, whereas the latter is known as a Kerr-type nonlinearity. We now focus on both effects separately and estimate the strength of the resulting interactions.

4.5.1 Thermal lensing

Thermal lensing is the phenomenon that the index of refraction n depends on the temperature of the medium. In the experiment of interest to us, non-radiative decay of the dye molecules, local fluctuations in the photon number and the external pumping with a laser lead to temperature fluctuations around the average temperature T_0. As the photon energy depends

on the index of refraction, these temperature fluctuations couple to the photons.

We now consider the following action in imaginary time for the photon field $\phi(\mathbf{r},\tau)$ and temperature fluctuation field $\delta T(\mathbf{r},\tau)$

$$S = \int d\mathbf{r} \int d\tau \left[\frac{\delta T(\mathbf{r},\tau)}{2T_0}\left(c_p + \frac{\kappa\nabla^2}{i\partial_\tau}\right)\delta T(\mathbf{r},\tau)\right] \tag{4.9}$$
$$+ \int d\mathbf{r} \int d\tau \left[\phi^*(\mathbf{r},\tau)\left(\hbar\frac{\partial}{\partial\tau} - \frac{\hbar^2\nabla_{\mathbf{x}}^2}{2m} - \frac{mc^2}{n^2} + \frac{1}{2}m\omega^2|\mathbf{x}|^2 - \mu\right)\phi(\mathbf{r},\tau)\right],$$

where $\mathbf{r} = (x, y, z)$ is a three-dimensional vector, $\nabla_{\mathbf{x}}^2$ denotes that we only consider motion in the transversal direction, c_p is the heat capacity and κ the thermal conductivity. The part which is quadratic in the temperature fluctuations is constructed such that it has the correct diffusive pole and diffusion propagator.

We now assume that the temperature fluctuations are small, and we write for the index of refraction $n(T) = n(T_0) + \alpha\delta T(\mathbf{r},\tau)$. Substituting this into the action and expanding for small temperature fluctuations, we obtain

$$\begin{aligned} S &:= S_{\text{temp}} + S_{\text{coup}} + S_{\text{ph}} \\ &= \int d\mathbf{r} \int d\tau \left[\frac{\delta T(\mathbf{r},\tau)}{2T_0}\left(c_p + \frac{\kappa\nabla^2}{i\partial_\tau}\right)\delta T(\mathbf{r},\tau)\right] \\ &+ \int d\mathbf{r} \int d\tau \left[\frac{2mc^2\alpha}{n^3(T_0)}\delta T(\mathbf{r},\tau)\phi^*(\mathbf{r},\tau)\phi(\mathbf{r},\tau)\right] \\ &+ \int d\mathbf{r} \int d\tau \left[\phi^*(\mathbf{r},\tau)\left(\hbar\frac{\partial}{\partial\tau} - \frac{\hbar^2\nabla_{\mathbf{x}}^2}{2m} + \frac{1}{2}m\omega^2|\mathbf{x}|^2 - \mu'\right)\phi(\mathbf{r},\tau)\right], \end{aligned} \tag{4.10}$$

where we shifted away the constant offset in the energy by setting $\mu' = \mu + mc^2/n^2(T_0)$. Since we want to describe thermal lensing, we can ignore S_{ph} and from now on we focus on the first two terms of Eq. (4.10).

To find the effective photon-photon interaction, it is more confinient to work in Fourier space. Therefore, we define the Fourier transforms as

$$\begin{aligned} \phi(\mathbf{r},\tau) &= \frac{1}{\sqrt{\hbar\beta V}}\sum_{\mathbf{p},n} a_{\mathbf{p},n} e^{i(\mathbf{p}\cdot\mathbf{r}-\omega_n\tau)}, \\ \delta T(\mathbf{r},\tau) &= \frac{1}{\sqrt{\hbar\beta V}}\sum_{\mathbf{p},n} \delta T_{\mathbf{p},n} e^{i(\mathbf{p}\cdot\mathbf{r}-\omega_n\tau)}. \end{aligned} \tag{4.11}$$

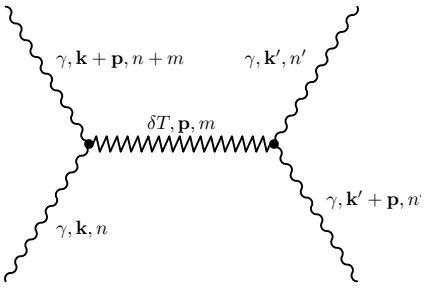

Figure 4.3: Feynman diagram for the photon-photon interaction due to the diffusion of temperature fluctuations.

By substituting this into S_{temp} and S_{coup}, we find

$$S = \sum_{\mathbf{p},n} \delta T^*_{\mathbf{p},n}(-\hbar G_T^{-1}(\mathbf{p}, i\omega_n))\delta T_{\mathbf{p},n} \tag{4.12}$$
$$+ \frac{1}{\sqrt{\hbar\beta V}}\left(\frac{mc^2\alpha}{n^3(T_0)}\right)\sum_{\substack{n,m,\\ \mathbf{k},\mathbf{p}}}\left(a^*_{\mathbf{k}+\mathbf{p},m+n}a_{\mathbf{k},n}\delta T_{\mathbf{p},m} + a^*_{\mathbf{k},n}a_{\mathbf{k}+\mathbf{p},m+n}\delta T^*_{\mathbf{p},m}\right),$$

where we used $\delta T^*_{\mathbf{p},n} = \delta T_{-\mathbf{p},-n}$. In the process we defined the inverse propagator in Fourier space for the temperature fluctuations

$$-\hbar G_T^{-1}(\mathbf{p}, \omega_n) = \frac{1}{T_0}\left(c_p - \frac{\kappa|\mathbf{p}|^2}{\omega_n}\right). \tag{4.13}$$

Subsequently, we complete the square, perform the Gaussian path integral over the temperature fluctuations $\delta T_{\mathbf{p},n}$, and re-exponentiate to arrive at the effective action

$$S = -\hbar\text{Tr}\log\left[-G_T^{-1}(\mathbf{p}, \omega_n)\right] \tag{4.14}$$
$$-\frac{1}{\hbar^2\beta V}\left(\frac{mc^2\alpha}{n^3(T_0)}\right)^2\sum_{\mathbf{k},\mathbf{k}',\mathbf{p}}\sum_{n,n',m} a^*_{\mathbf{k}+\mathbf{p},n+m}a_{\mathbf{k},n}a^*_{\mathbf{k}',n'}a_{\mathbf{k}'+\mathbf{p},n'+m}G_T(\mathbf{p}, \omega_m).$$

The last term is depicted as a Feynman diagram in Fig. 4.3. From the effective action we read off the photon-photon four-point vertex

$$\Gamma^{(4)}(\mathbf{p}, m) = -\frac{2}{\hbar}G_T(\mathbf{p}, \omega_m)\left(\frac{mc^2\alpha}{n^3(T_0)}\right)^2. \tag{4.15}$$

Because the photon gas is confined to two dimensions this is not the photon-photon interaction of the condensed photons. However, we can obtain this

interaction by using the fact that the longitudinal part decouples from transversal part of the photon field. Therefore, we define

$$\phi_{\text{long}}(z) = \sqrt{2/D_0}\sin(q\pi z/D_0), \tag{4.16}$$

with D_0 the length of the cavity in the longitudinal direction and $q = 7, 8$ the fixed longitudinal wavenumber of the photons. Thus, the photon-photon interaction in the two-dimensional photon gas is

$$\Gamma^{(4)}(\mathbf{p}, m) \to \left(\int_0^{D_0} |\phi_{\text{long}}(z)|^4\, dz\right)\Gamma^{(4)}(\mathbf{p}, m) = \frac{2\Gamma^{(4)}(\mathbf{p}, m)}{3D_0}. \tag{4.17}$$

Moreover, taking the photons in the condensate amounts to setting the Matsubara frequency equal to zero and only taking a nonzero momentum of k_z in the z-direction. Hence, we obtain

$$\tilde{g} = \frac{2\Gamma^{(4)}(\mathbf{0}, 0)m}{3\hbar^2 D_0} = \frac{4m^3c^4\alpha^2 T_0}{3D_0\hbar^2 n^6(T_0)c_p}. \tag{4.18}$$

Typical values for the experimental parameters are: $m = 6.7 \cdot 10^{-36}$ kg, $T_0 = 300$ K, $D_0 = 1.46 \cdot 10^{-6}$ m [32], $n = 1.34$, $\alpha = -5 \cdot 10^{-4}$ K^{-1} [97], $c_p = \tilde{c}_p/V_m$ with $\tilde{c}_p = 79.5$ J mol^{-1} K^{-1} and $V_m = 40.0 \cdot 10^{-6}$ m^3 mol^{-1} [98]. These values yield an estimate for the interaction strength of $\tilde{g} \sim 10^{-9}$.

4.5.2 Dye-mediated photon-photon scattering

We now neglect the temperature depence of the index of refraction and focus on dye-mediated photon-photon scattering. We therefore consider an model which includes the interactions between the photons and dye that is modeled as a two-level model. Therefore, we use a similar model as already encountered in Eq. (2.2) of Chapter 2, and we consider the Euclidean action

$$\begin{aligned} S = &\sum_{\mathbf{k},n} a^*_{\mathbf{k},n} G^{-1}(\mathbf{k}, i\omega_n) a_{\mathbf{k},n} + + \sum_{\mathbf{p},\rho,n} b^*_{\mathbf{p},\rho,n} G^{-1}_\rho(\mathbf{p}, i\omega_n) b_{\mathbf{p},\rho,n} \\ &+ \frac{g_{\text{mol}}}{\sqrt{\hbar\beta V}} \sum_{\mathbf{k},\mathbf{p},n,n'} \left(a_{\mathbf{k},n} b_{\mathbf{p},\downarrow,n'} b^*_{\mathbf{p}+\mathbf{k},\uparrow,n+n'} + a^*_{\mathbf{k},n} b_{\mathbf{p}+\mathbf{k},\uparrow,n+n'} b^*_{\mathbf{p},\downarrow,n'}\right), \end{aligned} \tag{4.19}$$

where

$$\begin{aligned} G^{-1}(\mathbf{k}, i\omega_n) &= -i\hbar\omega_n + \epsilon_\gamma(\mathbf{k}) - \mu, \\ G^{-1}_\rho(\mathbf{p}, i\omega_n) &= -i\hbar\omega_n + \epsilon(\mathbf{p}) - \mu_\rho + K_\rho. \end{aligned} \tag{4.20}$$

Here the quantities are defined in a similar way as in Sec. 2.2.

Instead of the second order perturbation theory that is performed in

Chapter 2, we here expand up to fourth order in the coupling constant $g_{\rm mol}$. By performing the Wick rotations, we find for the effective action

$$S^{\rm eff} = \sum_{\mathbf{k},n} a^*_{\mathbf{k},n}(-i\hbar\omega_n + \epsilon_\gamma(\mathbf{k}) - \mu + \hbar\Sigma(\mathbf{k}, i\omega_n))a_{\mathbf{k},n} \tag{4.21}$$
$$+ \frac{1}{2\hbar\beta V}\sum_{\substack{n,n',n''\\ \mathbf{k},\mathbf{k}',\mathbf{k}''}} \Gamma^{(4)}(\mathbf{k},\mathbf{k}',\mathbf{k}'',\omega_n,\omega_{n'},\omega_{n''})a^*_{\mathbf{k},n}a_{\mathbf{k}',n'}a^*_{\mathbf{k}'',n''}a_{\mathbf{k}-\mathbf{k}'+\mathbf{k}'',n-n'+n''},$$

where we defined the self-energy as

$$\hbar\Sigma(\mathbf{k}, i\omega_n) := \frac{g^2_{\rm mol}}{\hbar^2\beta V}\sum_{\mathbf{p},m} G_\downarrow(\mathbf{p}, i\omega_m)G_\uparrow(\mathbf{p}+\mathbf{k}, i(\omega_n+\omega_m)), \tag{4.22}$$

and the photon-photon interaction vertex is given by

$$\Gamma^{(4)}(\mathbf{k},\mathbf{k}',\mathbf{k}'',\omega_n,\omega_{n'},\omega_{n''}) := -\frac{g^4_{\rm mol}}{\hbar^4\beta V}\sum_{\mathbf{p},m} G_\uparrow(\mathbf{p}+\mathbf{k}, i(\omega_m+\omega_n)) \tag{4.23}$$
$$\times G_\downarrow(\mathbf{p}, i\omega_m)G_\uparrow(\mathbf{p}+\mathbf{k}', i(\omega_m+\omega_{n'}))G_\downarrow(\mathbf{p}+\mathbf{k}'-\mathbf{k}'', i(\omega_m+\omega_{n'}-\omega_{n''})).$$

In principle we can use the value of the parameters as given in Chapter 2, to find an estimate for this photon-photon interaction strength. However, it turns out to be more convenient to use a slightly different model. Namely, instead of an two-level model for the dye with an effective mass, we use the real mass and introduce a finite lifetime Γ for the excited molecular state. Hence, we define the spectral function

$$\rho_\uparrow(\mathbf{k},\omega) = \frac{1}{\sqrt{2\pi}\hbar\Gamma}\exp\left\{-\frac{(\hbar\omega - \epsilon(\mathbf{k}) - \Delta + \mu_\uparrow)^2}{2(\hbar\Gamma)^2}\right\}, \tag{4.24}$$

and the corresponding Green's function by using

$$G_\uparrow(\mathbf{k}, i\omega_n) = \int_\infty^\infty d(\hbar\omega)\,\frac{\rho_\uparrow(\mathbf{k},\omega)}{i\omega_n - \omega}. \tag{4.25}$$

Similarly as in Chapter 2, we need to calculate the imaginary part of the self-energy and fix the numerical value of the constants by fitting to the absorption spectrum. By starting from the definition as given in Eq. (4.22) and substituting Eqs. (4.24) and (4.25), we find for the imaginary part of the retarded self-energy

$$R(\mathbf{k}_+,\omega) := -{\rm Im}\left[\hbar\Sigma^{(+)}(\mathbf{k}_+,\omega)\right] \tag{4.26}$$
$$= -{\rm Im}\left[\frac{g^2_{\rm mol}}{V}\sum_{\mathbf{p}}\int_{-\infty}^{\infty}{\rm d}\hbar\omega'\,\rho_\uparrow(\mathbf{p}+\mathbf{k},\omega')\frac{N_{\rm FD}(\hbar\omega') - N_{\rm FD}(\epsilon(\mathbf{p})-\mu_\downarrow)}{-\hbar\omega^+ + \hbar\omega' - \epsilon(\mathbf{p}) + \mu_\downarrow}\right],$$

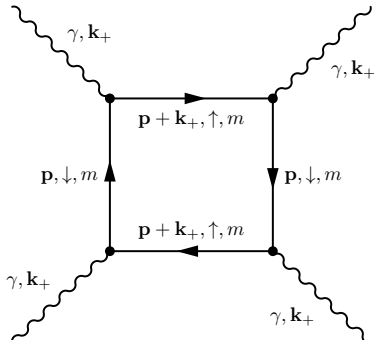

Figure 4.4: Feynman diagram for a fourth-order photon-photon interaction. The photons γ are considered to be part of the condensate and are thus at zero frequency and momentum $\mathbf{k}_+ = (0, 0, k_z)$, as their z-component momentum is fixed and $k_x = k_y = 0$ for the ground state of the homogeneous photon gas. The molecule forms a closed loop of ground ($\downarrow$) and excited ($\uparrow$) states, with momentum $\mathbf{p}$ and Matsubara frequency ω_m.

where $N_{\mathrm{FD}}(x) = 1/(\exp\{\beta x\} + 1)$ is the Fermi-dirac distribution function. Since we are considering a bath of molecules at room temperature and the spectral function is almost zero for negative ω, we are allowed to take the limit $N_{\mathrm{FD}}(x) \to N_{\mathrm{MB}}(x) := \exp\{-\beta x\}$. Hence,

$$R(\mathbf{k}_+, \omega) = \frac{\sqrt{\pi} g_{\mathrm{mol}}^2 \beta \ \exp\{\beta \mu_\downarrow\}}{\Lambda_{\mathrm{th}}^3 \sqrt{2(2\beta\epsilon(\mathbf{k}_+) + (\hbar\beta\Gamma)^2)}} \tag{4.27}$$
$$\times (1 - \exp\{-\beta\hbar\omega\}) \exp\left\{ \frac{-\beta(\epsilon(\mathbf{k}_+) + \Delta - \Delta\mu - \hbar\omega)^2}{2((\hbar\beta\Gamma)^2 + 2\beta\epsilon(\mathbf{k}_+))} \right\},$$

with $\mathbf{k}_+ = (0, 0, k_z)$ the wave number for photons in the condensate. By setting $\Delta\mu = 0$ and $k_z = \omega/c_{\mathrm{med}}$, and taking the part that is proportional to $N_\downarrow$, we obtain the absorption cross section at equilibrium. As it turns out the result is in very good approximation independent of the exact value k_z, and therefore from now onwards we take $k_z = 0$. In this case we find

$$\sigma(\omega)|_{k_z=0} = \frac{\sqrt{2\pi} g_{\mathrm{mol}}^2}{\hbar^2 \Gamma c_{\mathrm{med}}} \exp\left\{ -\frac{(\hbar\omega - \Delta)^2}{2\hbar^2\Gamma^2} \right\}. \tag{4.28}$$

Now we compare the absorption cross section for $k_z = 0$ to the experimental data for the fluorescent dye [57, 58]. The absorption spectrum for the dye is asymmetric and impossible to fully reproduce within this simple treatment. However, we can perform a fit to the line shape and obtain the coupling constant g_{mol}, the lifetime Γ and detuning Δ. Typical values we find are $g_{\mathrm{mol}} = 4 \cdot 10^{-33}$ J m$^{3/2}$, $\Gamma = 1.15 \cdot 10^{14}$ Hz and $\Delta = 3.8 \cdot 10^{-19}$ J.

We now evaluate the photon-photon interaction strength in the condensate, i.e., with Matsubara frequency zero, and is depicted in Fig. 4.4. By using

$$G_{\downarrow}^{2}(\mathbf{p},m)=-\hbar\partial_{\downarrow}G_{\downarrow}(\mathbf{p},m), \tag{4.29}$$

we obtain

$$\Gamma^{(4)}(\mathbf{0},\mathbf{0},\mathbf{0},0,0,0):=\frac{g_{\mathrm{mol}}^{4}\beta n_{\mathrm{mol}}}{\hbar^{2}\Gamma^{2}}f(\beta\mu-\beta\delta), \tag{4.30}$$

with

$$f(\beta\mu-\beta\delta)=\frac{1}{(\beta\hbar\Gamma)^{2}}\int_{-\infty}^{\infty}d\omega\int_{-\infty}^{\infty}d\omega'\,\frac{1}{\omega-\omega'}\exp\left\{-\frac{\omega^{2}+(\omega')^{2}}{2(\beta\hbar\Gamma)^{2}}\right\} \tag{4.31}$$
$$\times\left(\frac{1-e^{\beta\mu-\beta\delta-\omega}}{\beta\mu-\beta\delta-\omega}-\frac{1-e^{\beta\mu-\beta\delta-\omega'}}{\beta\mu-\beta\delta-\omega'}\right)\frac{(\beta\hbar\Gamma)^{2}+\omega+\omega'}{2\pi\{1+\exp\{\beta\mu-\beta\delta+(\beta\hbar\Gamma)^{2}/2\}\}}.$$

Here we set $\Delta\mu-\Delta:=\mu-\delta$, we introduced the dimensionless quantities $\omega:=\beta\hbar\omega$, $\omega':=\beta\hbar\omega'$. Furthermore, $f(\beta\mu-\beta\delta)$ is a smooth dimensionless function peaked around zero. Again we must scale $\Gamma^{(4)}\to 2\Gamma^{(4)}/3D_0$ to obtain the effective coupling constant g of the photons in the condensate.

Having found the expression Eq. (4.30) we have to solve for $\tilde{g}(\mu)$ self-consistently with the Gross-Pitaevskii equation. Considering the center of the trap, i.e., $V^{\mathrm{ex}}=0$, this amounts to solving $\tilde{g}(\mu)=(m/\hbar^{2}n_{\mathrm{ph}})\mu$ for μ, with n_{ph} the photon density. Graphically, this means that we need to find the intersection of $\tilde{g}(\mu)$ and $(m/\hbar^{2}n_{\mathrm{ph}})\mu$. Using typical experimental parameters we find $\tilde{g}\sim 10^{-8}-10^{-7}$. However, the magnitude of $\tilde{g}$ is rather uncertain due to the simplification of the rovibrational energy spectrum of the dye molecules.

4.6 Conclusion

In conclusion, we have calculated the effect of self-interactions on number fluctuations in Bose-Einstein condensates. Comparing our results with recent experiments on a condensate of light, we find good agreement. Moreover, we have considered two different possible photon-photon interactions. Both thermal lensing and dye-mediated photon-photon scattering give interaction strengths that are several orders of magnitude smaller than observed experimentally. Therefore, systematic measurements of the interaction strength are necessary to understand the true nature of the interaction. If the interaction is indeed a contact interaction at long wavelengths, then this would imply that the photon condensate is also a superfluid.

Chapter 5

Phase diffusion

We study phase diffusion in a Bose-Einstein condensate of light in a dye-filled optical microcavity, i.e., the spreading of the probability distribution for the condensate phase. To observe this phenomenon, we propose an interference experiment between the condensed photons and an external laser. We determine the average interference patterns, considering quantum and thermal fluctuations as well as dissipative effects due to the dye. Moreover, we show that a representative outcome of individual measurements can be obtained from a stochastic equation for the global phase of the condensate.[1]

5.1 Introduction

Phase transitions are every-day phenomena that have many high-tech applications in daily life, one example being the isotropic-nematic phase transition in LCD screens. Additionally, phase transitions are often encountered in fundamental research, such as in the description of superconductivity [99] and the electroweak and QCD phase transition in cosmology [100–102]. As a result, throughout history much effort has been put into understanding phase transitions. A crucial step was the development of Landau theory in 1937 [103], which provided a general framework to describe symmetry-breaking phase transitions.

Many phase transitions are associated with spontaneous symmetry breaking [104, 105]. In these transitions the state of the system after the phase transition does not show the same symmetry as the Hamiltonian. As an

[1] This Chapter is directly based on *Phase Diffusion in a Bose-Einstein Condensate of Light*, A.-W. de Leeuw, E.C.I. van der Wurff, R.A. Duine, and H.T.C. Stoof, Phys. Rev. A **90**, 043627 (2014). The content of this Chapter is also part of the Master's thesis of E.C.I. van der Wurff, who was supervised by A.-W. de Leeuw, R.A. Duine and H.T.C. Stoof.

illustration of spontaneous symmetry breaking, we consider the Heisenberg model for ferromagnetism [106]. In this system the Hamiltonian is invariant under rotations of the spins. After undergoing the transition the spins align in a particular direction, and the state of the system breaks spin rotation invariance. However, the original symmetry still has consequences because a global rotation of all spins leaves the energy invariant. Therefore, the ordered phase is infinitely degenerate and spontaneous symmetry breaking by itself does not predict which particular ground state the system will choose.

We can investigate this problem by looking at the probability distribution of the quantum-mechanical observable that acquires a nonzero expectation value upon undergoing the transition. In the context of atomic gases and Bose-Einstein condensation [1, 2], the Hamiltonian is invariant under global $U(1)$ transformations associated with the conservation of the number of atoms. Therefore, the number of condensed particles and the phase of the condensate are conjugate variables. Heisenberg's uncertainty principle implies that, for a fixed number of condensed particles, the phase of the condensate fluctuates. Thus, in finite-sized condensates the phase is not fixed and the system is not in a state with a definite phase. Rather, the phase of the condensate is characterized by a probability distribution, which can have nontrivial dynamics of its own. In Bose-Einstein condensates this phenomenon is known as phase diffusion [6, 107].

Considerable theoretical work has been done on phase diffusion in atomic condensates [108–113]. Experimentally, there have also been some attempts to measure this phenomenon [114, 115], but up to now there is no experimental evidence of phase diffusion. The only dynamical evolution of the phase of a Bose-Einstein condensate was measured in an optical lattice by quenching the system into the Mott-insulator phase [116]. As a result, this phase dynamics is not a consequence of spontaneous $U(1)$ symmetry breaking and having a finite number of condensed particles, and is fundamentally different from the phase diffusion discussed in this Chapter.

More recently, quasiparticle Bose-Einstein condensates, such as condensates of magnons, exciton-polaritons, and photons have been observed [29–32]. Since the phase of light can be obtained from a relatively simple interference experiment, the discovery of Bose-Einstein condensation of photons, in particular, opens up a new avenue to investigate phase diffusion in Bose-Einstein condensates.

In this Chapter, we therefore study phase diffusion in a Bose-Einstein condensate of photons. We propose an interference experiment between the condensed photons and an external laser to measure phase diffusion in the

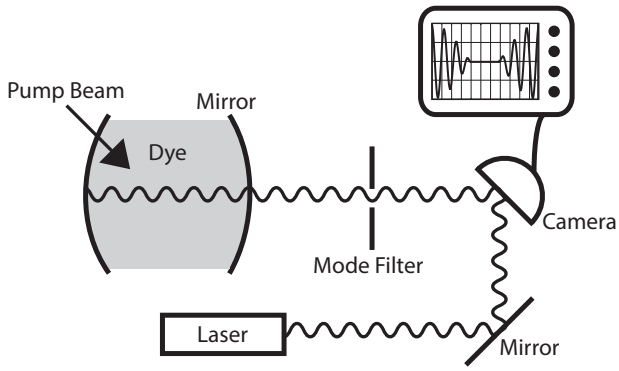

Figure 5.1: Proposal for an experimental setup to measure the phase diffusion of the Bose-Einstein condensate of photons in a dye-filled microcavity. The mode filter selects the condensate mode of the light that leaks through the mirror. These condensed photons interfere with an external laser, and by measuring the intensity of the combined signal, we obtain information about the phase diffusion of the Bose-Einstein condensate of photons.

photonic condensate. Since phase diffusion is governed by both quantum and thermal fluctuations of the number of condensed particles, we calculate average interference patterns for both cases separately. Moreover, for the present experimentally-most-relevant situation where thermal fluctuations dominate, we show that representative results of individual measurements can be obtained from a stochastic equation for the phase of the condensate.

5.2 Quantum fluctuations

Experimentally, information on the phase of the condensate can be inferred from interfering the electric field of the photon condensate with an external laser and measuring the intensity of the combined signal. We assume that the laser is frequency locked to the homogeneous noninteracting energy of a condensed photon, and without loss of generality we assume that the distance from the laser and the condensed photons to the detector is the same. A schematic picture of the experimental setup is shown in Fig. 5.1.

Since, for a finite-size condensate of photons, the phase is not well defined, we introduce a density operator $\hat{\rho}$ that takes into account that the photons can be in a superposition of different coherent states with different phases. Following Ref. [96], we write the following for the intensity of the combined signal of the laser and the condensate at the detector: $\bar{I}(\mathbf{r},t) = \mathrm{Tr}[\hat{\rho}\hat{E}^{-}(\mathbf{r},t)\hat{E}^{+}(\mathbf{r},t)]$, where the bar denotes the average and with $\hat{E}^{-}(\mathbf{r},t)$ and $\hat{E}^{+}(\mathbf{r},t)$ being, respectively, the negative- and positive-

frequency part of the sum of the electric field of the laser and the Bose-Einstein condensate.

For our system the relevant basis states are the coherent states $|\theta\rangle|\theta_{\rm L}\rangle$, where $|\theta_{\rm L}\rangle$ is a coherent state of the laser with phase $\theta_{\rm L}$ and $|\theta\rangle$ is a coherent state of the Bose-Einstein condensate with a certain phase θ. In the following, we assume without loss of generality that $\theta_{\rm L} = 0$. By using properties of these coherent states (see e.g., Ref. [117]), we obtain for the interference contribution of the intensity

$$\begin{aligned}\bar{I}_{\rm I}(\mathbf{r},t) &:= \bar{I}(\mathbf{r},t) - I_{\rm L}(\mathbf{r},t) - I_{\rm C}(\mathbf{r},t) \\ &= 2A_{\rm I}(\mathbf{r},t)\int_0^{2\pi} d\theta\, P(\theta,t)\cos(\theta),\end{aligned} \tag{5.1}$$

where $I_{\rm L}(\mathbf{r},t)$ and $I_{\rm C}(\mathbf{r},t)$ are the intensity of the laser and the condensed photons, respectively. Furthermore, $A_{\rm I}(\mathbf{r},t)$ is a prefactor that is the product of the amplitude of the electric field of the condensed photons and of the external laser. Moreover, $P(\theta,t)$ is the probability for the Bose-Einstein condensate to have phase θ. Since the intensity of the photons coming from the condensate is independent of the phase, this interference part of the intensity is the only relevant contribution for observing phase diffusion.

For an explicit expression of the intensity as a function of time, we need to determine the probability $P(\theta,t)$. In analogy with Ref. [59], we obtain this probability by quantizing a field theory that describes the dynamics of the phase of a Bose-Einstein condensate of photons. These photons are equivalent to a two-dimensional harmonically trapped gas of bosons with effective mass m [32]. Furthermore, they have an effective contact interaction with strength T^{2B} and a constant zero-momentum energy mc^2, with c being the speed of light in the medium. Note that we have assumed the laser to be frequency locked to mc^2. Therefore, in imaginary time the relevant action is given by

$$\begin{aligned}S[\psi^*,\psi] &= \frac{T^{2B}}{2}\int_0^{\hbar\beta} d\tau \int d\mathbf{x}\,|\psi(\mathbf{x},\tau)|^4 \\ &+ \int_0^{\hbar\beta} d\tau \int d\mathbf{x}\,\psi^*(\mathbf{x},\tau)\left\{\hbar\frac{\partial}{\partial\tau} - \frac{\hbar^2\nabla^2}{2m} - \mu + \frac{1}{2}m\Omega^2|\mathbf{x}|^2\right\}\psi(\mathbf{x},\tau),\end{aligned} \tag{5.2}$$

where $\beta = 1/k_{\rm B}T$ with T being the temperature, μ is the chemical potential of the photons with respect to the energy mc^2, and Ω is the harmonic trapping frequency. In the following we use numerical values for Ω, T^{2B}, and m as given in Ref. [32].

To extract the dynamics of the global phase, we substitute $\psi(\mathbf{x},\tau) =$

$\sqrt{\rho(\mathbf{x},\tau)}e^{i\theta(\tau)}$. Moreover, we consider the Thomas-Fermi limit relevant for experiments and therefore can neglect the gradient of the density profile $\rho(\mathbf{x},\tau)$. By integrating out the density field $\rho(\mathbf{x},\tau)$ and performing a Wick rotation $\tau \to it$, we find an effective action for the global phase. Quantizing this theory, we find that the wave function $\Psi(\theta,t)$ obeys

$$i\hbar\frac{\partial\Psi(\theta,t)}{\partial t} = -D\left(\frac{\partial}{\partial\theta} + iN_0\right)^2\Psi(\theta,t), \tag{5.3}$$

where $N_0 = \int d\mathbf{x}\,\bar{\rho}(\mathbf{x})$ is the average number of condensed photons, and the diffusion constant is defined as $D = T^{2B}/2\pi R_{\mathrm{TF}}^2$ with R_{TF} being the Thomas-Fermi radius of the photon condensate. The general solution to this equation reads

$$\Psi(\theta,t) = \sum_{n\in\mathbb{Z}} c_n \exp\left\{-\frac{iD(n+N_0)^2 t}{\hbar} + in\theta\right\}, \tag{5.4}$$

where the coefficients c_n are determined by the initial condition for the wave function.

In order to demonstrate the phase diffusion and to calculate a typical interference pattern, we consider the example that the initial wave function is a superposition of Gaussians centered around $\theta = 0 \bmod 2\pi$,

$$\Psi(\theta,0) = \frac{1}{(\pi\sigma^2)^{1/4}}\sum_{n\in\mathbb{Z}} \exp\left\{-\frac{(\theta+2\pi n)^2}{2\sigma^2}\right\}. \tag{5.5}$$

Taking this superposition ensures that the wave function is periodic, i.e., $\Psi(\theta,0) = \Psi(\theta+2\pi,0)$. In principle we have a slightly different normalization factor, but for the small values of $\sigma < 1$ considered here, this is a very good approximation. In experiments one would measure the phase of the condensate and then look at its dynamics. Hence, we start from a wave function that is strongly peaked and therefore we can use in good approximation that $\sigma < 1$.

For this initial wave function, we can determine c_n exactly and obtain an analytic expression for the probability $P(\theta,t) = |\Psi(\theta,t)|^2$. Typical plots of this probability are shown in Fig. 5.2. At $t = 0$ we have a sharp peak and therefore the phase of the condensate is well-defined. However, if time evolves the peak smears out and moves its position linearly with time. As time evolves even further, the probability again regains its original shape. This phenomenon is known as collapse and revival of the wave function, and is a consequence of the invariance of the wave function for $t \to t + 2\pi k\hbar/D$ for every integer k, as can be deduced from Eq. (5.4). Hereafter, cycles of

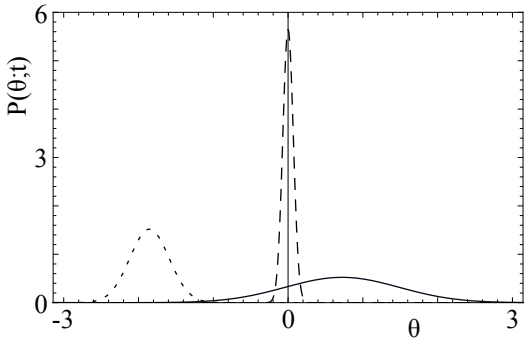

Figure 5.2: The probability $P(\theta, t)$ for the Bose-Einstein condensate of photons at different times for $N_0 = 5 \cdot 10^4$ and $\sigma = 10^{-1}$. The dashed, dotted, and solid curve are the probability at $t = 0$, $t = t_{\text{col}}$, and $t = 3t_{\text{col}}$. We clearly see the diffusion of the phase of the condensate if time evolves.

collapse and revival of the wave function occur.

Moreover, we use our expressions for the probability to obtain the average interference pattern as defined in Eq. (5.1). Again for small $\sigma < 1$, we find

$$\bar{I}_{\text{I}}(\mathbf{r}, t) = \frac{2\sigma A_{\text{I}}(\mathbf{r}, t)}{\sqrt{\pi}} \cos\left(\frac{5(1+2N_0)\sigma t}{2t_{\text{col}}}\right) \sum_{n\in\mathbb{Z}} e^{-n(n+1)\sigma^2} \cos\left(\frac{5n\sigma t}{t_{\text{col}}}\right), \quad (5.6)$$

with $t_{\text{col}} = 5\hbar\sigma/2D$. This time gives a measure of the time needed for this pattern to vanish for the first time. Furthermore, this expression contains two other important timescales. The first scale is the oscillation time of the interference pattern, which for a relatively large number of condensed photons $N_0 \gg 1$ is given by $t_{\text{osc}} = \hbar/2DN_0$. Physically this corresponds to $\hbar/\mu$, with μ being the chemical potential of the condensate. Note that this calculation gives a factor of two difference because of the quadratic expansion of the grand canonical energy. The second timescale, given by $t_{\text{rev}} = 2\pi\hbar/D$, is the revival time for which the interference pattern returns to its original shape. Note that this timescale is larger than t_{osc} by a factor $4\pi N_0$. Furthermore, in the thermodynamic limit $N_0 \to \infty$, we find that $D \propto 1/\sqrt{N_0} \to 0$ and both $t_{\text{col}} \to \infty$ and $t_{\text{rev}} \to \infty$. Hence, in the thermodynamic limit the condensate can be described as a symmetry-broken phase.

In the previous calculations we ignored that the photons are in a dye-filled optical microcavity, and that there is dissipation through the interaction with these dye molecules. As is shown in Ref. [75] by fitting to experimental results, for low energies these interaction effects can in very

good approximation be represented by one single dimensionless damping parameter α. To incorporate this damping into our calculation, we note that damping results into finite lifetimes for states with a nonzero energy. Therefore, as a first attempt to include dissipation, we change Eq. (5.4) to

$$\Psi(\theta,t) = \sum_{n\in\mathbb{Z}} c_n \int dE\, \rho(E,n) \exp\left\{-\frac{iEt}{\hbar} + in\theta\right\}, \tag{5.7}$$

where the spectral function $\rho(E,n)$ is given by

$$\rho(E,n) = \frac{1}{\pi}\frac{\alpha E}{(E - D(n+N_0)^2)^2 + \alpha^2 E^2}. \tag{5.8}$$

A consequence of approximating the dissipation effects with its low-energy limit is a violation of the sum rule, since the integral of the spectral function over all energies gives $1/(1+\alpha^2)$. However, the experimental value of α is rather small and therefore this approximation only leads to a small deviation.

For a relatively small number of condensed photons, the interference pattern with dissipation reads

$$\bar{I}(\mathbf{r},t;\alpha) \simeq e^{-t/t_{\rm dis}} \bar{I}_{\rm I}(\mathbf{r},t), \tag{5.9}$$

where $t_{\rm dis} = \hbar/4\alpha D N_0^2$ and $\bar{I}_{\rm I}(\mathbf{r},t)$ is given by Eq. (5.6). Thus with dissipation there is another timescale $t_{\rm dis}$, which indicates the decay time of the interference pattern. Furthermore, for relatively small times t we can simplify Eq. (5.6) and obtain

$$\bar{I}(\mathbf{r},t;\alpha) \simeq 2A_{\rm I}(\mathbf{r},t) e^{-t/t_{\rm dis} - (5t/2t_{\rm col})^2} \cos\left(\mu t/\hbar\right), \tag{5.10}$$

which shows the different qualitative behavior of decay due to dye and quantum effects, respectively. For very large condensates $N_0 \gg 1$, the low-energy approximation of the dissipation is no longer valid and we have to incorporate the complete energy dependence of the photon decay rate $\Gamma(E)$ as calculated in Ref. [75]. In a good approximation the dissipation timescale is then found by replacing $\alpha D N_0^2$ by $\hbar\Gamma(DN_0^2)/2$.

5.3 Thermal fluctuations

Analogously with Ref. [56], we describe the thermal fluctuations with a Langevin field equation. As mentioned before, we incorporate the interaction with the molecules by one dimensionless parameter α. Furthermore,

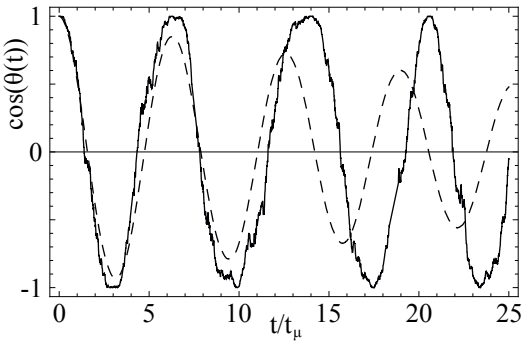

Figure 5.3: The result of $\cos(\theta(t))$ as a function of $t/t_{\rm osc}$ with $t_{\rm osc} = \hbar/\mu \simeq 5{\cdot}10^{-10}$ s. Here $\theta(t)$ is a solution to the Langevin equation describing the dynamics of the phase of the condensate for $N(t) = \langle N\rangle = 4\cdot 10^4$, $\alpha = 10^{-1}$, and $\hbar\beta \simeq 2.5\cdot 10^{-14}$ s. The solid curve is the result for an arbitrary noise configuration and the dashed curve represents the average over 500 different configurations of the noise.

we neglect the effects of the noncondensed photons. Following Ref. [118], we separate the dynamics of the number of photons $N(t)$ and their global phase $\theta(t)$, and find

$$\begin{aligned}(1+\alpha^2)\hbar\dot\theta(t) &= -\mu + \sqrt{(1+\alpha^2)/N(t)}\nu(t),\\ (1+\alpha^2)\hbar\dot N(t) &= -2\alpha\mu N(t) + 2\hbar\sqrt{N(t)(1+\alpha^2)}\eta(t),\end{aligned} \tag{5.11}$$

where the stochastic generalized forces $\eta(t)$ and $\nu(t)$ are Gaussian and obey

$$\begin{aligned}\langle\nu(t)\rangle = \langle\eta(t)\rangle = \langle\eta(t)\nu(t')\rangle &= 0,\\ \langle\nu(t)\nu(t')\rangle = \hbar^2\langle\eta(t)\eta(t')\rangle &\simeq \alpha\hbar\delta(t-t')/\beta.\end{aligned} \tag{5.12}$$

Since we are dealing with Bose-Einstein condensation, we used the fluctuation-dissipation theorem for large occupation numbers. Because the photons are at room temperature, we expect this to be a very good approximation. Furthermore, we note that the strength of the noise for the number $N(t)$ and phase $\theta(t)$ of the condensed photons scales differently with the number of condensed photons. For larger number of photons the fluctuations in the particle number increase, but the fluctuations in the global phase decrease. Moreover, in the thermodynamic limit the noise for the global phase vanishes, and we obtain again a condensate with a well-defined phase.

As the description of the thermal fluctuations is different from the quantum fluctuations, we need to modify our expression for the interference pattern. In the previous section we found an expression by taking the average

over an ensemble consisting of various quantum states, each with a certain probability. A single experimental measurement, however, typically yields

$$I_{\rm I}(\mathbf{r},t) = 2A_{\rm I}(\mathbf{r},t)\cos(\theta(t)), \tag{5.13}$$

where $\theta(t)$ is the solution of Eqs. (5.11) for one realization of the noise. As mentioned before, the fluctuations of the phase of the condensate are only present in this interference part of the intensity, and therefore we are primarily interested in this part of the intensity. Moreover, to highlight the fluctuations of the phase we would like to minimize the fluctuations in the intensity of the external laser and the light coming from the condensate. Since the intensity of the condensate is proportional to the number of condensed photons, we are interested in the regime with small number fluctuations. As can be deduced from the experimental results in Ref. [83] and Eqs. (5.11), the number fluctuations decrease for increasing condensate fractions. Therefore, we consider large condensate fractions such that the fluctuations in the interference pattern are dominated by phase fluctuations, and we take $N(t) = \langle N(t)\rangle := N_0$.

In Fig. 5.3 we show the result for $\cos(\theta(t))$, where $\theta(t)$ is a solution to the stochastic Eqs. (5.11) for a condensate fraction of roughly 35 %. The solid curve gives the interference pattern for a certain realization of the stochastic forces. Every realization of the noise results in a different interference pattern, and therefore every individual measurement will give a different result. However, once we average over more and more noise realizations $\langle\cos(\theta(t))\rangle$ converges, and we do observe the decay associated with the dissipation.

In order to get more information about this decay of the intensity $I_{\rm I}(\mathbf{r},t)$, we have to take the average of Eq. (5.13) over all noise configurations. By using the Fokker-Planck equation as derived in Ref. [118], we find

$$\begin{aligned}(1+\alpha^2)\hbar\frac{\partial}{\partial t}\langle\cos(\theta)\rangle &= \mu\langle\sin(\theta)\rangle - \frac{\alpha}{2\beta N_0}\langle\cos(\theta)\rangle,\\ (1+\alpha^2)\hbar\frac{\partial}{\partial t}\langle\sin(\theta)\rangle &= -\mu\langle\cos(\theta)\rangle - \frac{\alpha}{2\beta N_0}\langle\sin(\theta)\rangle.\end{aligned} \tag{5.14}$$

These equations admit analytic solutions and, by neglecting contributionsof order α^2, we find for the average of the interference part of the intensity

$$\langle I_{\rm I}(\mathbf{r},t)\rangle = 2A_{\rm I}(\mathbf{r},t)e^{-\alpha t/2\hbar\beta N_0}\cos\left(\mu t/\hbar\right), \tag{5.15}$$

which coincides with the result in Fig. 5.3 where we averaged over 500 noise realizations.

5.4 Discussion and conclusion

In the previous sections, we gave a discussion on phase diffusion governed by quantum and thermal fluctuations. Since thermal fluctuations are dominant for the current experiment, there are two important timescales $t_{\rm osc} = \hbar/\mu$ and $t_{\rm dis} = 2\hbar\beta N_0/\alpha$. For typical values for the trap frequencies Ω, we obtain that $t_{\rm osc}$ is of the order of picoseconds. Since this is rather small, we expect that it is challenging to measure these oscillations experimentally. However, for large condensate numbers $N_0 \gg 1$ and α ranging from 10^{-1} to 10^{-2} the decay time $t_{\rm dis}$ is in the nanoseconds regime, which is within the precision of current devices.

In conclusion, we have calculated the phase diffusion of a Bose-Einstein condensate of photons. We propose an interference experiment of the condensed photons with an external laser to observe this phase diffusion experimentally. Furthermore, we have shown that the typical outcome of individual experiments can be obtained from a stochastic equation for the phase of the condensate. Finally, we have demonstrated that thermal fluctuations dominate, and we obtained that the decay time of the average interference pattern is in the nanosecond regime, which is a accessible timescale in experiments.

Although the calculations in this Chapter are specific to a Bose-Einstein condensate of photons, the concepts and ideas presented here are also applicable to Bose-Einstein condensation of exciton-polaritons. Namely, also in these Bose-Einstein condensates we can get experimental information about the global phase of the condensate. For example, in Refs. [119, 120] the relative global phase of two coupled exciton-polariton condensates is measured in order to investigate Josephson oscillations. Therefore, it is worthwhile to apply the present theory to Bose-Einstein condensation of exciton-polaritons.

Chapter 6

Superfluid-Mott-insulator transition

We investigate the superfluid-Mott-insulator transition of a two-dimensional photon gas in a dye-filled optical microcavity and in the presence of a periodic potential. We show that in the random-phase approximation the effects of the dye molecules, which generally lead to dissipation in the photonic system, can be captured by two dimensionless parameters that only depend on dye-specific properties. Within the mean-field approximation, we demonstrate that one of these parameters decreases the size of the Mott lobes in the phase diagram. By considering also Gaussian fluctuations, we show that the coupling with the dye molecules results in a finite lifetime of the quasiparticle and quasihole excitations in the Mott lobes. Moreover, we show that there are number fluctuations in the Mott lobes even at zero temperature and therefore that the true Mott-insulating state never exists if the interactions with the dye are included.[1]

6.1 Introduction

In physics there are many theoretically predicted phenomena that are hard to verify directly in experiments. This can have several reasons, such as that predictions are outside the limits of current devices or that other physics overshadows the desired effect. In the latter category examples are the effects of disorder on top of effects predicted for clean systems, or a combination of various kinds of interactions. Therefore, there is a constant search for systems that exhibit interesting physics, are relatively simple, and are described by few parameters of which many are controllable experimentally.

[1] This Chapter is directly based on *Effects of dissipation on the superfluid-Mott-insulator transition of photons*, A.-W. de Leeuw, O. Onishchenko, R.A. Duine, and H.T.C. Stoof, Phys. Rev. A **91**, 033609 (2015).

A prime example of such a system is obtained by combining cold atoms with an optical lattice. In this case there is almost full control over the interactions between the atoms and over the lattice structure. Therefore, there exists a broad variety of experimental possibilities in these systems that demonstrate many phenomena in condensed-matter physics, (see, e.g., Refs. [121–129]). Nowadays this research area is still very active. One of the reasons is that cold fermionic atoms in an optical lattice possibly are quantum simulators for high-temperature superconductivity [130–132].

An interesting property of cold bosonic atoms in optical lattices is that there is a so-called quantum phase transition [21]. By reducing the depth of the optical lattice the system undergoes a transition from the Mott insulator, where each site is filled with an equal and integer amount of particles and number fluctuations are suppressed, to the superfluid phase with a fluctuating number of atoms per site. This transition was first observed experimentally by Greiner *et al.* [19], and subsequently has been studied extensively both theoretically and experimentally [18, 133–140]. Although most studies focus on the superfluid-Mott-insulator transition for cold atoms, this phase transition is not restricted only to cold atomic gases. For example, it also has been studied in systems consisting of polaritons [141–147]. Furthermore, the transition has been investigated in interacting photon gases in coupled dissipative cavities [148–151].

More recently, a new candidate for a system that can display a superfluid-Mott-insulator transition has emerged, namely, photons in a dye-filled optical microcavity. After the first experiments, which are well described in terms of Bose-Einstein condensation of weakly interacting photons [32], a new experiment was recently proposed [152]. By periodically varying the index of refraction of the dye inside the cavity, an effective lattice potential for the photons can be induced. Therefore, it is expected that the photons can also undergo this superfluid-Mott-insulator phase transition. However, this system is fundamentally different from the standard cold atomic gases in optical lattices, since the photons can be absorbed and emitted by the dye molecules. Thus, the question arises as to how this coupling affects the behavior of the photons in this periodic potential, and in particular the properties of the quantum phase transition to the Mott insulator.

In this Chapter we study the dissipation effects for a photonic lattice in a dye-filled optical microcavity. Although we focus here on photons, the results in this Chapter also apply to other systems that have dissipation. First, in Sec. 6.2 we introduce the general theory and express all quantities that enter our theory in terms of experimentally known parameters. Subsequently, we determine the effect of the molecules on the Mott

lobes in mean-field theory in Sec. 6.3. We start by considering a simplified model that neglects the fixed longitudinal momentum of the photons and only considers absorption and emission of photons with zero momentum. We show that at the mean-field level the dye effects are captured in one parameter γ that can be calculated analytically, and we express this parameter in experimentally known quantities. Additionally, we show that incorporation of γ decreases the size of the Mott lobes. Thereafter, we consider the model that includes the fixed longitudinal momentum of the photons and also the absorption and emission of photons with an arbitrary momentum, and we study the effect of these extensions on the value of γ. In Sec. 6.4 we go beyond mean-field theory and we calculate in the random-phase-approximation the excitations inside the Mott lobes. We show that in this approximation the dimensionless damping parameter α_{lat} enters our model and therefore the excitations acquire a finite lifetime. Moreover, we show that even at zero temperature there are now number fluctuations inside the Mott lobes, which implies that the true Mott-insulating phase no longer exists if the interactions with the dye are taken into account. Finally, we end with a conclusion and outlook in Sec. 6.5.

6.2 Photonic lattice in dye-filled microcavity

In this section we write down a model for a lattice of photons in a dye-filled optical microcavity for the experimental set-up used in Ref. [32, 36]. In the particular experimental configuration the longitudinal momentum of the photons is fixed, and the photons behave equivalently to a massive harmonically trapped Bose gas in two dimensions. Since the photons interact with dye molecules, the imaginary-time action that describes the photon system contains three parts. The part that describes the photons reads

$$\begin{aligned} S_{\mathrm{ph}}[\phi^*,\phi] &= S_0[\phi^*,\phi] + S_{\mathrm{int}}[\phi^*,\phi] \qquad (6.1)\\ &= \int_0^{\hbar\beta} d\tau \int d\mathbf{x}\, \phi^*(\mathbf{x},\tau)\left\{\hbar\frac{\partial}{\partial\tau} - \frac{\hbar^2\nabla^2}{2m} + V^{\mathrm{ext}}(\mathbf{x}) - \mu\right\}\phi(\mathbf{x},\tau)\\ &\quad + \frac{1}{2}\int_0^{\hbar\beta} d\tau \int d\mathbf{x} \int d\mathbf{x}'\, \phi^*(\mathbf{x},\tau)\phi^*(\mathbf{x}',\tau)V(\mathbf{x}-\mathbf{x}')\phi(\mathbf{x}',\tau)\phi(\mathbf{x},\tau), \end{aligned}$$

where μ is the chemical potential of the photons, m denotes their effective mass, $\beta = 1/k_{\mathrm{B}}T$ with T the temperature, $V(\mathbf{x}-\mathbf{x}')$ is the interaction potential and

$$V^{\mathrm{ext}}(\mathbf{x}) = V_0 \sum_j \cos^2(2\pi x_j/\lambda), \qquad (6.2)$$

denotes the lattice potential with λ two times the lattice spacing. In the following we are primarily interested in how these photons are affected by the coupling to the molecules, and therefore we ignore the external harmonic potential that arises due to the curvature of the cavity mirrors. We model the dye as a two-level system with energy difference Δ and we introduce the effective mass m_{d} to model the rovibrational structure of the molecules. As is shown in Ref. [75], the value of this effective mass can be tuned such that the correct experimental results for the molecular absorption and emission spectra are obtained. A different way to achieve this has been put forward by Kirton and Keeling [34]. Hence, the molecular part of the action reads

$$S_{\mathrm{mol}}[\psi^*,\psi] = \sum_{\rho\in\{\uparrow,\downarrow\}} \int_0^{\hbar\beta} d\tau \int d\mathbf{r}\, \psi_\rho^*(\mathbf{r},\tau)\left\{\hbar\frac{\partial}{\partial\tau} - \frac{\hbar^2\nabla^2}{2m_{\mathrm{d}}} + K_\rho - \mu_\rho\right\}\psi_\rho(\mathbf{r},\tau), \tag{6.3}$$

where $K_\uparrow = \Delta$, $K_\downarrow = 0$ and μ_ρ denotes the chemical potential of the excited and ground-state molecules. Contrary to the photon part, here the integration is over three-dimensional space. From now on, we use the convention that $\mathbf{x}$ is a two-dimensional vector and $\mathbf{r}$ is three dimensional. The last part of the action consists of interaction terms between photons and molecules, and reads

$$S_{\mathrm{c}}[\psi^*,\psi,\phi^*,\phi] = g\int_0^{\hbar\beta} d\tau \int d\mathbf{r}\, \left\{\phi^*(\mathbf{r},\tau)\psi_\downarrow^*(\mathbf{r},\tau)\psi_\uparrow(\mathbf{r},\tau) + \phi(\mathbf{r},\tau)\psi_\uparrow^*(\mathbf{r},\tau)\psi_\downarrow(\mathbf{r},\tau)\right\}, \tag{6.4}$$

with g a coupling constant. Furthermore, $\phi^*(\mathbf{r},\tau)$ is related to the photon field $\phi^*(\mathbf{x},\tau)$ in Eq. (6.8) according to

$$\phi(\mathbf{r},\tau) = \sqrt{2/L}\sin(k_\gamma z)\,\phi(\mathbf{x},\tau). \tag{6.5}$$

Here we assume that in one direction the photons are confined by a box of length L with impenetrable barriers at either end. Furthermore, in agreement with the experiments, we only take into account a single longitudinal momentum k_γ.

To make further progress, we expand the photonic fields in Wannier functions as

$$\phi(\mathbf{x},\tau) = \sum_{\mathbf{n},i} a_{\mathbf{n},i}(\tau) w_{\mathbf{n}}(\mathbf{x}-\mathbf{x}_i), \tag{6.6}$$

where $a_{\mathbf{n},i}(\tau)$ and its complex conjugate respectively annihilates or creates a photon in a Wannier state $w_{\mathbf{n}}(\mathbf{x}-\mathbf{x}_i)$ at lattice site i and in the band with the band index $\mathbf{n}$. Furthermore, the molecular field is expanded as

$$\psi_\rho(\mathbf{r},\tau) = \sum_{\mathbf{p}} b_{\mathbf{p},\rho}(\tau)\frac{e^{i\mathbf{p}\cdot\mathbf{r}}}{\sqrt{V}}, \tag{6.7}$$

where $b_{\mathbf{p},\rho}(\tau)$ and $b^*_{\mathbf{p},\rho}(\tau)$ annihilates or creates a molecule with momentum $\mathbf{p}$ and internal state $|\rho\rangle$. Next we consider the tight-binding limit, where each site can be seen as a harmonic oscillator and the Wannier functions are known exactly. Furthermore, we consider the limit where the photons only occupy the lowest band $\mathbf{n}=\mathbf{0}$. In this approximation the three parts of the action can be simplified, and by using the result of Ref. [153] we obtain

$$\begin{aligned} S_{\mathrm{ph}}[a^*,a] = &-\int_0^{\hbar\beta} d\tau \sum_{i\neq j} a_i^*(\tau) t_{i,j} a_j(\tau) \\ &+ \int_0^{\hbar\beta} d\tau \sum_i a_i^*(\tau)\left\{\hbar\frac{\partial}{\partial\tau} + \epsilon_i - \mu + \frac{U}{2}|a_i(\tau)|^2\right\} a_i(\tau), \end{aligned} \tag{6.8}$$

where ϵ_i is the energy at lattice site i, $t_{i,j}$ is the hopping strength between sites i and j, and U is the on-site interaction strength. The expression of these quantities in terms of Wannier functions can be found in Ref. [153]. Since we consider the tight-binding limit, we know the analytic expression for $w_{\mathbf{0}}(\mathbf{x}-\mathbf{x}_i)$. It is given by

$$w_{\mathbf{0}}(\mathbf{x}-\mathbf{x}_i) = \left(\frac{m\omega}{\pi\hbar}\right)^{1/2} \exp\left\{-m\omega(\mathbf{x}-\mathbf{x}_i)^2/2\hbar\right\}, \tag{6.9}$$

where m is the effective mass of the photon and ω is the frequency of the harmonic potential at every site that can be obtained by performing a Taylor expansion of Eq. (6.2). Hence,

$$\omega = \frac{2\pi}{\lambda}\sqrt{\frac{2V_0}{m}}. \tag{6.10}$$

Note that the single-band approximation is only valid if we have that both the thermal energy $k_{\mathrm{B}}T$ and the on-site interaction strength U are smaller than the on-site energy of the photons $\hbar\omega$, i.e., $k_{\mathrm{B}}T \ll \hbar\omega$ and $U \ll \hbar\omega$. Furthermore,

$$S_{\mathrm{mol}}[b^*,b] = \int_0^{\hbar\beta} d\tau \sum_{\rho,\mathbf{p}} b^*_{\mathbf{p},\rho}(\tau)\left\{\hbar\frac{\partial}{\partial\tau} + \epsilon_{\mathbf{p}} + K_\rho - \mu_\rho\right\} b_{\mathbf{p},\rho}(\tau), \tag{6.11}$$

where $\epsilon_{\mathbf{p}} = \hbar^2\mathbf{p}^2/2m_{\mathrm{d}}$. Finally, the part that describes the interaction between the photons and molecules can be rewritten as

$$\begin{aligned} S_{\mathrm{c}}[a^*, a, b^*, b] = & \\ & \frac{i}{\sqrt{2AV}} \int_0^{\hbar\beta} d\tau \sum_{j,\mathbf{k},\mathbf{k}',q} g_{\mathbf{k},\mathbf{k}',j} a_j^*(\tau) b^*_{(\mathbf{k}',q),\downarrow}(\tau) b_{(\mathbf{k},q_-),\uparrow}(\tau) + \mathrm{h.c.} \\ & - \frac{i}{\sqrt{2AV}} \int_0^{\hbar\beta} d\tau \sum_{j,\mathbf{k},\mathbf{k}',q} g_{\mathbf{k},\mathbf{k}',j} a_j^*(\tau) b^*_{(\mathbf{k}',q),\downarrow}(\tau) b_{(\mathbf{k},q_+),\uparrow}(\tau) + \mathrm{h.c.}, \end{aligned} \tag{6.12}$$

where $\mathbf{k}$ and $\mathbf{k}'$ are two-dimensional and $q_\pm = q \pm k_\gamma$. Above and in the following, $\mathbf{p}$ is a three-dimensional momentum vector and $\mathbf{k}$ is two dimensional. Furthermore,

$$g_{\mathbf{k},\mathbf{k}',j} = g \int d\mathbf{x}\, w_{\mathbf{0}}(\mathbf{x} - \mathbf{x}_j) e^{i(\mathbf{k}-\mathbf{k}')\cdot\mathbf{x}}, \tag{6.13}$$

and by using Eq. (6.9),

$$g_{\mathbf{k},\mathbf{k}',j} = g_{\mathrm{m}} e^{i(\mathbf{k}-\mathbf{k}')\cdot\mathbf{x}_j - \hbar(\mathbf{k}-\mathbf{k}')^2/2m\omega}, \tag{6.14}$$

with $g_{\mathrm{m}} = \sqrt{4g^2\pi\hbar/m\omega}$. The total action given by the sum of Eqs. (6.8), (6.11), and (6.12), describes the photon gas coupled to dye molecules in a periodic lattice in the single-band approximation. All the parameters that enter in this theory are now expressed in the experimentally tunable parameters λ and V_0.

6.3 Mean-field theory

The model derived in the previous section is rather complicated due to the fixed longitudinal momentum k_γ and the dependence of $g_{\mathbf{k},\mathbf{k}',i}$ on two independent momenta. To get a better understanding of the physics involved in this system, we first consider a simplified model that neglects both the nonzero value of k_γ and the non-diagonal coupling in $g_{\mathbf{k},\mathbf{k}',i}$. We return to the effects of these approximations in the second part of this section.

6.3.1 Toy model

We consider a toy model consisting of photons and molecules, where the molecules can only absorb and emit photons with very small momenta compared to the typical molecular momenta. Thus, we consider a model

with $S_{\rm ph}[a^*,a]$ and $S_{\rm mol}[b^*,b]$ given by respectively Eqs. (6.8) and (6.11), and $S_{\rm c}[a^*,a,b^*,b]$ is changed into

$$S_{\rm c}[a^*,a,b^*,b] = \frac{g_{\rm m}}{\sqrt{A}\sqrt{V}}\int_0^{\hbar\beta} d\tau \sum_{i,\mathbf{p}} \left\{ a_i^*(\tau) b_{\mathbf{p},\downarrow}^*(\tau) b_{\mathbf{p},\uparrow}(\tau) + a_i(\tau) b_{\mathbf{p},\uparrow}^*(\tau) b_{\mathbf{p},\downarrow}(\tau) \right\}. \tag{6.15}$$

Now, we use a mean-field approach to calculate the phase diagram of the photons. Therefore, we introduce the order parameter $\psi = \langle a_i(\tau)\rangle$. However, due to the coupling with the molecules, an expectation value of $a_i(\tau)$ will also induce a nonzero value for $\phi_{\mathbf{p}} = \langle b_{\mathbf{p},\uparrow}^*(\tau) b_{\mathbf{p},\downarrow}(\tau)\rangle$. Physically this implies that the molecules are forced into a linear superposition of its internal states. In the language of magnetism this means that the pseudospin of the molecules gets also a component in the x-y plane.

In the end we are only interested in the photons, and therefore we want to calculate $\phi_{\mathbf{p}}$ as a function of ψ. Since $S_{\rm ph}[a^*,a]$ is irrelevant for this calculation, we first only consider $S_{\rm c}[a^*,a,b^*,b]$ and $S_{\rm mol}[b^*,b]$. Up to linear order in the fluctuations, $S_{\rm c}[a^*,a,b^*,b]$ is given by

$$\begin{aligned} S_{\rm c}[a^*,a,b^*,b] &= \tilde{g}_{\rm m}\int_0^{\hbar\beta} d\tau \sum_{i,\mathbf{p}} \phi_{\mathbf{p}} \left[a_i(\tau) + a_i^*(\tau) \right] \\ &+ \tilde{g}_{\rm m} N_{\rm s}\psi \int_0^{\hbar\beta} d\tau \sum_{\mathbf{p}} \left\{ b_{\mathbf{p},\downarrow}^*(\tau) b_{\mathbf{p},\uparrow}(\tau) + b_{\mathbf{p},\uparrow}^*(\tau) b_{\mathbf{p},\downarrow}(\tau) - 2\phi_{\mathbf{p}} \right\}, \end{aligned} \tag{6.16}$$

where $\tilde{g}_{\rm m} = g_{\rm m}/\sqrt{A}\sqrt{V}$, $N_{\rm s}$ is the number of lattice sites, and without loss of generality we assume that both ψ and $\phi_{\mathbf{p}}$ are real.

We focus on the last part of the right-hand side of Eq. (6.16) to obtain an expression for $\phi_{\mathbf{p}}$. By using a Matsubara expansion we can write for the part of the action that depends on the molecular fields $b_\uparrow$ and $b_\downarrow$,

$$S_{\rm mf}[b^*,b] = \sum_{\mathbf{p},n} \begin{bmatrix} b_{\mathbf{p},n,\uparrow}^*, b_{\mathbf{p},n,\downarrow}^* \end{bmatrix} \cdot \begin{bmatrix} G_\uparrow^{-1} & \tilde{g}_{\rm m} N_{\rm s}\psi \\ \tilde{g}_{\rm m} N_{\rm s}\psi & G_\downarrow^{-1} \end{bmatrix} \cdot \begin{bmatrix} b_{\mathbf{p},n,\uparrow} \\ b_{\mathbf{p},n,\downarrow} \end{bmatrix}, \tag{6.17}$$

where $G_\rho^{-1} = -i\hbar\omega_n + \epsilon_{\mathbf{p}} + K_\rho - \mu_\rho$. Now we perform a unitary transformation to diagonalize the action. Thus, we define

$$v_{\mathbf{p},n} = \begin{bmatrix} \beta_{\mathbf{p},n,\uparrow} \\ \beta_{\mathbf{p},n,\downarrow} \end{bmatrix} = \begin{bmatrix} \cos(\theta) & -\sin(\theta) \\ \sin(\theta) & \cos(\theta) \end{bmatrix} \begin{bmatrix} b_{\mathbf{p},n,\uparrow} \\ b_{\mathbf{p},n,\downarrow} \end{bmatrix}. \tag{6.18}$$

Rewriting the action in terms of $v_{\mathbf{p},n}$ diagonalizes the action with on the

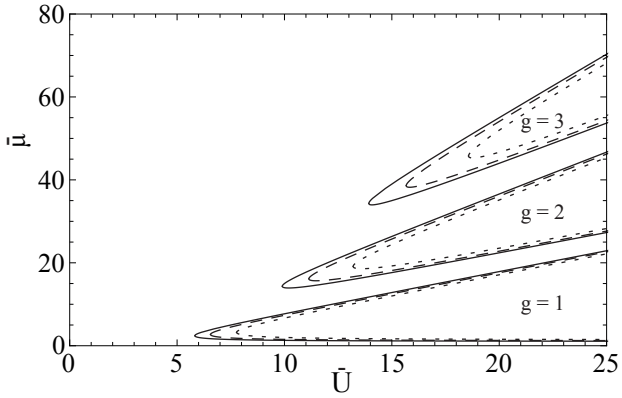

Figure 6.1: Phase diagram of the Bose-Hubbard Hamiltonian with the photon-molecule interaction parameter γ. From bottom to top, the three contributions are for, respectively, one, two or three particles per site. The solid, dashed, and dotted lines are for $\gamma = 0$, $\gamma = 1/2$ and $\gamma = 1$.

diagonal $-i\hbar\omega_n + \epsilon_{\mathbf{p}} + \Delta/2 - \lambda_{\pm}$ and

$$\lambda_{\pm} = \left(\mu_{\downarrow} + \mu_{\uparrow} \mp \sqrt{(\Delta - \Delta\mu)^2 + 4\tilde{g}_{\mathrm{m}}^2 N_{\mathrm{s}}^2 \psi^2}\right)/2. \tag{6.19}$$

Moreover,

$$\begin{aligned} \sin(2\theta) &= \frac{2\tilde{g}_{\mathrm{m}} N_{\mathrm{s}} \psi}{\sqrt{(\Delta - \Delta\mu)^2 + 4\tilde{g}_{\mathrm{m}}^2 N_{\mathrm{s}}^2 \psi^2}}, \\ \cos(2\theta) &= \frac{\Delta - \Delta\mu}{\sqrt{(\Delta - \Delta\mu)^2 + 4\tilde{g}_{\mathrm{m}}^2 N_{\mathrm{s}}^2 \psi^2}}. \end{aligned} \tag{6.20}$$

Here we define $\Delta\mu = \mu_{\uparrow} - \mu_{\downarrow}$. Furthermore, since $\langle \beta^*_{\downarrow,\mathbf{p}}(\tau)\beta_{\uparrow,\mathbf{p}}(\tau)\rangle = \langle \beta_{\downarrow,\mathbf{p}}(\tau)\beta^*_{\uparrow,\mathbf{p}}(\tau)\rangle = 0$, we obtain

$$\begin{aligned} \phi_{\mathbf{p}} = \langle b^*_{\mathbf{p},\downarrow}(\tau) b_{\mathbf{p},\uparrow}(\tau)\rangle &= \frac{\tilde{g}_{\mathrm{m}} N_{\mathrm{s}} \psi}{\sqrt{(\Delta - \Delta\mu)^2 + 4\tilde{g}_{\mathrm{m}}^2 N_{\mathrm{s}}^2 \psi^2}} \\ &\times \left\{ N_{\mathrm{MB}}(\epsilon_{\mathbf{p}} + \Delta/2 - \lambda_+) - N_{\mathrm{MB}}(\epsilon_{\mathbf{p}} + \Delta/2 - \lambda_-) \right\}, \end{aligned} \tag{6.21}$$

where we again considered the Maxwell-Boltzmann limit as the system is at room temperature. As already mentioned, this equation explicitly shows that $\psi \neq 0$ also implies a nonzero value of $\phi_{\mathbf{p}}$.

In order to further investigate the properties of the photons, we substitute this result into the action in Eq. (6.16). To compare with results for standard Hubbard models as in, for example, Ref. [153], we switch to the

Hamiltonian formalism. In the thermodynamic limit the effective Hamiltonian that describes the photons in the mean-field approximation is now given by

$$\begin{aligned}\hat{H}^{\text{eff}} = zt\psi^2 N_{\text{s}}\left[1+2\gamma\right] + \frac{U}{2}\sum_i \hat{n}_i\left(\hat{n}_i - 1\right) \\ - zt\psi\left[1+\gamma\right]\sum_i\left(\hat{a}_i + \hat{a}_i^\dagger\right) - \mu\sum_i \hat{n}_i,\end{aligned} \tag{6.22}$$

where we only consider tunneling between nearest neighbors, z is the number of nearest neighbors, $\hat{n}_i = \hat{a}_i^\dagger \hat{a}_i$ is the photon-number operator and

$$\gamma = \frac{\tilde{g}_{\text{m}}}{zt}\sum_{\mathbf{p}}\phi_{\mathbf{p}} = \frac{g_{\text{m}}^2}{zt}\frac{P(\Delta\mu)}{\Delta\mu - \Delta}\left(\frac{m_{\text{d}}}{m_{\text{d,real}}}\right)^{3/2} n_{\text{s}} n_{\text{mol}}. \tag{6.23}$$

Here $P(\Delta\mu)$ denotes the polarization of the molecules as defined in Ref. [75], $m_{\text{d,real}}$ is the real mass of the dye molecules, and n_{mol} equals the density of molecules. Furthermore, $n_{\text{s}} = N_{\text{s}}/A$ is the density of sites. Moreover, note that $\gamma > 0$ as the polarization $P(\Delta\mu)$ and $\Delta\mu - \Delta$ have the same sign for all values of $\Delta\mu$. Moreover, recall that we modeled the molecules as a two-level system with an effective mass, and therefore the ratio $m_{\text{d}}/m_{\text{d,real}}$ appears in the final result.

By introducing $\bar{U} = U/zt$ and $\bar{\mu} = \mu/zt$, we define $\hat{H}^{\text{eff}} = zt\sum_i \hat{H}_i$ and the Hamiltonian $\hat{H}_i$ at each site i as

$$\hat{H}_i = \frac{\bar{U}}{2}\hat{n}_i\left(\hat{n}_i - 1\right) + \psi^2\left[1+2\gamma\right] - \bar{\mu}\hat{n}_i - \psi\left[1+\gamma\right]\left(\hat{a}_i + \hat{a}_i^\dagger\right). \tag{6.24}$$

To calculate the phase diagram of the photons in the dye-filled cavity, we use the usual Landau theory for second-order phase transitions. Hence, we write the energy of the ground state as

$$E_{\text{g}}(\psi) = a_0(g, \bar{U}, \bar{\mu}) + a_2(g, \bar{U}, \bar{\mu})\psi^2 + \mathcal{O}(\psi^4), \tag{6.25}$$

and we minimize this energy. The corresponding value of ψ determines the phase of the system. For $a_2(g, \bar{U}, \bar{\mu}) \geq 0$, $\psi = 0$ and the system is inside a Mott lobe. Differently, for $a_2(g, \bar{U}, \bar{\mu}) < 0$ we have that $\psi \neq 0$ and the photons are in the superfluid phase. This distinction becomes clear if we consider the ground state of the system. At the level of mean-field theory, the ground state inside the Mott lobe is a state with a well-defined number of particles at each site. Therefore, we obtain $\psi = \langle \hat{a}_i \rangle = 0$ as the states with a different number of photons per site are orthogonal.

Furthermore, in the superfluid phase the number of particles per site is not sharply defined. Thus, the ground state is a linear superposition of number states and therefore $\psi \neq 0$.

To investigate the phase transition we determine $a_2(g, \bar{U}, \bar{\mu})$ by following Ref. [153] and perform second-order perturbation theory. Therefore, we split the Hamiltonian in an exactly solvable part $\hat{H}_0$ and a perturbation $\psi\,[1+\gamma]\,\hat{V}$. In this case

$$\hat{H}_0 = \frac{\bar{U}}{2}\hat{n}_i\left(\hat{n}_i - 1\right) + \psi^2\left[1 + 2\gamma\right] - \bar{\mu}\hat{n}_i, \tag{6.26}$$

and

$$\hat{V} = \left(\hat{a}_i + \hat{a}_i^\dagger\right). \tag{6.27}$$

In perturbation theory the second-order correction to the energy reads

$$E_{\mathrm{g}}^{(2)} = \psi^2\left[1+\gamma\right]^2 \sum_{n \neq g} \frac{|\langle n|\hat{V}|g\rangle|^2}{E_{\mathrm{g}}^{(0)} - E_{\mathrm{n}}^{(0)}}, \tag{6.28}$$

where $|n\rangle$ is the state with n particles and for $n = g$ this state is the ground state. Furthermore, $E_{\mathrm{n}}^{(0)}$ is the energy of the state $|n\rangle$ with respect to the exactly solvable Hamiltonian $\hat{H}_0$. Again analogous to Ref. [153], we obtain

$$a_2(g, \bar{U}, \bar{\mu}) = \left[1+\gamma\right]^2 \left(\frac{g}{\bar{U}(g-1) - \bar{\mu}} + \frac{g+1}{\bar{\mu} - \bar{U}g}\right) + 1 + 2\gamma \tag{6.29}$$

for $\bar{U}(g-1) < \bar{\mu} < \bar{U}g$. The boundary of the Mott lobes can be found by solving $a_2(g, \bar{U}, \bar{\mu}_\pm) = 0$ for $\bar{\mu}_\pm$. We find

$$\bar{\mu}_\pm = \frac{1}{2}\left((2g-1)\bar{U} - 1/\Gamma\right) \pm \frac{1}{2\Gamma}\sqrt{1 + \bar{U}\Gamma(\bar{U}\Gamma - 4g - 2)}, \tag{6.30}$$

where $\Gamma = (1+2\gamma)/(1+\gamma)^2 < 1$. In Fig. 6.1 we present a plot of the two branches of Eq. (6.30) for several values of γ. We obtain that for increasing γ, the size of the Mott lobes decreases. Physically this makes sense as the absorption and emission of photons by the molecules effectively increases the hopping of photons between different lattice sites. Furthermore, we note that for increasing number of particles in the ground state the effect of γ also increases. Moreover, the smallest $\bar{U}$ for each Mott lobe is equal to

$$\bar{U}_{\mathrm{c}} = \left(2g + 1 + \sqrt{(2g+1)^2 - 1}\right)/\Gamma = \bar{U}_{\mathrm{c},0}/\Gamma, \tag{6.31}$$

with $\bar{U}_{\mathrm{c},0}$ the result obtained in Ref. [153] for $\gamma = 0$ and correspondingly $\Gamma = 1$.

To estimate the value of γ, we want to express this coefficient in terms of the experimental parameters λ and V_0. As mentioned before, λ is twice the lattice spacing and V_0 is the depth of the lattice potential. From Eq. (6.23) it follows that we have to find an expression for t. From Ref. [154], we obtain

$$\tilde{t} = \frac{4\tilde{V}_0^{3/4}}{\pi^{1/4}} \left(\frac{\Lambda_{\mathrm{th}}}{\lambda}\right)^{1/2} \exp\left\{-2\left(\frac{\lambda}{\Lambda_{\mathrm{th}}}\right)\sqrt{\frac{\tilde{V}_0}{\pi}}\right\}. \tag{6.32}$$

Here $\Lambda_{\mathrm{th}} = (2\pi\hbar^2/mk_{\mathrm{B}}T)^{1/2}$ is the thermal de Broglie wavelength, $\tilde{V}_0 = V_0/k_{\mathrm{B}}T$ and $\tilde{t} = t/k_{\mathrm{B}}T$. For the two-dimensional squared periodic potential considered here, we take $n_{\mathrm{s}} = 4/\lambda^2$ and $z = 4$. Hence,

$$\gamma = \left(\frac{m_{\mathrm{eff}}}{m_{\mathrm{real}}}\right)^{\frac{3}{2}} \frac{n_{\mathrm{mol}}}{4\pi^{1/4}} \sqrt{\frac{\Lambda_{\mathrm{th}}}{\lambda}} \frac{g^2\beta}{\tilde{V}_0^{5/4}} \frac{P(\Delta\mu)}{\Delta\mu - \Delta} e^{\frac{2\lambda}{\Lambda_{\mathrm{th}}}\sqrt{\frac{\tilde{V}_0}{\pi}}}. \tag{6.33}$$

In Fig. 6.2 we use this expression for γ to illustrate the phase diagram for $\beta|\Delta\mu - \Delta| < 1$ and $z = 4$. For these chemical potentials we can approximate $P(\Delta\mu)/\beta(\Delta\mu - \Delta) \simeq 1/2$ and for other quantities such as g, m_{d}, and $m_{\mathrm{d,real}}$ we take the numerical values as found in Ref. [75].

6.3.2 Photon model

Up to now we only considered the terms with diagonal coupling in momentum space and we neglected the fixed momentum k_γ of the photon in the longitudinal direction. In the following we consider the effect of these approximations on the phase diagram presented in the previous section. Therefore, here we consider the full action consisting of the sum of Eqs. (6.8-6.12). In accordance with the previous calculation, we define $\langle b^*_{(\mathbf{k}',q),\downarrow}(\tau) b_{(\mathbf{k},q_-),\uparrow}(\tau)\rangle = \phi_{\mathbf{k},\mathbf{k}',q_-}$ and $\langle a_{\mathrm{i}}\rangle = \psi$. The expectation value of the molecular fields that depend on q_+ are denoted by $\phi_{\mathbf{k},\mathbf{k}',q_+}$.

Now we perform a mean-field approximation and we calculate $\phi_{\mathbf{k},\mathbf{k}',p_{\mathrm{z}}}$ as a function of ψ. Therefore, we consider $S_{\mathrm{mol}}[b^*, b]$ and

$$\begin{aligned} S_{\mathrm{c}}[a^*, a, b^*, b] = & \\ & \frac{iN_{\mathrm{s}}\psi}{\sqrt{2AV}} \int_0^{\hbar\beta} d\tau \sum_{\mathbf{k},\mathbf{G},q} g_{\mathbf{G}} b^*_{(\mathbf{k}+\mathbf{G},q),\downarrow}(\tau) b_{(\mathbf{k},q_+),\uparrow}(\tau) + \mathrm{h.c.} \\ & - \frac{iN_{\mathrm{s}}\psi}{\sqrt{2AV}} \int_0^{\hbar\beta} d\tau \sum_{\mathbf{k},\mathbf{G},q} g_{\mathbf{G}} b^*_{(\mathbf{k}+\mathbf{G},q),\downarrow}(\tau) b_{(\mathbf{k},q_-),\uparrow}(\tau) + \mathrm{h.c.}, \end{aligned} \tag{6.34}$$

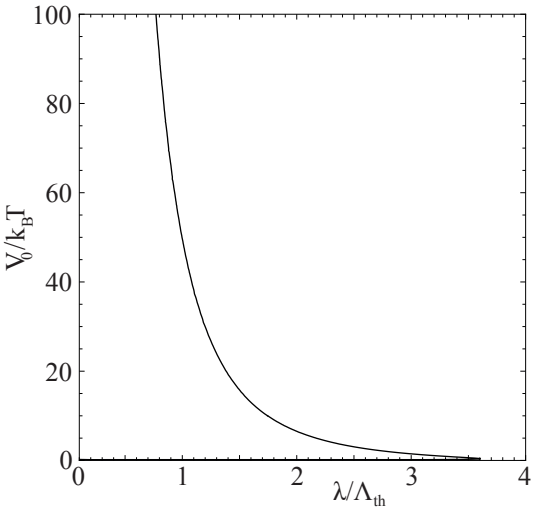

Figure 6.2: Plot of the values of γ in terms of the experimental parameters V_0 and λ. We used $n_{\mathrm{mol}} = 9 \cdot 10^{23}\,\mathrm{m}^{-3}$, $T = 300\,\mathrm{K}$, and $\beta|\Delta\mu - \Delta| < 1$. Furthermore, Λ_{th} is the thermal de Broglie wavelength. On the right-hand side of the solid line $\gamma > 1/2$ and the corrections to the Mott lobes are important. To the left of the solid line $\gamma < 1/2$ and the effect of the photon-molecule coupling γ on the Mott lobes is small. Finally, these results are only valid if thermal fluctuations are small $k_{\mathrm{B}}T \ll \hbar\omega$ or $4\pi V_0/k_{\mathrm{B}}T \gg (\lambda/\Lambda_{\mathrm{th}})^2$.

where without loss of generality we again assume that ψ is real. Furthermore, we perform the summation over the lattice sites. After this summation the coupling constant $g_{\mathbf{k},\mathbf{k}',i}$, given by Eq. (6.14), only depends on a two-dimensional reciprocal lattice vector $\mathbf{G}$. Here we consider Eq. (6.2), and therefore we have a cubic lattice with lattices sites $(n\lambda/2 - \lambda/4, m\lambda/2 - \lambda/4)$ with n and m integers. Therefore, $\mathbf{G} = 4\pi\mathbf{n}/\lambda$ with $\mathbf{n} = (n_x, n_y)$ and n_x and n_y integers. Hence,

$$g_{\mathbf{G}} = g_{\mathrm{m}} \exp\left\{ -\frac{2}{\tilde{\lambda}} \sqrt{\frac{\pi}{\tilde{V}_0}} \left(n_x^2 + n_y^2\right) \right\}, \tag{6.35}$$

where $\tilde{\lambda} = \lambda/\Lambda_{\mathrm{th}}$ and $\tilde{V}_0 = V_0/k_{\mathrm{B}}T$.

To calculate $\phi_{\mathbf{k},\mathbf{k}',q}$ we in principle have to invert an infinite-dimensional matrix. However, we are generally interested in the phase transition and therefore we only need to calculate the inverse of this infinite-dimensional matrix up to linear order in ψ. Since all the off-diagonal terms of this infinite dimensional matrix are already linear in ψ, we obtain up to linear

order in ψ

$$\phi_{\mathbf{k},\mathbf{k}+\mathbf{G},q_+} = \frac{-iN_\mathrm{s}\psi g_\mathbf{G}}{\sqrt{2AV}} \frac{N_\mathrm{MB}(\epsilon(\mathbf{k},q_+)-\mu_\uparrow+\Delta)-N_\mathrm{MB}(\epsilon(\mathbf{k}+\mathbf{G},q)-\mu_\downarrow)}{\epsilon(\mathbf{k},q_+)-\epsilon(\mathbf{k}+\mathbf{G},q)+\Delta-\Delta\mu}, \tag{6.36}$$

where we consider the classical limit. We again combine the effects of the molecules in the parameter γ, which in this case reads

$$\gamma = \frac{n_\mathrm{s}}{ztV} \sum_{\mathbf{k},n_x,n_y,q} g_\mathrm{m}^2 \exp\left\{-\frac{4}{\tilde{\lambda}}\sqrt{\frac{\pi}{\tilde{V}_0}}\left(n_x^2+n_y^2\right)\right\} \times \frac{N_\mathrm{MB}(\epsilon(\mathbf{k},q_+)-\mu_\uparrow+\Delta)-N_\mathrm{MB}(\epsilon(\mathbf{k}+\mathbf{G},q)-\mu_\downarrow)}{\Delta\mu-\Delta+\epsilon(\mathbf{k}+\mathbf{G},q)-\epsilon(\mathbf{k},q_+)}, \tag{6.37}$$

where we used that the contributions of both $\phi_{\mathbf{k},\mathbf{k}+\mathbf{G},q_+}$ and $\phi_{\mathbf{k},\mathbf{k}+\mathbf{G},q_-}$ are the same. Note that for $k_\gamma = 0$ and if we only consider $n_x = n_y = 0$, we recover our previous result from the simplified model.

To determine γ we have to evaluate a sum over an infinite number of terms. However, by performing a numerical analysis we obtain that the contribution rapidly decreases for increasing n_x and n_y. Therefore, it suffices to only take into account the terms where both $n_x \leq 1$ and $n_y \leq 1$. Since γ depends on $\Delta\mu$, we obtain a different phase diagram for every value of $\Delta\mu$. However, although there are quantitative differences, the qualitative results of the calculations are not dependent on the precise value of $\Delta\mu$. Therefore, in comparison with the previous calculation, we again take $\beta|\Delta-\Delta\mu| < 1$.

In Fig. 6.3 we show a comparison between the values of γ in the thermodynamic limit as a function of the experimental parameters V_0 and λ, for the full photon model discussed here and the simplified model used previously. As can be seen from the figure, both results are qualitatively the same. However, quantitatively there are some differences between both results. The largest difference occurs for relatively small values of V_0. Namely, for $V_0/k_\mathrm{B}T < 2$ the full photon model results in a larger region where the value of γ is relatively small. For larger V_0 both results are remarkably close, and the full model has only a marginally larger region where the effects of the molecule coupling are important.

6.4 Number fluctuations inside the Mott lobes

In the previous section we constructed a self-consistent mean-field theory to investigate the effect of the photon-molecule coupling on the phase diagram of the photonic lattice in a dye-filled optical microcavity. However, to

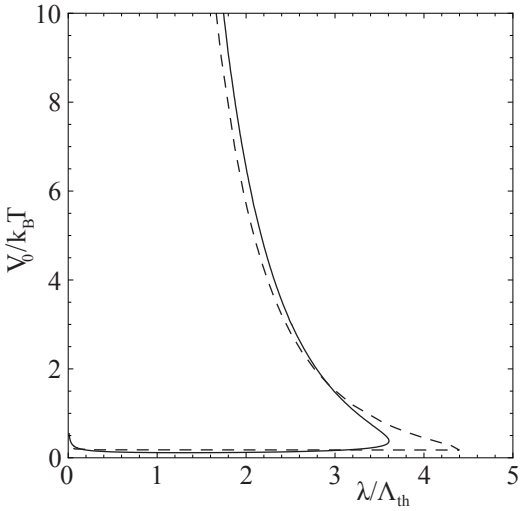

Figure 6.3: Plot of the values of γ for the complete photon model and the simplified model in terms of the experimental parameters V_0 and λ. The simplified model is represented by the solid line and the full model is depicted by the dashed line. On the right-hand side of both lines $\gamma > 1/2$ and here the Mott lobes are noticeably affected by the photon-molecule coupling. In this plot, we take $\Lambda_{\rm th} \simeq 1.6 \cdot 10^{-6}\,\mathrm{m}$ and the numerical values for the other parameters and the conditions are the same as given below Fig. 6.2.

obtain more information about the physics in the Mott lobes, we have to go beyond mean-field theory and also include fluctuations. Since the theory in the previous section cannot easily be generalized to describe these fluctuations, we now use functional methods instead of the operator methods used previously. This has the advantage that it is relatively straightforward to include fluctuations at zero temperature.

Similar to the approach in Ref. [75], we integrate out the molecules and expand up to second order in the coupling constant g. Thus, we obtain

$$S[a^*,a] = \int_0^{\hbar\beta} d\tau \sum_i a_i^*(\tau)\left(\hbar\frac{\partial}{\partial\tau} - \mu + \frac{U}{2}|a_i(\tau)|^2\right)a_i(\tau) \qquad (6.38)$$
$$- \int_0^{\hbar\beta} d\tau \int d\tau' \sum_{i,j} a_i^*(\tau) G_{i,j}^{-1}(\tau-\tau') a_j(\tau'),$$

with

$$G_{i,j}^{-1}(\tau-\tau') = t_{i,j}\delta(\tau-\tau') - \hbar\Sigma_{i,j}(\tau-\tau'), \qquad (6.39)$$

and

$$\hbar\Sigma_{i,j}(\tau-\tau') = \frac{1}{AV}\sum_{\mathbf{k},\mathbf{k}',p_z} g_{\mathbf{k},\mathbf{k}',i}\, g^*_{\mathbf{k},\mathbf{k}',j} G_{\downarrow}(\tau'-\tau,\mathbf{k}',p_z) G_{\uparrow}(\tau-\tau',\mathbf{k},p_z+k_\gamma). \tag{6.40}$$

Here, the coupling constant $g_{\mathbf{k},\mathbf{k}',i}$ is defined in Eq. (6.14) and the Green's function of the excited-state molecules or ground-state molecules is given by $G_\sigma(\tau'-\tau,\mathbf{k}',p_z)$. From these expressions we obtain that the interaction with the molecules is an additional mechanism for the photons to hop between different lattice sites. Since $\hbar\Sigma_{i,i}(\tau-\tau') \neq 0$, the interaction with the molecules also contributes to the on-site Green's function of the photons. To decouple the hopping term we perform a Hubbard-Stratonovich transformation to the action, and we write

$$S[a,a^*,\psi^*,\psi] = S[a^*,a] + \int_0^{\hbar\beta} d\tau \int_0^{\hbar\beta} d\tau' \sum_{i,j} \left(a_i^*(\tau)-\psi_i^*(\tau)\right) G^{-1}_{i,j}(\tau-\tau') \left(a_j(\tau')-\psi_j(\tau')\right), \tag{6.41}$$

where $\psi_i(\tau)$ is the complex order-parameter field. Following the procedure described in Ref. [153], we calculate the action up to second order in ψ and obtain

$$\begin{aligned} S^{(2)}[\psi^*,\psi] &= \int_0^{\hbar\beta} d\tau \int_0^{\hbar\beta} d\tau' \sum_{i,j} \psi_i^*(\tau) G^{-1}_{i,j}(\tau-\tau')\psi_j(\tau') \\ &- \frac{1}{\hbar}\int_0^{\hbar\beta} d\tau \int_0^{\hbar\beta} d\tau' \int_0^{\hbar\beta} d\tau'' \int_0^{\hbar\beta} d\tau''' \sum_{i,j,i',j'} \psi_i^*(\tau) \\ &\times G^{-1}_{i,j'}(\tau-\tau''')\langle a_{j'}(\tau''') a_{i'}^*(\tau'')\rangle_0 G^{-1}_{i',j}(\tau''-\tau')\psi_j(\tau'). \end{aligned} \tag{6.42}$$

Here $\langle ... \rangle_0$ denotes the expectation value with respect to the action defined in Eq. (6.41) for $G^{-1}_{i,j}(\tau-\tau') = 0$. Now, we separately calculate the first and second part of this action. First, we define

$$\psi_i(\tau) = \frac{1}{\sqrt{\hbar\beta N_{\mathrm{s}}}} \sum_{\mathbf{k},n} \psi_{\mathbf{k},n} e^{i(\mathbf{k}\cdot\mathbf{x}_i - \omega_n\tau)}, \tag{6.43}$$

where $\mathbf{k}$ only runs over the first Brillouin zone. We substitute the Fourier expansions of $\psi_i(\tau)$ and $\hbar\Sigma_{i,j}(\tau-\tau')$ and again we take t_{ij} equal to t for nearest neighbors and zero otherwise. By performing the integrations over

τ and τ', we obtain

$$\int_0^{\hbar\beta} d\tau \int_0^{\hbar\beta} d\tau' \sum_{i,j} \psi_i^*(\tau) G_{i,j}^{-1}(\tau-\tau')\psi_j(\tau') = -\sum_{\mathbf{k},n} G_{\mathrm{m}}^{-1}(\mathbf{k}, i\omega_n)\psi_{\mathbf{k},n}^*\psi_{\mathbf{k},n}, \tag{6.44}$$

where

$$G_{\mathrm{m}}^{-1}(\mathbf{k}, i\omega_n) = \epsilon_{\mathbf{k}} + \frac{16\pi\hbar}{m\lambda^2\omega}\hbar\Sigma(\mathbf{k}, k_\gamma, i\omega_n). \tag{6.45}$$

Here, we use that we are inside a Mott lobe where ω is sufficiently large and therefore we use the approximation that $|g_{\mathbf{k},\mathbf{k}',i}|^2 = |g_{\mathrm{m}}|^2$. Note that if we perform the Wick rotation to real frequencies in $\hbar\Sigma(\mathbf{k}, k_\gamma, i\omega_n)$, we obtain the retarded self-energy as calculated in Ref. [75]. Furthermore, the lattice dispersion $\epsilon_{\mathbf{k}}$ is given by

$$\epsilon_{\mathbf{k}} = -2t\sum_{j=1}^{2}\cos(k_j\lambda/2). \tag{6.46}$$

Similar to the calculation in the previous section, the periodicity of the photons induces the introduction of reciprocal lattice vectors for the molecules. The incorporation of these vectors gives additional contributions that are off-diagonal in momentum space. However, especially inside the Mott lobes these contributions are small. Since in this section we only consider that part of the phase diagram, these contributions are neglected throughout the rest of this section.

The calculation of the second term of Eq. (6.42) is more involved. However, we only consider the zero-temperature case and therefore we can use some results from Ref. [153]. Similarly, we obtain

$$\langle a_{j'}(\tau)a_{i'}^*(\tau')\rangle_0 = \delta_{i',j'}\langle a_{i'}(\tau)a_{i'}^*(\tau')\rangle_0, \tag{6.47}$$

with

$$\langle a_i(\tau)a_i^*(\tau')\rangle_0 = \Theta(\tau-\tau')(g+1)e^{(\mu-gU)(\tau-\tau')/\hbar} + \Theta(\tau'-\tau)ge^{(\mu-(g-1)U)(\tau-\tau')/\hbar}. \tag{6.48}$$

Again, by only taking into account nearest-neighbor hopping we can evaluate the second term of Eq. (6.42) explicitly. By using Eqs. (6.39), (6.40), (6.43), and (6.48), we can perform the integration over imaginary time and

summations over lattice sites. Combining this result with Eq. (6.44), we find

$$S^{(2)}[\psi^*,\psi] = -\hbar \sum_{\mathbf{k},n} \psi^*_{\mathbf{k},n} G^{-1}(\mathbf{k}, i\omega_n)\psi_{\mathbf{k},n}, \tag{6.49}$$

where the inverse Green's function obeys

$$\begin{aligned}\hbar G^{-1}(\mathbf{k}, i\omega_n) &= G^{-1}_{\mathrm{m}}(\mathbf{k}, i\omega_n) \\ &\times \left\{1 + G^{-1}_{\mathrm{m}}(\mathbf{k}, i\omega_n)\left(\frac{g+1}{-i\hbar\omega_n - \mu + gU} + \frac{g}{i\hbar\omega_n + \mu - (g-1)U}\right)\right\}.\end{aligned} \tag{6.50}$$

As the quadratic coefficient $a_2(g,\mu,U)$ of the Landau free energy coincides with $-\hbar G^{-1}(\mathbf{0},0)/zt$, this expression allows us to compare this theory with the result from the previous section. By using the expression for the self-energy in Ref. [75], we obtain

$$-\frac{\hbar G^{-1}(\mathbf{0},0)}{zt} = (1+\gamma)\left[1 + (1+\gamma)\left\{\frac{g}{\bar{U}(g-1) - \bar{\mu}} + \frac{g+1}{\bar{\mu} - \bar{U}g}\right\}\right]. \tag{6.51}$$

Since in this approach we do not take into account the nonzero expectation value of $\langle b^*_{\mathbf{p}',\downarrow}(\tau) b_{\mathbf{p},\uparrow}(\tau)\rangle$, we arrive at a slightly different coefficient $a_2(g,\mu,U)$ as found in Eq. (6.29). Both mean-field theories are however qualitatively the same as they lead to shrinking Mott lobes for increasing values for γ. Although the exact position of the phase boundary of the Mott lobes is slightly different, we expect that inside these loops both approaches are equivalent as in this region of the phase diagram the expectation value of the photon annihilation operator and therefore $\langle b^*_{\mathbf{p}',\downarrow}(\tau) b_{\mathbf{p},\uparrow}(\tau)\rangle$ is zero.

6.4.1 Quasiparticle excitations

We include the Gaussian fluctuations to obtain $\langle a_i(\tau) a^*_{i'}(\tau')\rangle$, and thereby calculate the quasihole and quasiparticle excitations in the Mott lobes. To obtain a relation between this correlator of photon operators and the correlator of the Hubbard-Stratonovich fields $\langle \psi^*_i(\tau)\psi_j(\tau')\rangle$, we add sources $J_i(\tau)$ and $J^*_i(\tau)$ that couple to $a_i(\tau)$ and $a^*_i(\tau)$. Instead of the Hubbard-Stratonovich transformation used in Eq. (6.41), we now add

$$\begin{aligned}\int_0^{\hbar\beta} d\tau \int_0^{\hbar\beta} d\tau' \sum_{i,j} &\left\{a^*_i(\tau) - \psi^*_i(\tau) + \left[J\cdot G\right]_i(\tau)\right\} \\ &\times G^{-1}_{i,j}(\tau-\tau')\left\{a_j(\tau') - \psi_j(\tau') + \left[G\cdot J\right]_j(\tau')\right\},\end{aligned} \tag{6.52}$$

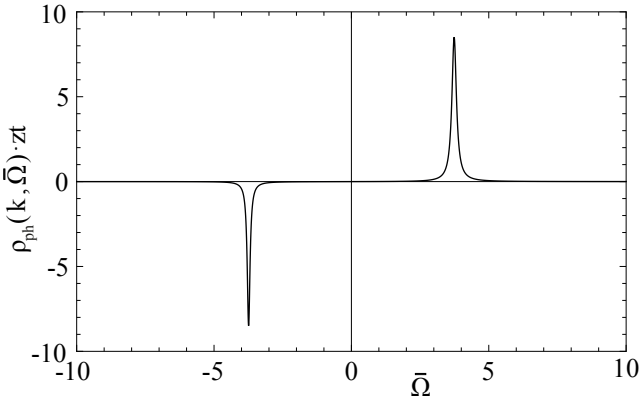

Figure 6.4: Plot of the spectral function of the photons $\rho_{\mathrm{ph}}(\mathbf{k}, \bar{\Omega})$ inside the $g = 1$ Mott lobe as a function of $\bar{\Omega} = \Omega/zt$ for $\mathbf{k} = 0$, $U/zt = 11$, $\mu/zt = 5$ and $\alpha_{\mathrm{lat}} = 10^{-2}$. The incorporation of the photon-molecule coupling broadens the peaks that are located at the quasihole and quasiparticle excitations.

to the action in Eq. (6.38). Here we introduce short-hand notation for the convolution

$$[J \cdot G]_i(\tau) = \sum_{i'} \int d\tau'' \, \hbar J^*_{i'}(\tau'') G_{i',i}(\tau'' - \tau). \tag{6.53}$$

By differentiation of the partition function with respect to the currents, we obtain

$$\langle a^*_i(\tau) a_j(\tau') \rangle = \langle \psi^*_i(\tau) \psi_j(\tau') \rangle - \hbar G_{i,j}(\tau - \tau'). \tag{6.54}$$

Denoting the Fourier transform of $\langle a^*_i(\tau) a_j(\tau') \rangle$ by $G_{\mathrm{ph}}(\mathbf{k}, i\omega_n)$, we therefore find that

$$\begin{aligned} -\frac{1}{\hbar} G_{\mathrm{ph}}(\mathbf{k}, i\omega_n) = &\left(\frac{g+1}{-i\hbar\omega_n - \mu + gU} + \frac{g}{i\hbar\omega_n + \mu - (g-1)U} \right) \\ &\times \left[1 + G^{-1}_{\mathrm{m}}(\mathbf{k}, i\omega_n) \left(\frac{g+1}{-i\hbar\omega_n - \mu + gU} + \frac{g}{i\hbar\omega_n + \mu - (g-1)U} \right) \right]^{-1}. \end{aligned} \tag{6.55}$$

The excitations of the photons in the Mott lobes correspond to the zeros of this inverse Green's function $G_{\mathrm{ph}}(\mathbf{k}, \Omega)$, where we perform an analytic continuation $i\omega_n \to \Omega$. Note that for large interactions U the excitations are also at large frequencies. At these large frequencies the self-energy vanishes and we obtain the usual results. However, for intermediate U for which we are inside a Mott lobe and the excitations are still at relatively small frequencies, the self-energy is important. In the following we ignore

the real part of the self-energy, since this part, to a good approximation, only results in a shift of dispersions.

By assuming that the excitation are at relatively small energies, we can approximate $\hbar\Sigma^{+}(\mathbf{k}, k_\gamma, \Omega) \simeq -i\alpha\hbar\Omega$. Here α is the small dimensionless damping parameter we calculated in previous work [75]. Up to linear order in α, we obtain

$$\begin{aligned}\hbar\Omega_{\mathbf{k}}^{\pm} &= (1 - i\alpha_{\mathrm{lat}})\hbar\omega_{\mathbf{k}}^{\pm} \\ &\quad - \frac{i}{2}\alpha_{\mathrm{lat}}\left\{U + \mu \pm \frac{(2g^2-1)U^2 - U\left[\epsilon_{\mathbf{k}} + \mu(1+2g)\right] - \epsilon_{\mathbf{k}}\mu}{\hbar\omega_{\mathbf{k}}^{+} - \hbar\omega_{\mathbf{k}}^{-}}\right\},\end{aligned} \tag{6.56}$$

where $\alpha_{\mathrm{lat}} = 8\pi\hbar\alpha/m\omega\lambda^2$. Furthermore, $\hbar\omega_{\mathbf{k}}^{+}$ and $\hbar\omega_{\mathbf{k}}^{-}$ denote the quasiparticle and quasihole excitations as calculated in Ref. [153].

Moreover, we can also calculate the spectral function that is defined as

$$\rho_{\mathrm{ph}}(\mathbf{k}, \Omega) = -\frac{1}{\pi\hbar}\mathrm{Im}\left[G_{\mathrm{ph}}(\mathbf{k}, \Omega)\right]. \tag{6.57}$$

In Fig. 6.4 we show a plot of the spectral function of the photons inside the $g = 1$ Mott lobe for $\mathbf{k} = \mathbf{0}$. The spectral function has two peaks, one around the quasihole excitations and the other located at the quasiparticle dispersion. Due to the interaction of the photons with the molecules, the peaks are broadened. The width of the peaks is determined by the value of α_{lat}, and the larger this parameter the broader the peaks become. Furthermore, due to the approximation of the self-energy, the sum rule is modified and reads

$$\int d(\hbar\Omega)\rho_{\mathrm{ph}}(\mathbf{k}, \Omega) = \frac{1}{1 + \alpha_{\mathrm{lat}}^2}, \tag{6.58}$$

which is the same sum rule as already encountered in Ref. [75]. Thus for relatively small α_{lat} the sum rule is to a very good approximation satisfied. Note that we can exactly satisfy the sum-rule, by taking the full energy dependence of the self-energy into account and not using only its low-energy approximation.

6.4.2 Number fluctuations

Apart from the excitations and the spectral function inside the Mott lobes, we can also use the presented theory to calculate the number fluctuations. For a Bose gas in an optical lattice that is described by the Bose-Hubbard model, the true Mott insulator state only exists at zero temperature as at this temperature the number fluctuations inside the Mott lobes vanish. However, for nonzero temperatures thermal fluctuations always induce

number fluctuations, and strictly speaking there is no Mott insulator. As we show next, in this system of photons in a dye-filled microcavity even at zero temperature the number of photons in the Mott lobes fluctuates. Therefore, for the photons in the dye-filled optical microcavity the true Mott-insulating state does not exist due to the fluctuations induced by the absorption and emission of photons by the dye molecules.

To calculate the number of photons inside the Mott lobes, we first determine the thermodynamic potential. After the Hubbard-Stratonovich transformation that decouples the hopping term, the thermodynamic potential consist of two separate parts. The exactly solvable part is given by the eigenvalue of the Hamiltonian $\hat{H}_0$ in Eq. (6.26) with $\psi = 0$. The other part is described by Eq. (6.49) and the contribution to the thermodynamic potential can be calculated by integrating out ψ in the Gaussian approximation. Hence,

$$\Omega = N_{\mathrm{s}} E_0 + \frac{1}{\beta} \mathrm{Tr} \left[\log \left(-\hbar \beta G^{-1} \right) \right], \tag{6.59}$$

where the inverse Green's function G^{-1} is defined in Eq. (6.50), and E_0 is the energy of the Hamiltonian in the Mott lobe with g photons. Thus,

$$E_0 = \frac{1}{2} U g(g-1) - \mu g. \tag{6.60}$$

Note that the thermodynamic potential also has a contribution from the fact that we change the partition function if we simply add a complete square to the action. Namely, by performing the Hubbard-Stratonovich transformation we should multiply exactly with one and therefore the thermodynamic potential has an additional contribution that depends on the self-energy induced by the molecules and the hopping parameter. However, both do not have an explicit dependence on the chemical potential of the photons. Therefore, if we calculate densities by taking a partial derivative of the thermodynamic potential with respect to this chemical potential, this additional contribution has no effect.

Thus the number of photons per site in the Mott lobe is given by

$$n = -\frac{1}{N_{\mathrm{s}}} \frac{\partial \Omega}{\partial \mu} = g - \frac{1}{\beta N_{\mathrm{s}}} \sum_{\mathbf{k},n} G(\mathbf{k}, i\omega_n) \frac{\partial G^{-1}(\mathbf{k}, i\omega_n)}{\partial \mu}. \tag{6.61}$$

In this expression we cannot simply perform the sum over Matsubara frequencies analytically, since the self-energy has a non-trivial imaginary part. Therefore, we define

$$\rho_{\mathrm{ml}}(\mathbf{k}, \Omega) = -\frac{1}{\pi} \mathrm{Im} \left[G(\mathbf{k}, \Omega^+) \frac{\partial G^{-1}(\mathbf{k}, \Omega^+)}{\partial \mu} \right], \tag{6.62}$$

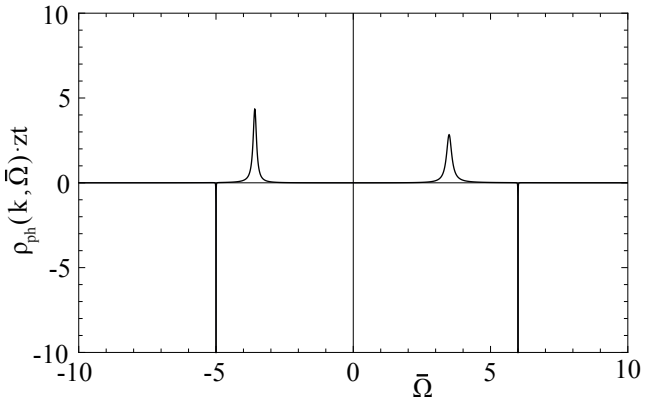

Figure 6.5: Plot of the spectral function $\rho_{\rm ml}(\mathbf{k},\bar{\Omega})$ inside the $g=1$ Mott lobe as a function of $\bar{\Omega}=\Omega/zt$ for $\mathbf{k}=0$, $U/zt=11$, $\mu/zt=5$ and $\alpha_{\rm lat}\simeq 10^{-2}$. The spectral function has a delta-peak contributions at $\Omega=-\mu$ and $\Omega=-\mu+gU$. Furthermore, the nonzero value of α broadens the contributions that are located at the quasihole and quasiparticle excitations.

where $\Omega^+=\Omega+i\epsilon$ with $\epsilon>0$ infinitesimally small. In Fig. 6.5 we show a typical plot of this spectral function. This function contains four different contributions. There are two delta-peaks at $\Omega=-(\mu-(g-1)U)/\hbar$ and $\Omega=-(\mu-gU)/\hbar$, and there are contributions at the quasiparticle and quasihole excitations that are broadened by the photon-molecule coupling.

By using the definition of $\rho_{\rm ml}(\mathbf{k},\Omega)$, we can rewrite

$$n=g+\frac{1}{N_{\rm s}}\sum_{\mathbf{k}}\int_{-\infty}^{\infty}d(\hbar\Omega)N_{\rm BE}(\hbar\Omega)\rho_{\rm ml}(\mathbf{k},\Omega). \tag{6.63}$$

Here $N_{\rm BE}(\hbar\Omega)$ denotes the Bose-Einstein distribution function. Here and in the following we consider the photon gas at zero temperature and only consider quantum fluctuations. This amounts to calculating

$$n=g-\frac{\lambda^2}{4}\int_{\rm BZ}\frac{d\mathbf{k}}{(2\pi)^2}\int_{-\infty}^{0}d(\hbar\Omega)\,\rho_{\rm ml}(\mathbf{k},\Omega), \tag{6.64}$$

where we only integrate the momenta over the first Brillouin zone. Recall that we consider a square lattice with spacing $\lambda/2$ and therefore the momenta run from $-2\pi/\lambda$ to $2\pi/\lambda$. Since in the low-energy approximation of the self-energy we obtain ultra-violet divergences, we consider the full expression of the self-energy as obtained in Ref. [75] and numerically evaluate the integrals. However, in the following we still use the parameter $\alpha_{\rm lat}$ to compare between results for different values of the self-energy.

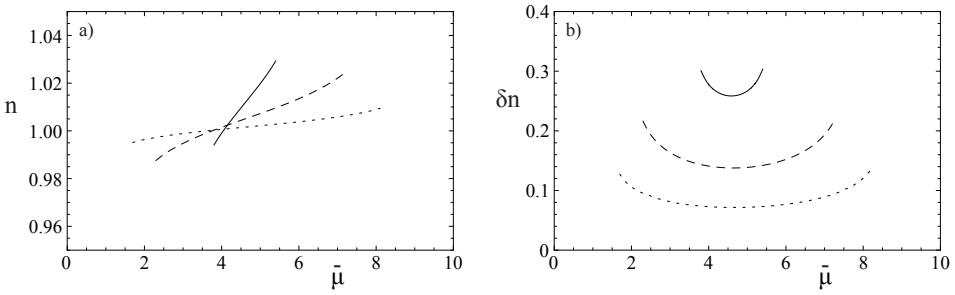

Figure 6.6: a) Average number of photons n and b) corresponding number fluctuation δn at zero temperature in the $g = 1$ Mott lobe as a function of μ/zt for $\mathbf{k} = 0$, $\lambda/\Lambda_{\rm th} = 1$, $V_0/k_{\rm B}T = 30$, $zt/k_{\rm B}T \simeq 0.3$ and $U/zt = 11$. The solid, dashed, and dotted curves correspond to $\alpha_{\rm lat} \simeq 9.8 \cdot 10^{-2}$, $\alpha_{\rm lat} \simeq 4.9 \cdot 10^{-2}$, and $\alpha_{\rm lat} \simeq 1.6 \cdot 10^{-2}$. Since increasing the value of $\alpha_{\rm lat}$ also increases the value of γ, the range of $\bar{\mu}$ where the photons are inside the $g = 1$ Mott lobe decreases for increasing $\alpha_{\rm lat}$. Moreover, the number fluctuation become larger if the value of $\alpha_{\rm lat}$ increases.

As an example, we now take $\lambda/\Lambda_{\rm th} = 1$ and $V_0/k_{\rm B}T = 30$ such that $\beta zt \simeq 0.3$. Furthermore, we calculate the number of photons for different values of the self-energy, which can be obtained, for example, by changing the density of molecules or changing the detuning. Moreover, these expressions are only valid in the Mott lobes and therefore the values of $\bar{\mu}$ are restricted. In agreement with this theory, we use the phase boundaries as calculated by solving $\hbar G^{-1}(\mathbf{0}, 0)/zt = 0$, where $\hbar G^{-1}(\mathbf{0}, 0)/zt$ is defined in Eq. (6.51).

In Fig. 6.6(a) we show the average number of photons in the $g = 1$ Mott lobe at zero temperature for several values of $\alpha_{\rm lat}$. We observe that inside the Mott lobe the average number of photons is not constant, and therefore the true Mott insulator never exists if the interactions with the dye molecules are included. Furthermore, for increasing values of $\alpha_{\rm lat}$ there are two effects. First, the range of $\bar{\mu}$ for which the photons are in the $g = 1$ Mott lobe decreases as larger values of $\alpha_{\rm lat}$ also correspond to larger values of γ. Moreover, the differences between the number of photons for different values of $\bar{\mu}$ inside the plateau become larger, i.e., the slope of the plateau increases. This slope is related to the fluctuations in the average number of photons, namely,

$$\delta n := \sqrt{\langle \hat{n}^2 \rangle - \langle \hat{n} \rangle^2} = \sqrt{\frac{\partial n}{\partial(\beta\mu)}} = \sqrt{\frac{\kappa}{zt}}, \tag{6.65}$$

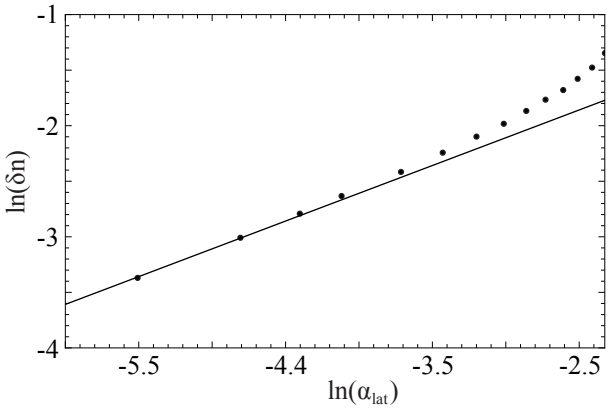

Figure 6.7: Minimal value of the number fluctuation $\ln(\delta n)$ as a function of $\ln(\alpha_{\rm lat})$ at zero temperature in the $g = 1$ Mott lobe for $\lambda/\Lambda_{\rm th} = 1$, $V_0/k_{\rm B}T = 30$, $zt/k_{\rm B}T \simeq 0.3$ and $U/zt = 11$. The points represent values of $\bar{\mu}$ for which the minimum in the number fluctuations is determined numerically. The solid line is a fit through the first points of a line with slope 0.5. For $\alpha_{\rm lat}$ smaller than roughly 10^{-2}, we find good agreement with the numerical points.

where we define $\kappa = \partial n/\partial(\beta\bar{\mu})$ as the compressibility.

To obtain the number fluctuations due to quantum fluctuations, we first consider the density as given by Eq. (6.63) and we take the derivative with respect to $\beta\bar{\mu}$. Then we only consider quantum fluctuations, by neglecting the Bose-Einstein distribution function of the photons and only integrating over negative frequencies. These number fluctuations are shown in Fig. 6.6(b). We observe that for increasing values of $\alpha_{\rm lat}$ the number fluctuations increase. Moreover, for a fixed value of $\alpha_{\rm lat}$ we obtain that the number fluctuations increase, closer to the phase boundary. Intuitively, this is because deeper in the Mott lobe, on average, the fluctuations in the number of photons decrease.

To obtain more information about how the value of $\alpha_{\rm lat}$ affects the number fluctuations, we determine the minimal value of δn for different values of $\alpha_{\rm lat}$. The results of this numerical calculation are shown in Fig. 6.7. We observe that for small values of $\alpha_{\rm lat}$, to a very good approximation $\delta n \propto \sqrt{\alpha_{\rm lat}}$. If $\alpha_{\rm lat}$ is larger than roughly 10^{-2}, this relation is no longer valid and the effect of $\alpha_{\rm lat}$ on the number fluctuations is larger. We also performed the same calculation for $U/zt = 14$ and obtained similar results for the scaling of δn.

Although the average number of photons inside a Mott lobe varies, the system is for all practical purposes still a Mott insulator if these number fluctuations are small. To distinguish this region from the regime where

the fluctuations are large enough to destroy the Mott insulator, we use our definition of the compressibility. A true Mott insulator is incompressible and this corresponds to $\kappa = 0$ or $\delta n = 0$. However, we anticipate that for $\delta n < 1/2$ it is still possible to make a distinction between different Mott lobes, and therefore we consider this regime practically as the Mott insulator. As can be seen in Fig. 6.6(b), this condition is satisfied for relatively large α_{lat}, even up to values of 10^{-1}. Thus, in most cases the photons are to a good approximation still in the Mott-insulating phase. Moreover, note that these number fluctuations at zero temperature imply that the transition from a superfluid to a Mott insulator is a crossover instead of a quantum phase transition as is the case for cold bosonic atoms in an optical lattice.

6.5 Conclusion and outlook

In this Chapter we have investigated the effects of the dye molecules on the superfluid-Mott-insulator phase transition of photons in a dye-filled optical microcavity. First, we derived expressions for the relevant parameters of our theory in terms of the experimental quantities. Then, we considered a simplified model that neglects the fixed longitudinal momentum of the photons and only takes into account absorption and emission of photons with zero momentum. We have shown that at the mean-field theory level the effect of the photon-molecule coupling can be captured in a single dimensionless parameter γ. By performing a self-consistent mean-field theory, we have found that a nonzero expectation value of the annihilation operator of the photons induces coherence between different internal molecular states. We have demonstrated that incorporation of γ decreases the size of the Mott lobes. We considered the full model that includes the fixed longitudinal momentum and takes into account absorption and emission of photons with nonzero momentum, and have found generally good agreement between the values of γ for this full model and simplified model. However, for small lattice potential depths V_0 in the full model there is a larger range of lattice spacings where the value γ is smaller.

Moreover, by first integrating out the molecules we calculated both the excitations and the number fluctuations inside the Mott lobes at zero temperature. We obtained that the quasiparticle and quasihole excitations in this system have a finite lifetime, which is visible in the finite width of both contributions in the spectral function. We have demonstrated that the coupling between the photons and dye molecules results in nonzero number fluctuations at zero temperature, and therefore, strictly speaking, the Mott

insulator does not exist. However, we have shown that for the most relevant values of α_{lat}, the compressibility is sufficiently small and the system is to a good approximation still in the Mott-insulating state. Subsequently, we obtained that for a relatively small coupling the number fluctuations scale with the square root of the dimensionless damping parameter α_{lat}.

For future research it would be interesting to investigate which regions are accessible in experiments. From Ref. [152], we know that for the lattice potential typical lattice spacings in the micron regime are expected. Since this is of the same order as discussed in this Chapter, we expect that for sufficiently deep lattice potentials the coupling with the molecules is important and could prevent the system from being inside a Mott lobe. For example, it is interesting to compare the state of the photons for different molecular densities, detunings or other dye-specific properties. Furthermore, we have found that in the superfluid phase of the photons the molecules are in a superposition of different internal states. Although our calculation does not incorporate the full rovibrational structure of the molecules, we expect that this phenomenon is also present in the experiment. Therefore, it would be interesting to measure and investigate the behavior of the molecules if the photons are in the superfluid phase.

Except for these experimental options, there are also some possibilities for future theoretical work. First of all, in the experimental system there is a harmonic trapping potential and for qualitative agreement this should be taken into account. In a first approximation this can be incorporated in the local-density approximation. Moreover, the presented theory beyond mean-field only takes into account the effect of Gaussian fluctuations at zero temperature. However, in the current experiment the photons are at room temperature. In analogy with the first-order correlation functions and phase fluctuations of a Bose-Einstein condensate of photons under similar conditions, we expect that the thermal fluctuations are also very important [155]. Finally, we note that the presented formalism is potentially also useful to describe the effects of relaxation on the superfluid to insulator transition in quantum magnets [156].

Chapter 7

Superfluidity

We construct a theory for Bose-Einstein condensation of light in nano-fabricated semiconductor microcavities. We model the semiconductor by one conduction and one valence band which consist of electrons and holes that interact via a Coulomb interaction. Moreover, we incorporate screening effects by using a contact interaction with the scattering length for a Yukawa potential and describe in this manner the crossover from exciton gas to electron-hole plasma as we increase the excitation level of the semiconductor. We then show that the dynamics of the light in the microcavities is damped due to the coupling to the semiconductor. Furthermore, we demonstrate that on the electron-hole plasma side of the crossover, which is relevant for the Bose-Einstein condensation of light, this damping can be described by a single dimensionless damping parameter that depends on the external pumping. Hereafter, we propose to probe the superfluidity of light in these nano-fabricated semiconductor microcavities by making use of the differences in the response in the normal or superfluid phase to a sudden rotation of the trap. In particular, we determine frequencies and damping of the scissors modes that are excited in this manner. Moreover, we show that a distinct signature of the dynamical Casimir effect can be observed in the density-density correlations of the excited light fluid.

7.1 Introduction

The first observation of Bose-Einstein condensation in a dilute atomic vapor opened up several different possibilities to explore many-body phenomena in a completely new regime. As before this observation it was hard to experimentally access the macroscopic quantum regime, the low temperatures of these systems created a playground for the investigation of several interesting quantum effects. One prominent example is the observation of

superfluidity via the existence of quantized vortices [157–159]. These developments were even more encouraged by the large experimental control that is available in the cold atomic gases, leading also to the possibility to investigate dynamical behavior.

More recently a class of Bose-Einstein condensates have been observed that are fundamentally different from atomic condensates and also allow for different experimental probes. These Bose-Einstein condensates of bosonic quasiparticles such as magnons [29], exciton-polaritons [30, 31] and photons [32] are dissipative systems. This leads to the possibility to investigate phenomena that are not not yet observed in atomic condensates, such as large number fluctuations in a Bose-Einstein condensate of photons [83,160]. Moreover, it is also interesting to investigate whether certain equilibrium phenomena are still present in these dissipative systems.

Although the Bose-Einstein condensate of light allows for dynamical measurements and new experimental probes, there are still some disadvantages to the current experimental approach [32,36]. First, it is inconvenient to dynamically change the trap geometry of the photons. Second, every possible change highly affects the interactions of the photons with the dye and therefore strongly influences the thermalization of the photons. Lastly, it is very hard to predict theoretically, and to a large extent it is still unknown experimentally, how strongly the photons interact and what the origin of the effective photon-photon interaction is. Therefore, this is a large disadvantage for studying various many-body phenomena of light.

To overcome these problems we propose to follow a different experimental approach, namely nano-fabricated semiconductor microcavities. In this system we use a semiconductor with a periodic array of holes filled with air to create a photonic crystal. The photons thermalize due to the interaction with the electrons and holes in the semiconductor. Moreover, by simply increasing the size of the holes when moving further away from the center of the semiconductor, the photons feel an effective harmonic trapping potential [161]. Finally, also in this case there is external pumping to compensate for photon losses out of the microcavity. Although this suggest that light in such nano-fabricated semiconductor microcavities is similar to photons in a dye-filled optical microcavity, the former system has several advantages. Most importantly, the interaction between the light and the semiconductor is well understood, see e.g. Ref. [162]. Therefore, there are good prospects of controlling the effective photon-photon interaction. Moreover, it is possible to change the cavity geometry and it is also achievable to influence the photon trap dynamically on a sub-picosecond timescale [163].

A prime example of a many-body phenomenon of light where the ad-

vantages of the semiconductor microcavity can be utilized is superfluidity. In Ref. [164] it is shown that in dissipative condensates a superfluid density can exist and therefore it is expected that also a Bose-Einstein condensate of photons can exhibit superfluidity. Although some work has been carried out that mainly focus on the frictionless flow of light through an obstacle, see e.g. Ref. [165–168], up to now the superfluidity of a Bose-Einstein condensate of photons has not yet been explored, since it is unclear how the superfluidity of this system can be probed in the current experiments. Namely, recall that the standard experiment for probing the superfluid behavior, i.e., observing the existence of quantized vortices after rotation of the condensate, appears not to be feasible in a dye-filled optical microcavity.

From studies in atomic Bose-Einstein condensates we know that there is another method to obtain direct evidence for superfluidity [169, 170]. By applying a small sudden rotation of the trapping potential the so-called scissors modes can be excited. The modes are quite different from the excitations in the of the atoms in the normal state. Therefore, the time evolution of the angle between the axial direction of the condensate and the new trap direction is distinct in the normal and superfluid phase. As mentioned before, in current experiments this is difficult to observe as a rotation of the cavity highly affects the interactions of the photons with the dye and therefore destroys the thermalization of the photons. In contrast, in a semiconductor microcavity the trap geometry can be changed on a subpicosecond timescale [163], which is much shorter than the inverse trapping frequency which is typically of the order of tens of gigahertz. Therefore, this fast change of the cavity geometry is non-adiabatic, which allows for the excitation of the scissors modes and probing the superfluidity of a Bose-Einstein condensate of light.

Nonetheless, there are still major differences between the dynamics of the scissors modes in Bose-Einstein condensates of atoms and photons. The former systems are very clean and therefore damping is typically not an issue, especially because most experiments are carried out in the collisionless regime. As a result, only for fine-tuned configurations of the experimental set-up, such as in Ref. [171], the scissors modes are damped by Beliaev processes. In a Bose-Einstein condensate of light on the other hand, the photons are, as envisaged here, coupled to electrons and holes in the solid-state cavity, that is pumped with an external laser beam. In the context of exciton-polariton systems it is shown that this pumping of the external bath affects the superfluid properties [172, 173]. We show here that the coupling with the external bath gives rise to damping of the scissors

modes and in addition that this damping offers the possibility to observe a dynamical Casimir effect. Moreover, we demonstrate that the amount of damping also depends on the external pumping.

In this Chapter we study light in nano-fabricated semiconductor microcavities. The layout of the Chapter is as follows. In Sec. 7.2 we model the semiconductor by one conduction and one valence band and describe the interactions between the electrons and holes by an effective contact interaction, which is especially appropriate in the electron-hole plasma regime of interest to us here where the Coulomb potential is screened to a short-range interaction. We include screening effects by calculating the scattering length for the appropriate Yukawa potential. Hereafter, we consider the coupling between light and the semiconductor in Sec. 7.3. We show that the coupling results into damping of the light and we demonstrate that this damping can be characterized by a single dimensionless parameter that depends on the external pumping. After this, we apply our model and study an example of a many-body phenomena of light where the advantages of semiconductor microcavities are particularly useful. Namely, in Sec. 7.4 we propose to investigate the superfluidity of light via the excitation of scissors modes. In Sec. 7.5 we consider a sudden rotation of the trapping potential of an elongated photon condensate and we calculate the decay rates of the excitations in the Thomas-Fermi limit. Hereafter, in Sec. 7.6 we propose to measure the density-density correlations of the excited light fluid, since the decay products of the scissors mode quanta also demonstrate an analog of the dynamical Casimir effect. Finally, we end with conclusions and discussion in Sec. 7.7.

7.2 Semiconductor

To investigate Bose-Einstein condensation of light in a nano-fabricated semiconductor we in first instance ignore the light and start with a model for a homogeneous semiconductor. We consider the following action

$$S_{\rm sc}[\phi^*,\phi] = -\hbar\sum_{i,\alpha}\int_0^{\hbar\beta} d\tau \int d\mathbf{r}\, \phi^*_{i,\alpha}(\mathbf{r},\tau)G_{0i}^{-1}\phi_{i,\alpha}(\mathbf{r},\tau) \tag{7.1}$$

$$-\sum_{\alpha,\alpha'}\int_0^{\hbar\beta} d\tau \int d\mathbf{r}\, d\mathbf{r}'\, \phi^*_{e,\alpha}(\mathbf{r},\tau)\phi^*_{h,\alpha'}(\mathbf{r}',\tau)V_s(\mathbf{r}-\mathbf{r}')\phi_{h,\alpha'}(\mathbf{r}',\tau)\phi_{e,\alpha}(\mathbf{r},\tau).$$

In this model we only take into account one valence and conduction band and i denotes the electron e or hole h respectively. The generalization to for instance one conduction band and three valance bands is straightforward

and can be easily achieved once the experimentally relevant semiconductor is known. The electron field and hole field are denoted by $\phi_{i,\alpha}$ and $\phi^*_{i,\alpha}$ with α and α' representing the spin degeneracy that is denoted by $\uparrow$ or $\downarrow$. The noninteracting Green's function G^{-1}_{0i} is defined as

$$G^{-1}_{0i} = -\frac{1}{\hbar}\left\{\hbar\frac{\partial}{\partial\tau} - \frac{\hbar^2\nabla^2}{2m_i} - \mu_i\right\}, \tag{7.2}$$

where μ_i is the chemical potential and m_i is the corresponding mass of the electron or hole. Note that the band gap of the semiconductor is absorped in our definitions of the chemical potentials. The same is true for the bandgap renormalization due to the electron-electron and hole-hole Coulomb interactions. The electron-hole interaction, however, needs to be considered explicitly due to the possibility of exciton formation.

In a semiconductor there are usually Coulomb interactions. However, since we are mostly interested in the highly excited regime where excitons do not exist and screening plays a dominant role, we may simplify the theory and replace the interaction potential by a contact interaction

$$V_s(\mathbf{r}-\mathbf{r}') \to -V_0\delta(\mathbf{r}-\mathbf{r}'), \tag{7.3}$$

with V_0 the effective interaction strength that we determine selfconsistently later on.

Now we perform a Hubbard-Stratonovich transformations to the pairing fields and integrate out the fermionic fields [174]. Note that we have to perform four different transformations and therefore we introduce the fields $\Delta_{\alpha\alpha'}(\mathbf{x},\tau)$, of which the averages are given by

$$\langle\Delta_{\alpha\alpha'}(\mathbf{r},\tau)\rangle = V_0\langle\phi_{h,\alpha}(\mathbf{r},\tau)\phi_{e,\alpha'}(\mathbf{r},\tau)\rangle. \tag{7.4}$$

We apply here the Nozières-Schmitt-Rink approximation and only consider terms up to quadratic order in the pairing fields [175], which is the simplest approximation that correctly incorporates the crossover between an exciton gas and an electron-hole plasma that occurs as a function of excitation, i.e., pumping, of the semiconductor. In this approximation we find that the thermodynamic potential Ω is given by

$$\begin{aligned}\Omega &:= \Omega_1 + \Omega_2 \\ &= \frac{4}{\beta}\sum_{\mathbf{P},n}\ln\left(-1/\hbar T^{\mathrm{MB}}(i\Omega_n,\mathbf{P})\right) - \frac{2}{\beta}\sum_{\mathbf{p},i}\ln\left(1+e^{-\beta(\epsilon_{\mathbf{p},i}-\mu_i)}\right),\end{aligned} \tag{7.5}$$

where Ω_n are bosonic Matsubara frequencies and $\epsilon_{\mathbf{p},i} = \hbar^2\mathbf{p}^2/2m_i$ is the kinetic energy of the particle or hole. The thermodynamic potential thus

consists of the sum of the ideal electron and hole contributions and a fluctuation correction. The many-body T-matrix in the above expression is defined as

$$\frac{1}{T^{\mathrm{MB}}(i\Omega_n,\mathbf{P})} = \frac{1}{V_0} - \frac{1}{V}\sum_{\mathbf{p}'}\frac{1}{\epsilon_{\mathbf{p}',e}+\epsilon_{\mathbf{p}',h}} + \frac{1}{V}\sum_{\mathbf{p}'}\frac{1-N_{\mathrm{FD}}(\epsilon_{\mathbf{P}-\mathbf{p}',e}-\mu_e)-N_{\mathrm{FD}}(\epsilon_{\mathbf{p}',h}-\mu_h)}{-i\hbar\Omega_n+\epsilon_{\mathbf{P}-\mathbf{p}',e}+\epsilon_{\mathbf{p}',h}-\mu_e-\mu_h}, \tag{7.6}$$

where $N_{\mathrm{FD}}(x) = 1/(e^{\beta x}+1)$ is the Fermi-Dirac distribution function. From now on we simplify the notation by omitting the arguments of the many-body T-matrix.

7.2.1 Interactions

To obtain a better understanding of the effect of the interactions in our model, we now focus on the many-body T-matrix. For simplicity we consider relatively small densities of electrons and holes, such that the many-body effects, i.e., the Fermi-Dirac distribution function in Eq. (7.6), can be neglected. In this regime we find

$$\frac{1}{T^{\mathrm{MB}}} = \frac{1}{V_0} - \frac{m_r^{3/2}}{2\pi\hbar^3}\sqrt{-2(z-\epsilon_{\mathbf{P},e+h}+\mu_e+\mu_h)}, \tag{7.7}$$

where z is the complex center-of-mass energy associated with the Matsubara frequencies $i\Omega_n$ and m_r is the so-called reduced mass which is defined as

$$m_r = \left(\frac{m_e m_h}{m_e+m_h}\right). \tag{7.8}$$

Moreover, $\epsilon_{\mathbf{P},e+h}$ is the kinetic energy of the center-of-mass motion of the electron and hole involved in the interaction that is given by

$$\epsilon_{\mathbf{P},e+h} = \frac{\hbar^2\mathbf{P}^2}{2(m_e+m_h)}. \tag{7.9}$$

We write the effective interaction strength as $V_0 = 4\pi\hbar^2 a/m_r$ with a the so-called effective scattering length of the potential between the electron and hole.

From the expression for the many-body T-matrix in Eq. (7.7) we obtain two features as a function of the complex energy z. First, we find that for positive values of V_0 there is a pole on the real axis. This corresponds

to the exciton that is a bound state of an electron and a hole. Second, we find that there is a branch cut on the real axis, which corresponds to the continuum of electron-hole scattering states. To see this explicitly we calculate the density of electrons in the semiconductor. As we only consider optical excitations, the electron density n_e is equal to the hole density n_h. Hence, we define a carrier density n as

$$n = n_e = n_h = -\frac{1}{V}\left(\frac{\partial\Omega}{\partial\mu_e}\right)_T. \tag{7.10}$$

Since we have an analytical expression for the many-body T-matrix, we can also calculate the density analytically. By using similar techniques as shown in Ref. [59], we perform the summation over Matsubara frequencies by contour integration. Note that we have to be careful with the branch cut and the pole when choosing the contours. Ultimately, we find

$$n = n_{\mathrm{id}} + n_{\mathrm{ex}} + n_{\mathrm{sc}}, \tag{7.11}$$

where

$$\begin{aligned}
n_{\mathrm{id}} &= \frac{1}{2\pi^2}\left(\frac{2m_i}{\hbar^2}\right)^{3/2}\int_0^\infty d\epsilon\,\sqrt{\epsilon}\,N_{\mathrm{FD}}(\epsilon-\mu_i), \qquad (7.12)\\
n_{\mathrm{ex}} &= \frac{\Theta(a)}{\pi^2}\left(\frac{2(m_e+m_h)}{\beta\hbar^2}\right)^{3/2}\int_0^\infty d\epsilon\,\sqrt{\epsilon}\,N_{\mathrm{BE}}(\epsilon_{\mathrm{ex}}),\\
n_{\mathrm{sc}} &= -\frac{1}{2\pi^3}\frac{\Lambda_{\mathrm{th}}}{4a\sqrt{\pi}}\left(\frac{2(m_e+m_h)}{\beta\hbar^2}\right)^{3/2}\\
&\quad\times\int_0^\infty d\epsilon\int_{-\infty}^\infty dy\,\sqrt{\epsilon}\frac{N_{\mathrm{BE}}(\epsilon-\beta(\mu_e+\mu_h)+y^2)}{y^2+\left(\Lambda_{\mathrm{th}}/4a\sqrt{\pi}\right)^2},
\end{aligned}$$

with Θ the Heaviside step function, $\beta = 1/k_{\mathrm{B}}T$, $\Lambda_{\mathrm{th}} = \left(2\pi\hbar^2\beta/m_r\right)^{1/2}$ the thermal de Broglie wavelength, $N_{\mathrm{BE}}(x) = 1/(e^x+1)$ the Bose-Einstein distribution function and we defined the dimensionless exciton energy ϵ_{ex} as

$$\epsilon_{\mathrm{ex}} = \epsilon - \beta(\mu_e+\mu_h) - \frac{1}{16\pi}\left(\frac{\Lambda_{\mathrm{th}}}{a}\right)^2. \tag{7.13}$$

We see that there are three contributions to the carrier density. The first contribution is simply the ideal gas result. The second part originates from the exciton bound state and the third part describes the scattering continuum of electron-hole states. We can calculate the separate contributions to the density as a function of the value of the scattering length. In order

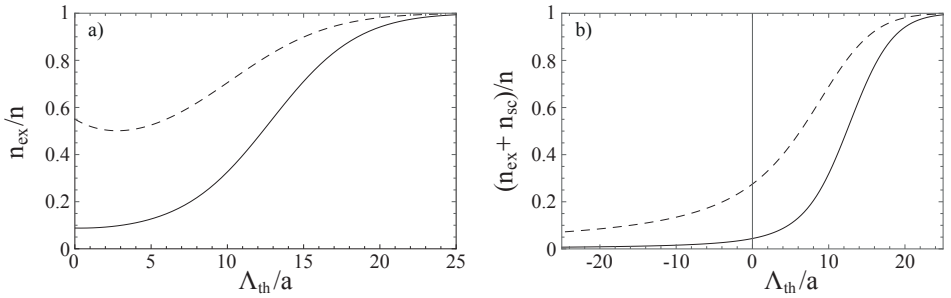

Figure 7.1: a) Number of electrons in excitons and b) total number of electrons in the excitons and the scattering contributions as a function of the interaction parameter a for ZnO. The solid and dashed lines correspond to a carrier density of $n = 10^{23}\,\mathrm{m}^{-3}$ and $n = 10^{24}\,\mathrm{m}^{-3}$, respectively. We obtain a smooth crossover from $\Lambda_{\mathrm{th}}/a \ll 0$ where the electrons and holes behave as an ideal gas and form an electron-hole plasma, to $\Lambda_{\mathrm{th}}/a \gg 0$ where almost all electrons and holes form excitons.

to obtain these values, we first take a certain carrier density n. Then we can find the chemical potentials as a function of the scattering length, by using Eqs. (7.11) and (7.12) for both $i = e$ and $i = h$. By resubstituting the chemical potentials, we obtain that every contribution to the density only depends on the scattering length and the carrier density. Therefore, we investigate the effect of changing the value of these physical parameters. Of course, because of screening the effective scattering length will also depend on the carrier density, but we ignore this in first instance and come back to this problem in a moment.

In Fig. 7.1 we show the exciton contribution n_{ex} and the sum with the scattering contribution n_{sc} as a function of the scattering length. As an example, we take ZnO at room temperature and use $m_e = 0.28m_0$, $m_h = 0.59m_0$ with m_0 the bare electron mass, see Ref. [174]. First, we note from Eqs. (7.12) that there are only excitons for positive values of the scattering length and therefore we only show the number of excitons in this regime. For smaller values of the scattering length the contribution of the excitons becomes larger. Furthermore, by looking at the sum of the exciton and scattering contribution as a function of the interactions, we note that there is a smooth crossover from $\Lambda_{\mathrm{th}}/a \ll 0$ when the electrons behave as an ideal gas, to $\Lambda_{\mathrm{th}}/a \gg 0$ where almost all electrons form excitons. Therefore, we note that this model for the semiconductor describes both the exciton regime and the regime where there is a electron-hole plasma. Moreover, we note that the sum of the exciton and the scattering contribution is an analog for the behavior of the Cooper-pair density in the

BEC-BCS crossover [176].

7.2.2 Scattering length

Up to now we have considered the scattering length as a free parameter. However, in a semiconductor the interaction depends on the value of the carrier density due to screening effets. Here we only consider the effects of static screening that can be described by using a Yukawa potential. Therefore, we can make our model selfconsistent by calculating the scattering length for the Yukawa potential.

The standard procedure for calculating the scattering length is via the so-called Born series. However, for a Yukawa potential this will lead to divergences and taking into account only the first term of this expansion is not sufficient. Therefore, we here use a different approach. First, we note that the scattering length is associated with a low-energy two-body scattering wavefunction that is given by

$$\psi(r) \overset{r\to\infty}{=} A\left(1-\frac{a}{r}\right), \tag{7.14}$$

where A is a normalization constant that is usually taken to be 1 for many-body applications. Moreover, if we define $u(r) = r\psi(r)$ than this function satisfies the following radial Schrödinger equation

$$\frac{\hbar^2}{2m_r}\frac{d^2u(r)}{dr^2} = V(r)u(r), \tag{7.15}$$

where $V(r)$ is a potential and r is the relative coordinate between the electron and hole. Note that this is an equation for the relative motion between the electron and hole and therefore we have to use the reduced mass m_r in the kinetic energy part. For relatively large distances the potential vanishes and therefore the wavefunction given by Eq. (7.14) is a solution to this equation. Hence, we have to solve this equation and look at the solution at large distances. To find the scattering length, we use that

$$-a = \lim_{r\to\infty}\left(\frac{u(r)}{u'(r)} - r\right). \tag{7.16}$$

Thus by solving the radial Schrödinger equation as written in Eq. (7.15) we can find the scattering length.

For the semiconductor we assume that there is only static screening and therefore we are allowed to take a Yukawa potential that is defined as

$$V(r) = -\frac{e^2}{4\pi\epsilon_0\epsilon_r r}e^{-r/\lambda_s}, \tag{7.17}$$

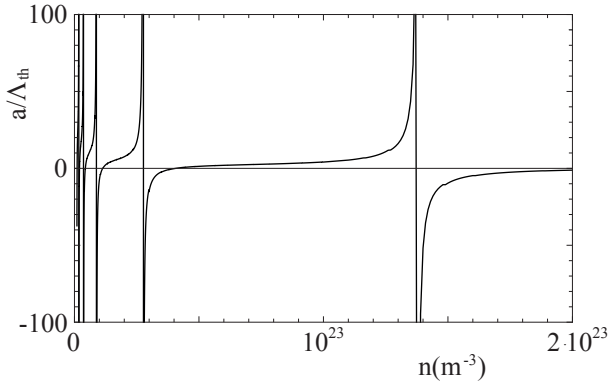

Figure 7.2: The scattering length for ZnO as a function of the carrier density by using the Yukawa potential with a screening length that is calculated for the ideal-gas parts of the electron and hole densities. We obtain that the last resonance occurs at the Mott-density $n_{\mathrm{M}} \simeq 2.3 \cdot 10^{24}\,\mathrm{m}^{-3}$.

with e the electron charge, ϵ_0 the vacuum permittivity, ϵ_r the appropriate relative dieletric constant and λ_s the screening length. We calculate the screening length by assuming that only the unbound carriers screen the potential. Although this approximation leads to an overestimation of the screening length, we expect that this is a small effect since screening by bound carriers is weaker than screening by unbound carriers.

In this approximation the screening length λ_s satisfies $\lambda_s^{-2} = \lambda_e^{-2} + \lambda_h^{-2}$ with

$$\lambda_i = \sqrt{\frac{\epsilon_0 \epsilon_r}{e^2} \frac{\partial \mu_i^0}{\partial n}}, \tag{7.18}$$

the screening lengths of the electron and hole plasmas respectively. Note that in this formula the superscript 0 of the chemical potential indicates that we calculate from the unbound carrier density by treating the electron and hole as ideal Fermi gases. To find the scattering length for the Yukawa potential we still need to specify the boundary conditions in Eq. (7.15). Since the potential is infinite at $r = 0$, we must take $u(0) = 0$. Moreover, we set $u'(0) = 1$. Note that this latter boundary condition is simply a matter of normalization and does not affect the value of the scattering length.

In Fig. 7.2 we display the scattering length as a function of the carrier density by determining the screening length with the ideal-gas parts of the electron and hole densities. For convenience we again consider ZnO with the values as stated in Ref. [174]. We observe that there are multiple resonances or equivalently values of the carrier density where the scattering length

diverges. This is a consequence of the changing value of the screening length for different carrier densities. For larger carrier densities, the screening length becomes smaller and therefore roughly speaking the potential is less deep. Hence, for small carrier densities the Yukawa potential supports more bound states. Furthermore, every resonance corresponds to a bound state and we find that the last resonance occurs at the Mott-density $n_{\mathrm{M}} \simeq 2.3 \cdot 10^{24}\,\mathrm{m}^{-3}$. After that value of the carrier density, the scattering length always remains negative. Therefore, this calculation shows that there are only excitons for carrier densities that are smaller than the Mott-density. Note that this is in agreement with previously obtained results and the value for the Mott-density is within the range of published data [174].

For large carrier densities we only have to take into account the last resonance. Moreover, for carrier densities that are close to n_M we can approximate

$$\frac{a(n)}{\Lambda_{\mathrm{th}}} \simeq 2.1 \frac{n_{\mathrm{M}}}{n_{\mathrm{M}} - n}. \tag{7.19}$$

7.2.3 Many-body effects

We are primarly interested in the regime where the amount of excitons is negligible, because this is the regime where Bose-Einstein condensation of light is possible. From the results in the last section, we know that we therefore have to consider large carrier densities. At these high densities the many-body effects, i.e., the Fermi-Dirac distribution functions in Eq. (7.6), become important. Therefore, we now focus on these contributions and we consider the part of the many-body T-matrix that has been neglected before, namely

$$\frac{1}{(2\pi)^3} \int d\mathbf{p}' \frac{N_{\mathrm{FD}}(\epsilon_{\mathbf{P}-\mathbf{p}',e}) + N_{\mathrm{FD}}(\epsilon_{\mathbf{p}',h})}{i\hbar\Omega_n - \epsilon_{\mathbf{P}-\mathbf{p}',e} - \epsilon_{\mathbf{p}',h} + \mu_e + \mu_h}. \tag{7.20}$$

In first instance we only consider the imaginary part and we neglect the real part. For further purposes we need to calculate this many-body T-matrix for $i\Omega_n \to \omega^+ = \omega + i\epsilon$, where $\epsilon > 0$ is infinitesimally small. By switching to spherical coordinates and performing the angular integration, we find that there is only a nonzero imaginary part if

$$y := \hbar\omega + \mu_e + \mu_h - \epsilon_{\mathbf{P},e+h} > 0. \tag{7.21}$$

The imaginary part is given by

$$\frac{\Theta(y)}{4\pi\hbar^2 P} \left[\int_{p^h_{\mathrm{min}}}^{p^h_{\mathrm{max}}} dp\, k\, m_e\, N_{\mathrm{FD}}(\epsilon_{\mathbf{p},h}) + \langle e \leftrightarrow h \rangle \right], \tag{7.22}$$

where $P = |\mathbf{P}|$ and $\langle e \leftrightarrow h \rangle$ denotes that there is a similar contribution as the first integral where the indices e and h are interchanged. Furthermore,

$$p^h_{\rm min} = \frac{1}{\hbar}\sqrt{2y\frac{m_e m_h}{m_e+m_h}} - \frac{m_h}{m_e+m_h}P, \tag{7.23}$$
$$p^h_{\rm max} = \frac{1}{\hbar}\sqrt{2y\frac{m_e m_h}{m_e+m_h}} + \frac{m_h}{m_e+m_h}P,$$

where $p^e_{\rm min}$ and $p^e_{\rm max}$ are given by similar expression with again the indices e and h interchanged.

By using

$$\int_{p^h_{\rm min}}^{p^h_{\rm max}} dp\, p\; N_{\rm FD}(\epsilon_{\mathbf{p},h}) = -\frac{m_h}{\beta\hbar^2}{\rm Log}\left[\frac{e^{-\beta\mu_h}+e^{-\beta\hbar^2(p^h_{\rm max})^2/2m_h}}{e^{-\beta\mu_h}+e^{-\beta\hbar^2(p^h_{\rm min})^2/2m_h}}\right], \tag{7.24}$$

we obtain for the full many-body T-matrix,

$$\frac{1}{T^{\rm MB}} = \frac{1}{V_0} - \Theta(-y)\frac{m_r^{3/2}}{\pi\hbar^3}\sqrt{-\frac{y+i\epsilon}{2}} \tag{7.25}$$
$$-\frac{im_e m_h}{4\pi\beta\hbar^4 P}\Theta(y){\rm Log}\left[\frac{\cosh\left(\frac{\beta}{2}\left\{\hbar\omega+C_{e+h}\right\}\right)+\cosh\left(\frac{\beta}{2}C_{e-h}\right)}{\cosh\left(\frac{\beta}{2}\left\{\hbar\omega-C_{e+h}\right\}\right)+\cosh\left(\frac{\beta}{2}C_{e-h}\right)}\right],$$

where

$$C_{e+h} = 4\frac{\sqrt{m_e m_h}}{m_e+m_h}\sqrt{y\,\epsilon_{\mathbf{P},e+h}}, \tag{7.26}$$
$$C_{e-h} = \mu_e - \mu_h + \frac{m_e-m_h}{m_e+m_h}\left(y-\epsilon_{\mathbf{P},e+h}\right).$$

Note that this results includes the two-body result as given by Eq. (7.7). Moreover, in the context of ultracold Fermi gases a similar calculation has already been performed in Ref. [177]. As expected, we agree with that result if we put $m_e = m_h = m$ and $\mu_e = \mu_h = \mu$.

Now we use this result to find a self-consistent solution for the chemical potential of the electrons and holes. Recall that

$$n_i = -\frac{1}{V}\left(\frac{\partial\Omega}{\partial\mu_i}\right)_T \tag{7.27}$$
$$= \frac{2}{V}\sum_{\mathbf{p}} N_{\rm FD}(\epsilon_{\mathbf{p},i}) - \frac{4\hbar}{V}\sum_{\mathbf{P}}\int d(\hbar\omega)\,\rho_i(\omega,\mathbf{P})N_{\rm BE}(\omega),$$

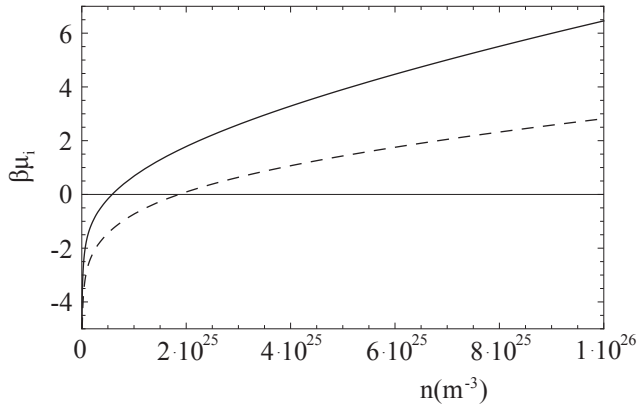

Figure 7.3: Chemical potential of the electrons μ_e (solid) and the chemical potential of the holes μ_h (dashed) for ZnO as a function of the carrier density by using the self-consistent scattering length for the Yukawa potential.

where

$$\rho_i(\omega, \mathbf{P}) = -\frac{1}{\pi\hbar}\mathrm{Im}\left[T^{\mathrm{MB}}(\omega, \mathbf{P})\frac{\partial}{\partial\mu_i}\frac{1}{T^{\mathrm{MB}}(\omega, \mathbf{P})}\right]. \tag{7.28}$$

As in the previous sections, we only want to consider optical excitation. Therefore, we for simplicity from now on neglect the dependence of the many-body T-matrix on $\mu_e - \mu_h$ and set

$$C_{e-h} = \frac{m_e - m_h}{m_e + m_h}\left(y - \epsilon_{\mathbf{P},e+h}\right). \tag{7.29}$$

In this case the spectral function is the same for $i = e$ and $i = h$ and we again define the carrier density as $n = n_e = n_h$.

The spectral function $\rho(\omega, \mathbf{P}) = \rho_e(\omega, \mathbf{P}) = \rho_h(\omega, \mathbf{P})$ of the pairs contains two different contributions that we can separate by considering either $y < 0$ or $y > 0$. For $y < 0$, we obtain that the Logarithm does not contribute in Eq. (7.25). In this case we can analytically determine the spectral function and we find

$$\rho(\omega, \mathbf{P}) = \frac{\Theta(a)}{\hbar}\delta\left(\hbar\omega - \epsilon_{\mathbf{P},e+h} + \mu_e + \mu_h + \frac{\Lambda_{\mathrm{th}}^2}{16\pi\beta a^2}\right). \tag{7.30}$$

By using the result of Eq. (7.13) we recognize that this contribution to the spectral function is simply a delta-function at the exciton energy. Again recall that this contribution is only present when the scattering length is positive and from the results in the previous section this implies that

for carrier densities larger than the Mott density this contribution is not present. The other contribution to the spectral function is obtained by taking $y > 0$. In this case the square root in the expression for the many-body T-matrix vanishes and we are left with the contribution from the logarithm. This represents the scattering continuum of electrons and holes.

In Fig. 7.3 we show the result for the chemical potentials of electrons and holes as a function of the carrier density n for ZnO as discussed in Ref. [174]. In comparison with the calculation in that article, where the chemical potentials are determined by treating the electron and holes as two ideal Fermi gases, we find slightly smaller values for both chemical potentials. For example, we find for the value of the carrier density that corresponds to population inversion, i.e., $\mu_e + \mu_h > 0$, a value that is roughly two times larger than stated in Ref. [174].

7.3 Light in semiconductor microcavities

Now that we worked out the model for the semiconductor, we consider the full situation and include the coupling to an external light field. Similar to Bose-Einstein condensation of light in a dye-filled cavity, we can describe the complete dynamics using the Schwinger-Keldysh formalism as presented in Ref. [75]. As will follow from the results in this section, in this case the self-energy as given in the Langevin field equation in Ref. [75] is proportional to the susceptibility of the semiconductor. However, also for Bose-Einstein condensation of light in nano-fabricated semiconductor microcavities the system relaxes towards a steady state that can be described by standard equilibrium methods. It is important to realize here that throughout our paper we are always considering the thermalized case, and in particular are not discussing the fully non-equilibrium laser regime of this system. We start from the action

$$
\begin{aligned}
S[a_{\mathbf{k}}, a^*_{\mathbf{k}}, \phi_{\mathbf{k}}, \phi^*_{\mathbf{k}}] &= S_{\rm sc}[\phi_{\mathbf{k}}, \phi^*_{\mathbf{k}}] \\
&+ \sum_{\mathbf{k}} \int_0^{\hbar\beta} d\tau\, a^*_{\mathbf{k}}(\tau) \left\{ \hbar \frac{\partial}{\partial \tau} + \epsilon_{\rm ph}(\mathbf{k}) - \mu_{\rm ph} \right\} a_{\mathbf{k}}(\tau) \\
&- \frac{g_{eh}}{\sqrt{V}} \sum_{\mathbf{k},\mathbf{p},\alpha} \int_0^{\hbar\beta} d\tau\, a^*_{\mathbf{k}}(\tau) \phi_{h,\mathbf{p},-\alpha}(\tau) \phi_{e,\mathbf{k}-\mathbf{p},\alpha}(\tau) \\
&- \frac{g_{eh}}{\sqrt{V}} \sum_{\mathbf{k},\mathbf{p},\alpha} \int_0^{\hbar\beta} d\tau\, a_{\mathbf{k}}(\tau) \phi^*_{e,\mathbf{k}-\mathbf{p},\alpha}(\tau) \phi^*_{h,\mathbf{p},-\alpha}(\tau).
\end{aligned}
\tag{7.31}
$$

This action contains several parts. First, $S_{\rm sc}[\phi_{\mathbf{k}}, \phi^*_{\mathbf{k}}]$ describes the semiconductor, which is the momentum-space representation of Eq. (7.1). The second part describes the light with $a^*_{\mathbf{k}}(\tau)$ and $a_{\mathbf{k}}(\tau)$ the photon fields. Here, $\epsilon_{\rm ph}(\mathbf{k})$ is the kinetic energy of the photons. By performing a full band structure calculation, e.g. see Ref. [161], we know that

$$\epsilon_{\rm ph}(\mathbf{k}) \cong E_0 + \frac{\hbar^2(\mathbf{k}-\mathbf{k}_0)^2}{2m}, \tag{7.32}$$

with E_0 the energy of the photon at the minimum of the band with respect to the energy of the band gap of the semiconductor, $\mathbf{k}_0$ the wavenumber at the minimum of the band and m the effective mass that arises from the local curvature of the band. In equilibrium, the sum of the number of electron and photons and the sum of holes and photons is conserved. Therefore, in equilibrium we have

$$\mu_{\rm ph} = \mu_e + \mu_h. \tag{7.33}$$

The last two terms of Eq. (7.31) describe the interaction of the light with the semiconductor. The first of these terms corresponds to the annihilation of electron-hole pairs by the electric field and the second term is the creation of electron-hole pairs by the electric field. Recall that α represents the spin degeneracy of the electrons and holes and can be either $\uparrow$ or $\downarrow$. In the interactions terms we only consider electrons and holes with opposite spin and therefore we only take into account transitions without spin-flip. Moreover, we introduced the coupling constant g_{eh} and we assumed that the coupling is independent of energy. Finally, note that the photons and the corresponding momentum $\mathbf{k}$ are two dimensional. However, the electron and holes are three dimensional and therefore $\mathbf{p}$ is also a three-dimensional vector. This convention will be used throughout the remainder of this Chapter.

To obtain the effect of the coupling to the semiconductor on the behaviour of the photon gas, we use second order perturbation theory in the coupling constant g_{eh}. By following the same steps as in the appendix of Ref. [174], we find the effective action for the photons to be

$$S^{\rm eff}[a_{\mathbf{k}}, a^*_{\mathbf{k}}] = \sum_{\mathbf{k},n} a^*_{\mathbf{k},n} \left\{ -i\hbar\omega_n + \epsilon_{\rm ph}(\mathbf{k}) - \mu_{\rm ph} - \chi_{\mathbf{k}}(\omega_n) \right\} a_{\mathbf{k},n}. \tag{7.34}$$

Here the susceptibility $\chi_{\mathbf{k}}(\omega_n)$ acts as a self-energy for the photons. In the Nozières-Schmitt-Rink approximation it is given by

$$\chi_{\mathbf{k}}(\omega_n) = \frac{g^2_{eh}}{V} \sum_{\mathbf{p}} \chi_{\mathbf{k},\mathbf{p}}(\omega_n), \tag{7.35}$$

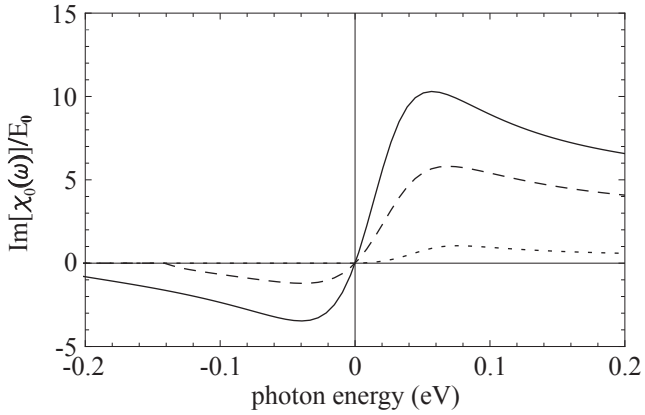

Figure 7.4: The imaginary part of the susceptibility $\chi_{\mathbf{0}}(\omega)$ divided by the energy of the photon at the minimum of the band E_0 as a function of the photon energy for $g_{eh} \simeq 1.7 \cdot 10^{-32}\,\mathrm{J}\cdot\mathrm{m}^{3/2}$ and $E_0 = 0.72\,\mathrm{eV}$. The dotted, dashed and solid curves corresponds to a carrier density of $n = 10^{25}\,\mathrm{m}^{-3}$, $n = 5 \cdot 10^{25}\,\mathrm{m}^{-3}$ and $n = 10^{26}\,\mathrm{m}^{-3}$ respectively.

with

$$\chi_{\mathbf{k},\mathbf{p}}(\omega_n) = \chi^0_{\mathbf{k},\mathbf{p}}(\omega_n)\left(1 - \frac{V_0}{V}\sum_{\mathbf{p}'}\chi_{\mathbf{k},\mathbf{p}'}(\omega_n)\right). \tag{7.36}$$

Hence,

$$\chi_{\mathbf{k},\mathbf{p}}(\omega_n) = \frac{\chi^0_{\mathbf{k},\mathbf{p}}(\omega_n)}{1 + \frac{V_0}{V}\sum_{\mathbf{p}'}\chi^0_{\mathbf{k},\mathbf{p}'}(\omega_n)}, \tag{7.37}$$

where

$$\chi^0_{\mathbf{k},\mathbf{p}}(\omega_n) = \frac{1 - N_{\mathrm{FD}}(\epsilon_{\mathbf{k}-\mathbf{p},e}) - N_{\mathrm{FD}}(\epsilon_{\mathbf{p},h})}{i\hbar\omega_n - \epsilon_{\mathbf{k}-\mathbf{p},e} - \epsilon_{\mathbf{p},h} + \mu_e + \mu_h}. \tag{7.38}$$

From the previous section we know the effective interaction strength V_0 and the chemical potentials as a function of the carrier density. Therefore, we can determine the finite- lifetime effects of the photons due to the interaction with the electron-hole plasma by calculating the imaginary part of the susceptibility $\chi_{\mathbf{k}}(\omega)$ for every carrier density. In principle we can determine the susceptibility for arbitrary photon momentum $\mathbf{k}$. However, since we are primarily interested in Bose-Einstein condensation of the photons, we from now onwards only consider $\mathbf{k} = \mathbf{0}$.

In Fig. 7.4 we display the imaginary part of the susceptibility for $g_{eh} \simeq$

$1.7 \cdot 10^{-32}\,\mathrm{J}\cdot\mathrm{m}^{3/2}$. Note that this values only changes the absolute value of the imaginary part and does not affect the qualitative behaviour. However, the actual value for these physical parameter should be obtained from experiments on optical spectra of the semiconductor. We find that for small carrier densities the imaginary part is only nonzero for positive photon energies. However, for carrier densities that are large enough, we also obtain negative contributions for negative energies. This is a consequence of the fact that only for large enough carrier densities there is gain of photons by emission processes. Moreover, we find that for large carrier densities, where there is substantial gain of photons, the imaginairy part of the susceptibility is linear for small values of the photon energy. Note that this is similar to the result for Bose-Einstein condensation of light in a dye-filled optical microcavity as presented in Ref. [75]. In this regime of large carrier densities we can combine the finite-lifetime effects of the photons in a single dimensionless parameter α, which is simply the slope of the imaginairy part of the susceptibility at the origin. Note that we considered a homogeneous semiconductor coupled to an external light field. However, in the proposed experiment as envisaged here, the semiconductor contains airholes, in which there are of course no electron or holes. In this case we need to multiply α by $1-\eta_{\mathrm{air}}$, where η_{air} corresponds to the fraction of the volume of the holes of the semiconductor.

Up to now we only considered carrier densities that are larger than the Mott density. In this case we are in the pure photon regime, whereas for carrier densities that are smaller than the Mott density the photons are coupled to the exciton and therefore exciton-polaritons excitations exist. To emphasize the difference between the two density regimes, we now investigate the spectral function of the photons in the two different regimes. We define the spectral function of the photons as

$$\rho_\gamma(\mathbf{k},\omega) = \frac{-1}{\pi\hbar}\mathrm{Im}\left[G_\gamma(\mathbf{k},\omega^+)\right], \tag{7.39}$$

where $G_\gamma(\mathbf{k}, i\omega_n)$ is defined in Eq. (7.34) and $\omega^+ = \omega + i\epsilon$ with ϵ infinitesimally small.

In Fig. 7.5 we show the dimensionless spectral function $\rho_\gamma(\mathbf{k},\omega)\cdot\mathrm{eV}$ for $g_{eh} \simeq 9\cdot 10^{-34}\,\mathrm{J}\cdot\mathrm{m}^{3/2}$ and $E_0 = 0.4\,\mathrm{eV}$ as a function of the photon energy. Below the Mott density we have two distinct contributions. Due to the coupling of the excitons to the photons, we have two peaks corresponding to the lower and upper exciton-polariton branches. Note that the photons that are part of the upper exciton-polariton acquire a finite lifetime, since their energy is larger than the energy threshold for the scattering continuum of electrons and holes. However, for carrier densities that are larger

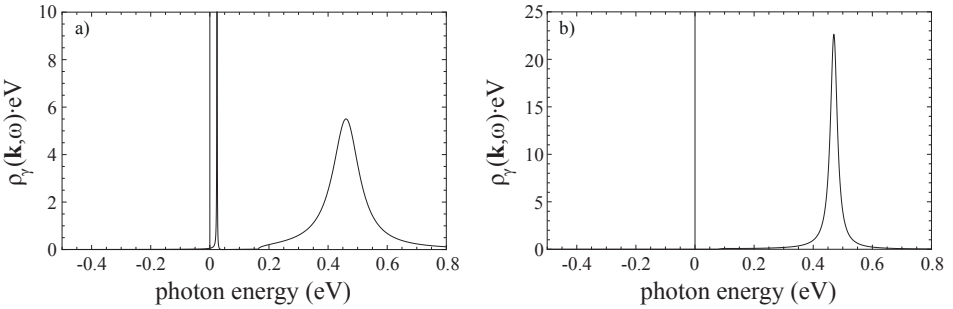

Figure 7.5: The spectral function of the photons above and below the Mott density of $n \simeq 2.3 \cdot 10^{24}\,\mathrm{m}^{-3}$ for $g_{eh} \simeq 9 \cdot 10^{-34}\,\mathrm{J} \cdot \mathrm{m}^{3/2}$ and $E_0 = 0.4\,\mathrm{eV}$. In Figure a) the density is $n = 3.1 \cdot 10^{23}\,\mathrm{m}^{-3}$ and Figure b) is for a carrier density of $n = 1 \cdot 10^{25}\,\mathrm{m}^{-3}$. Below the Mott density there are two different contributions corresponding to the upper and lower exciton-polaritons. However, above the Mott density excitons do not exist and therefore there are only pure photons that acquire a finite lifetime through the interaction with the electrons and holes. This is the regime in which Bose-Einstein condensation of light is possible.

than the Mott density, the excitons are no longer present. In this case the spectral function only has a pure photon contribution, where the interaction with the semiconductor results into a finite lifetime of the photon. Therefore, in this spectral function we clearly find the physical differences between the exciton-polariton and the photon limits of the crossover. It is important to note that Bose-Einstein condensation of photons appears only in the regime described in Fig. 7.5(b).

7.4 Scissors modes

In the previous section we constructed a model for Bose-Einstein condensation of light in nano-fabricated semiconductor microcavities. From now onwards we focus on an example of a many-body phenomenon of light that cannot be studied the currents experiments on Bose-Einstein condensation of photons, but can be investigated in the proposed experimental set-up. Namely, we consider probing the superfluidity of light via the excitation of scissor modes.

We consider a two-dimensional photon gas with effective mass m and an effective point-like interaction g in an external harmonic trapping potential $V^{\mathrm{ext}}(\mathbf{x})$ with trapping frequencies ω_x and ω_y. Note that in the nano-fabricated semiconductor microcavities the harmonic potential arises by systematically increasing the size of the holes from the center to the edge

of the semiconductor. Furthermore, in the previous section we showed that there is an excitation exchange between the photon gas and the electron-hole plasma, but, apart from such processes, photons are assumed to be conserved. Therefore, we are allowed to consider this quasi-equilibrium photon gas in the grand-canonical ensemble and to introduce the chemical potential μ of the photons. Moreover, we introduce a dimensionless interaction parameter g that describes the interactions between the photons. Note that an explicit expression for the parameter can be obtained from Eq. (7.31) by applying fourth order perturbation theory in the coupling constant g_{eh}. However, here we simply use a phenomenological approach to incorporate the interactions between the photons and leave the calculation of the photon-photon interaction for future work.

We are interested in the dynamics of a condensate of light after a sudden rotation of the trap. In the following, we treat the local density and local phase of the condensate separately and we consider a condensate with a large number of photons such that we can use the Thomas-Fermi approximation. In this approximation the equilibrium condensate density $n_0(\mathbf{x})$ is equal to

$$n_0(\mathbf{x}) = \frac{\mu}{g}\left[1 - (x/R_{\mathrm{TF},x})^2 - (y/R_{\mathrm{TF},y})^2\right], \tag{7.40}$$

with $R^2_{\mathrm{TF},i} = 2\mu/m\omega_i^2$ the Thomas-Fermi radius in the corresponding direction. Furthermore, the density is zero outside the ellipse that is spanned by these two radii. A rotation of the trap by a small angle results into a change in the condensate density $\delta n(\mathbf{x})$ that is given by

$$\delta n(\mathbf{x}, t) := \left[n_0(\mathbf{x}') - n_0(\mathbf{x})\right] e^{-i\omega t} = Cxye^{-i\omega t}, \tag{7.41}$$

where $\mathbf{x}'$ are the coordinates after the sudden rotation of the trap and C is a normalization constant. Here we used that for an eigenmode the time dependence is harmonic with angular frequency ω. To obtain more information about the fluctuations of the local phase, we consider the hydrodynamic equations of the condensate as for example can be found in Ref. [43]. By assuming that both the velocity of the condensate and the density fluctuations $\delta n(\mathbf{x})$ are small, we find for the phase of the condensate

$$\delta\phi(\mathbf{x}, t) = \frac{g}{i\hbar\omega} Cxye^{-i\omega t}. \tag{7.42}$$

Moreover, for a harmonic trapping potential the frequency of the scissors mode is given by $\omega = (\omega_x^2 + \omega_y^2)^{1/2}$. The normalization constant C can be

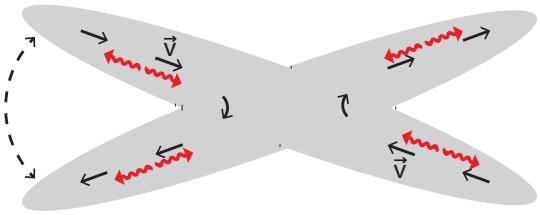

Figure 7.6: The cigar-shaped superfluid photon gas after a sudden rotation of the trapping potential by a small angle. The dashed lines indicates the oscillations of the condensate and the solid arrows denote the irrotational velocity $\vec{v}$ of the condensed photons. The red wiggly arrows represent the decay products of the scissors mode quanta that can be used to demonstrate the dynamical Casimir effect.

determined from the normalization condition of the corresponding Bogoliubov amplitudes and we find

$$C := \sqrt{\frac{12\hbar\omega}{\pi g R_{\mathrm{TF},y}^3 R_{\mathrm{TF},x}^3}}. \tag{7.43}$$

In the normal state the dynamics after a sudden rotation is different and we have to distinguish between the collisional and collisionless regime. In the collisional regime the frequency of the excitations is the same as in the superfluid phase [169]. However, if the gas is dilute and the interactions are weak, the system is in the collisionless regime and the analog of the scissors-mode frequency is equal to $\omega_x + \omega_y$. By comparing the classical collision rate with the trap frequencies, we can make a distinction between both regimes. By using the expressions as specified in Ref. [169], we know how to construct the experiment conditions such that we are in the collisionless regime and we can distinguish whether the photons are superfluid or not by measuring the frequencies of the excitations of the photon gas after applying a rotation to the trap.

7.5 Damping of scissors modes

We have just seen that the superfluidity of the photons can be studied by looking at the frequencies of the excitations after applying a sudden rotation to the trap. These scissors modes result in oscillations that can directly be observed in experiments. However, due to the coupling of the photons with the electron-hole plasma it is worthwhile investigating how this coupling leads to the damping of these oscillations.

We have demonstrated that for a Bose-Einstein condensate of light, at large carrier densities the effects of the electron-hole plasma can be characterized by a single dimensionless damping parameter α that depends on the external pumping. Moreover, the photon gas equilibrates to a steady state that is a dynamical balance between particle losses and external pumping. In the following we start from this steady state and we investigate the associated decay processes of the scissors modes. In particular, we show that the decay rate depend on the value of α and thereby on the external pumping.

To observe properties of the damping, we are primarily interested in configurations that allow for many decay processes. For an elongated trap, the difference between the energies of two adjacent modes in the direction with the small trap frequency is small. Therefore, we expect that in that case the energy of the excitations in the long direction almost forms a continuum and the scissors mode quanta can decay into many other modes. Hence, this elongated trap is particularly interesting and we only consider this configuration throughout the remainder of this Chapter. A summary of the proposed structure is displayed in Fig. 7.6.

We are interested in damping processes where fluctuations of the condensate induce the creation of non-condensed excitations and therefore we only have to consider the interaction part of the hamiltonian. We substitute for the creation and annihilation operator of the photons $\hat{\psi}(\mathbf{x},t) = \langle\hat{\psi}(\mathbf{x},t)\rangle + \delta\hat{\psi}(\mathbf{x},t)$ and we only consider terms up to quadratic order in the fluctuations $\delta\hat{\psi}(\mathbf{x},t)$. In this Bogoliubov approximation, we therefore study

$$\begin{aligned}\hat{H}_{\rm int}(t) = 2g\int d\mathbf{x}\,|\langle\hat{\psi}(\mathbf{x},t)\rangle|^2\delta\hat{\psi}^\dagger(\mathbf{x},t)\delta\hat{\psi}(\mathbf{x},t) \\ + \frac{g}{2}\int d\mathbf{x}\,\left\{\langle\hat{\psi}(\mathbf{x},t)\rangle^2[\delta\hat{\psi}^\dagger(\mathbf{x},t)]^2 + \langle\hat{\psi}^\dagger(\mathbf{x},t)\rangle^2[\delta\hat{\psi}(\mathbf{x},t)]^2\right\}.\end{aligned} \tag{7.44}$$

Now we explicitly separate the dynamics of the local phase and density of the condensate by writing $\langle\hat{\psi}(\mathbf{x},t)\rangle = \sqrt{n_0(\mathbf{x})+\delta n(\mathbf{x},t)}e^{i\delta\phi(\mathbf{x},t)}$, with $n_0(\mathbf{x})$ the equilibrium condensate density and both $\delta n(\mathbf{x},t)$ and $\delta\phi(\mathbf{x},t)$ fluctuations that are known from the calculations in the previous section. Since these fluctuations are small, we only consider the first non-vanishing term in the condensate fluctuations. For the harmonic potential that is considered here, the parts of the hamiltonian that are linear in the condensate fluctuations $\delta n(\mathbf{x},t)$ and $\delta\phi(\mathbf{x},t)$ vanish, since the fluctuations are odd under $y \to -y$. Hence, there is no decay of a single scissors mode quantum at this level of approximation and we have to consider the parts of the hamiltonian that are quadratic in the condensate fluctuations.

We introduce the Bogoliubov amplitudes $u_j(\mathbf{x})$ and $v_j(\mathbf{x})$ according to

$$\delta\hat{\psi}(\mathbf{x},t) = \sum_j \left[u_j(\mathbf{x})\hat{b}_j(t) - v_j^*(\mathbf{x})\hat{b}_j^\dagger(t)\right], \tag{7.45}$$
$$\delta\hat{\psi}^\dagger(\mathbf{x},t) = \sum_j \left[u_j^*(\mathbf{x})\hat{b}_j^\dagger(t) - v_j(\mathbf{x})\hat{b}_j(t)\right],$$

where $j = 1, 2, ...$ indicates the mode number of the excitation. Note that we neglect the contributions coming from $j = 0$, since we are only interested in the decay into non-condensed excitations and the $j = 0$ term correspond to the dynamics of the global phase of the condensate. Therefore, we have

$$\hat{H}_I(t) = e^{-2i\omega t}\sum_{j,j'\neq 0} H_{j,j'}\hat{b}_j^\dagger(t)\hat{b}_{j'}^\dagger(t) \tag{7.46}$$
$$= \frac{(gC)^2}{\hbar\omega}e^{-2i\omega t}\sum_{j,j'\neq 0}\left[H^1_{j,j'} + \frac{gH^2_{j,j'}}{\hbar\omega}\right]\hat{b}_j^\dagger(t)\hat{b}_{j'}^\dagger(t),$$

where

$$H^1_{j,j'} = \int d\mathbf{x}\, x^2y^2\left[u_j^*(\mathbf{x})u_{j'}^*(\mathbf{x}) - v_j^*(\mathbf{x})v_{j'}^*(\mathbf{x})\right], \tag{7.47}$$
$$H^2_{j,j'} = \int d\mathbf{x}\, x^2y^2 n_0(\mathbf{x})\left[u_j^*(\mathbf{x})u_{j'}^*(\mathbf{x}) + v_j^*(\mathbf{x})v_{j'}^*(\mathbf{x})\right].$$

To make further progress, we need to determine the Bogoliubov amplitudes and determine the time dependence of the operators $\hat{b}_j(t)$ and $\hat{b}_j^\dagger(t)$. Hence, we need to solve the Bogoliubov-de Gennes equations.

In two dimensions the general solution of the Bogoliubov-de Gennes equations is not known. However, in the elongated configuration we expect that the dynamics of the long-wavelength photons is approximately one dimensional. Therefore, we use the exact solution of the Bogoliubov-de Gennes equations in one dimension, see e.g. Ref. [79], in order to make a proper variational ansatz for the form of the non-condensed fluctuations in the elongated configuration. Thus, we consider the ansatz

$$u_j(\mathbf{z}) = \frac{1}{2\sqrt{C_j}}\left[\alpha_j\sqrt{1-|\mathbf{z}|^2} + \frac{\beta_j}{\sqrt{1-|\mathbf{z}|^2}}\right]P_j(\tilde{x}), \tag{7.48}$$
$$v_j(\mathbf{z}) = \frac{1}{2\sqrt{C_j}}\left[\alpha_j\sqrt{1-|\mathbf{z}|^2} - \frac{\beta_j}{\sqrt{1-|\mathbf{z}|^2}}\right]P_j(\tilde{x}),$$

with $\mathbf{z} = (\tilde{x}, \tilde{y}) = (x/R_{\mathrm{TF},x}, y/R_{\mathrm{TF},y})$ and $P_j(\tilde{x})$ the j-th Legendre polynomial. Furthermore, the constants α_j and β_j are given by

$$\alpha_j = \frac{1}{\sqrt{R_{\mathrm{TF},x} R_{\mathrm{TF},y}}} \sqrt{\frac{\mu}{\hbar\Omega_j}}, \qquad \beta_j = \frac{1}{2\sqrt{R_{\mathrm{TF},x} R_{\mathrm{TF},y}}} \sqrt{\frac{\hbar\Omega_j}{\mu}}, \tag{7.49}$$

with $\Omega_j = \omega_x \sqrt{j(j+1)/2}$ the energy eigenvalues of the one dimensional problem. Also $R_{\mathrm{TF},x}$ and $R_{\mathrm{TF},y}$ correspond to the Thomas-Fermi radius of the condensate in the specified direction. Moreover, we defined the constant C_j which is given by

$$C_j = \int_{-1}^{1} d\tilde{x}\, (1-\tilde{x}^2)^{1/2} \left[P_j(\tilde{x})\right]^2 . \tag{7.50}$$

This ansatz corresponds to a solution for an elongated trap where the excitation only propagates in the direction with the small trapping frequency. Note that if from the start we would have removed the y-dependence, our ansatz simplifies to the exact solution in one dimension as given in Ref. [79].

Since the photons are in a good first approximation equivalent to non-relativistic particles with an effective mass m and point-like interaction with strength g, we consider the following action within the functional-integral formalism in the Bogoliubov approximation

$$\begin{aligned} S[\phi^*, \phi] = &\int d\tau \int d\mathbf{x}\, \phi^*(\mathbf{x},\tau) G^{-1}(\mathbf{x},\tau) \phi(\mathbf{x},\tau) \\ &+ \frac{g}{2} \int d\tau \int d\mathbf{x}\, n_0(\mathbf{x}) \left\{ \left[\phi^*(\mathbf{x},\tau)\right]^2 + \left[\phi(\mathbf{x},\tau)\right]^2 \right\} . \end{aligned} \tag{7.51}$$

Here we defined

$$G^{-1}(\mathbf{x},\tau) = \hbar \frac{\partial}{\partial \tau} - \frac{\hbar^2 \nabla^2}{2m} + V^{\mathrm{ext}}(\mathbf{x}) - \mu + 2gn(\mathbf{x}). \tag{7.52}$$

Furthermore, $\phi(\mathbf{x},\tau)$ and $\phi^*(\mathbf{x},\tau)$ are the fields that describe the fluctuations that originate from the Bogliubov approximation $\psi(\mathbf{x},\tau) = \langle \psi(\mathbf{x},\tau) \rangle + \phi(\mathbf{x},\tau)$, $n_0(\mathbf{x})$ is the condensate density, $n(\mathbf{x})$ equals the total density and $V^{\mathrm{ext}}(\mathbf{x})$ corresponds to the external trapping potential. We consider the usual Bogoliubov transformation with

$$\phi(\mathbf{x},\tau) = \sum_j \left[u_j(\mathbf{x}) b_j(\tau) - v_j^*(\mathbf{x}) b_j^*(\tau) \right], \tag{7.53}$$

and the ansatz from Eq. (7.48) for the coherence factors. This allows us to rewrite

$$S = \frac{1}{2}\int d\tau \sum_{j,j'} \begin{bmatrix} b_j(\tau) \\ b_j^*(\tau) \end{bmatrix}^\dagger \cdot \begin{bmatrix} G_{j,j',11} & G_{j,j',12} \\ G_{j,j',12} & G_{j,j',11} \end{bmatrix} \begin{bmatrix} b_{j'}(\tau) \\ b_{j'}^*(\tau) \end{bmatrix} \tag{7.54}$$
$$+ \frac{1}{2}\int d\tau \sum_{j,j'} \begin{bmatrix} b_j(\tau) \\ b_j^*(\tau) \end{bmatrix}^\dagger \cdot \begin{bmatrix} G_{j,j'} & 0 \\ 0 & -G_{j,j'} \end{bmatrix} \cdot \hbar\frac{\partial}{\partial\tau} \begin{bmatrix} b_{j'}(\tau) \\ b_{j'}^*(\tau) \end{bmatrix},$$

with

$$G_{j,j'} = \int d\mathbf{x} \left[u_j(\mathbf{x})u_{j'}(\mathbf{x}) - v_j(\mathbf{x})v_{j'}(\mathbf{x})\right], \tag{7.55}$$
$$G_{j,j',11} = -g\int d\mathbf{x}\, n_0(\mathbf{x}) \left[u_j(\mathbf{x})v_{j'}(\mathbf{x}) + u_{j'}(\mathbf{x})v_j(\mathbf{x})\right]$$
$$+ \int d\mathbf{x} \left[u_j(\mathbf{x})G^{-1}(\mathbf{x})u_{j'}(\mathbf{x}) + v_j(\mathbf{x})G^{-1}(\mathbf{x})v_{j'}(\mathbf{x})\right],$$
$$G_{j,j',12} = g\int d\mathbf{x}\, n_0(\mathbf{x}) \left[u_j(\mathbf{x})u_{j'}(\mathbf{x}) + v_j(\mathbf{x})v_{j'}(\mathbf{x})\right]$$
$$- \int d\mathbf{x} \left[u_j(\mathbf{x})G^{-1}(\mathbf{x})v_{j'}(\mathbf{x}) + v_j(\mathbf{x})G^{-1}(\mathbf{x})u_{j'}(\mathbf{x})\right].$$

Here we used that $u_n(\mathbf{x})$ and $v_n(\mathbf{x})$ are real. Furthermore,

$$G^{-1}(\mathbf{x}) = G^{-1}(\mathbf{x},\tau) - \hbar\frac{\partial}{\partial\tau} = -\frac{\hbar^2}{2m}\frac{\partial^2}{\partial x^2} + gn_0(\mathbf{x}), \tag{7.56}$$

where we used the Gross-Pitaevski equation in the Thomas-Fermi limit. Moreover, in this limit we can also neglect the second-order derivative with respect to y. This is valid as G^{-1} acts on $u_n(\mathbf{x})$ and $v_n(\mathbf{x})$ that only have y-dependence in the density.

We consider $F_j(\mathbf{x}) = u_j(\mathbf{x}) + v_j(\mathbf{x})$ and $G_j(\mathbf{x}) = u_j(\mathbf{x}) - v_j(\mathbf{x})$ with $u_j(\mathbf{x})$ and $v_j(\mathbf{x})$ as given by Eq. (7.48). Then,

$$-\frac{\hbar^2}{2m}\frac{\partial^2}{\partial x^2}u_j(\mathbf{x}) = -\frac{\hbar^2}{4m}\frac{\partial^2}{\partial x^2}(F_j(\mathbf{x}) + G_j(\mathbf{x})) \tag{7.57}$$
$$= -\frac{\hbar^2}{4m}\frac{\partial^2}{\partial x^2}F_j(\mathbf{x}) = \frac{1-\tilde{x}^2-\tilde{y}^2}{1-\tilde{x}^2}\frac{\hbar\Omega_j}{2}G_j(\mathbf{x}),$$

where we used the results of Ref. [59] and the fact that we are in the Thomas-Fermi limit and therefore neglected the derivatives of the densities. Namely, all these derivatives result into second-order derivatives of densities

or terms that contain $n_0'(\mathbf{x})/n_0(\mathbf{x})$, which are all small in the Thomas-Fermi limit. Similarly, we find that

$$-\frac{\hbar^2}{2m}\frac{\partial^2}{\partial x^2}v_j(\mathbf{x}) = \frac{1-\tilde{x}^2-\tilde{y}^2}{1-\tilde{x}^2}\frac{\hbar\Omega_j}{2}G_j(\mathbf{x}). \tag{7.58}$$

Now, we define

$$I_{j,j'} = \frac{1}{\sqrt{C_j C_{j'}}}\int_{-1}^{1} d\tilde{x}\, P_j(\tilde{x})P_{j'}(\tilde{x})\sqrt{1-\tilde{x}^2}. \tag{7.59}$$

Then,

$$G_{j,j'} = \frac{1}{2}\left[\sqrt[4]{\frac{j'(j'+1)}{j(j+1)}} + \sqrt[4]{\frac{j(j+1)}{j'(j'+1)}}\right] I_{j,j'}, \tag{7.60}$$

$$G_{j,j',11} = \left(\frac{\hbar\Omega_{j'}}{3} + \frac{\hbar\Omega_j}{2}\right)\sqrt[4]{\frac{j'(j'+1)}{j(j+1)}} I_{j,j'},$$

$$G_{j,j',12} = \left(\frac{\hbar\Omega_j}{2} - \frac{\hbar\Omega_{j'}}{3}\right)\sqrt[4]{\frac{j'(j'+1)}{j(j+1)}} I_{j,j'}.$$

For now we ignore the coupling between modes where $j \neq j'$. Note that this is in general a good approximation as the integral $I_{j,j'}$ has a maximal value for $j = j'$ and gradually decreases if j is further and further away from j'. This allows us to rewrite

$$S = \frac{\hbar\Omega_j}{12}\int d\tau \sum_j \left\{[b_j(\tau)]^2 + \left[b_j^*(\tau)\right]^2\right\} \tag{7.61}$$

$$+ \frac{1}{2}\int d\tau \sum_j \left\{b_j^*(\tau)\left[\hbar\frac{\partial}{\partial\tau} + \frac{5\hbar\Omega_j}{6}\right] b_j(\tau) - b_j(\tau)\left[\hbar\frac{\partial}{\partial\tau} - \frac{5\hbar\Omega_j}{6}\right] b_j^*(\tau)\right\}$$

To complete our variational approach we determine the equations of motion, which allows us to determine the time dependence of the operators $b_j(\tau)$ and $b_j^*(\tau)$. We find for the equations of motion

$$\left(\hbar\frac{\partial}{\partial\tau} + \frac{5\hbar\Omega_j}{6}\right) b_j(\tau) + \frac{\hbar\Omega_j}{6}b_j^*(\tau) = 0, \tag{7.62}$$

$$\left(\hbar\frac{\partial}{\partial\tau} - \frac{5\hbar\Omega_j}{6}\right) b_j^*(\tau) - \frac{\hbar\Omega_j}{6}b_j(\tau) = 0,$$

for every $j = 0, 1, ...$ Hence,

$$b_j(\tau) = c_n^* e^{\sqrt{\frac{2}{3}}\Omega_j\tau} + d_j e^{-\sqrt{\frac{2}{3}}\Omega_j\tau}, \tag{7.63}$$

$$b_j^*(\tau) = c_n e^{-\sqrt{\frac{2}{3}}\Omega_j\tau} + d_j^* e^{\sqrt{\frac{2}{3}}\Omega_j\tau}.$$

Thus the energy of the excitations for $j = 0, 1, 2, ...$ is equal to

$$\hbar\omega_j = \hbar\Omega_j\sqrt{2/3} = \hbar\omega_x\sqrt{j(j+1)/3}. \tag{7.64}$$

To quantify the effect of neglecting the non-diagonal terms, we numerically determine the eigenvalues of the full problem, where we consider terms from $j = 1$ to $j = 75$. The largest error of roughly 15 percent occurs for $j = 1$. For the other values of j the error is even smaller and less than 10 percent. Therefore, it is indeed a good first approximation to neglect the non-diagonal terms. Furthermore, by resubstituting the expressions in Eqs. (7.63) into Eqs. (7.62) we obtain

$$\begin{aligned} d_j^* &= -\left(5 + 2\sqrt{6}\right) c_j^*, \\ c_j &= \left(2\sqrt{6} - 5\right) d_j. \end{aligned} \tag{7.65}$$

Hence, up to an overal normalization constant

$$\phi(\mathbf{x}, \tau) = \sum_j \left[\tilde{u}_j(\mathbf{x}) d_j e^{-\omega_j\tau} - \tilde{v}_j^*(\mathbf{x}) d_j^* e^{\omega_j\tau}\right], \tag{7.66}$$

where

$$\begin{aligned} \tilde{u}_j(\mathbf{x}) &= u_j(\mathbf{x}) + \left(5 - 2\sqrt{6}\right) v_j^*(\mathbf{x}), \\ \tilde{v}_j^*(\mathbf{x}) &= v_j^*(\mathbf{x}) + \left(5 - 2\sqrt{6}\right) u_j(\mathbf{x}). \end{aligned} \tag{7.67}$$

By using these expressions for the Bogoliubov amplitudes, we find for $H_{j,j'}$ as defined in Eqs. (7.46) and (7.47),

$$\begin{aligned} H_{j,j'} = &\frac{2g}{\pi R_{\mathrm{TF},y} R_{\mathrm{TF},x}} \frac{1}{\sqrt{Z_{j,j}^{0,1} Z_{j',j'}^{0,1}}} \\ &\times \left[\left(\sqrt{\frac{\omega_{j'}}{\omega_j}} + \sqrt{\frac{\omega_j}{\omega_{j'}}} + \frac{\sqrt{\omega_j\omega_{j'}}}{2\omega}\right) Z_{j,j'}^{2,3} + \frac{16\mu^2}{35\hbar\omega\sqrt{\hbar\omega_j\hbar\omega_{j'}}} Z_{j,j'}^{2,7}\right], \end{aligned} \tag{7.68}$$

where we used the shorthand notation

$$Z_{j,j'}^{m,n} = \int_{-1}^{1} d\tilde{x}\, \tilde{x}^m \left(1 - \tilde{x}^2\right)^{n/2} P_j(\tilde{x}) P_{j'}(\tilde{x}). \tag{7.69}$$

To investigate the damping of the scissors modes, we are interested in the transition rate for creating two excitations with frequency ω_j and

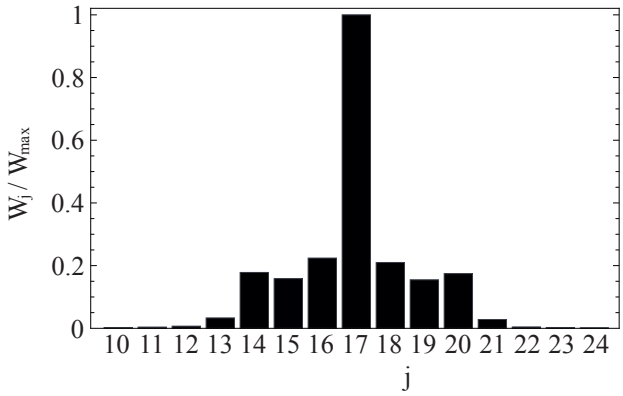

Figure 7.7: The decay rate of two scissors mode quanta into a non-condensed mode $W_j = \sum_{j'} W_{j,j'}(1 + \delta_{j,j'})$ with mode number j for $\mu = 10\,\omega_y$, $\omega_y = 10\,\omega_x$ and $\alpha = 10^{-2}$.

$\omega_{j'}$ from the vacuum through the decay of two scissors mode quanta. By applying Fermi's Golden Rule, we obtain

$$W_{j,j'} \simeq \frac{8\pi |H_{j,j'}|^2}{\hbar(1+\delta_{j,j'})}\rho(\omega_j + \omega_{j'}), \tag{7.70}$$

where

$$\rho(\omega_j + \omega_{j'}) = \frac{1}{\pi\hbar}\frac{\alpha(\omega_j + \omega_{j'})}{(\omega_j + \omega_{j'} - 2\omega)^2 + [\alpha(\omega_j + \omega_{j'})]^2}. \tag{7.71}$$

Here we introduced a final density of states $\rho(E)$ to incorporate that, due to the interaction with the molecules, there is a probability that the photon is in a state with an energy that is within a small band around $\omega_j + \omega_{j'}$. Note that for the current experiments we have that $\beta(\hbar\omega_j + \hbar\omega_{j'}) \ll 1$ with $\beta = 1/k_{\rm B}T$ the inverse of the thermal energy. Therefore, we used the low-energy approximation for the density of states [75]. As the dimensionless damping parameter α is small, we directly satisfy $W_{j,j'} \simeq 0$ to a very good approximation if the photons scatter into a state with energy outside the small band around $\omega_j + \omega_{j'}$. Note that the nonzero value of α makes our calculation specific to dissipative Bose-Einstein condensates and not immediately applicable to a cold atomic gas, where $\alpha = 0$ and Beliaev damping of the scissors modes is only possible in the presence of fine-tuned degeneracies [171].

In Fig. 7.7 we show the decay rate $W_j = \sum_{j'} W_{j,j'}(1+\delta_{j,j'})$ for $\mu = 10\,\omega_y$, $\omega_y = 10\,\omega_x$ and $\alpha = 10^{-2}$. Because the frequency of the scissors mode ω is roughly equal to ω_{17}, we obtain a peak for $j = 17$. Furthermore, we find

that the decay of the scissors modes indeed leads to population of several non-condensed modes.

7.6 Density-density correlation function

We now consider the situation that the scissors modes are being excited and we consider the density-density correlation function in the operator formalism. Thus, we define

$$g^{(2)}(\mathbf{x},\mathbf{x}',t) = \frac{\langle\hat{\rho}(\mathbf{x},t)\hat{\rho}(\mathbf{x}',t)\rangle}{\langle\hat{\rho}(\mathbf{x},t)\rangle\langle\hat{\rho}(\mathbf{x}',t)\rangle} - 1, \tag{7.72}$$

where $\hat{\rho}(\mathbf{x},t) = \hat{\psi}^\dagger(\mathbf{x},t)\hat{\psi}(\mathbf{x},t)$ is the density operator. We again take $\hat{\psi}(\mathbf{x},t) = \langle\hat{\psi}(\mathbf{x},t)\rangle + \delta\hat{\psi}(\mathbf{x},t)$ and we explicitly separate the fluctuations that are described as scissors modes and Bogoliubov excitations by writing $\delta\hat{\psi}(\mathbf{x},t) = \delta\hat{\psi}_s(\mathbf{x},t) + \delta\hat{\psi}_B(\mathbf{x},t)$. As a consequence, the density-density correlation function contains the density-density correlations from the scissors modes and also a term from the density-density correlations between the Bogoliubov modes. From now onwards we take $y = y' = 0$ such that the contribution of the scissors modes vanishes, as can be seen explicitly in Eqs. (7.41) and (7.42).

For the part with the Bogoliubov excitations we can use Eq. (7.45) to rewrite the result in terms of the Bogoliubov amplitudes $u(\mathbf{x})$ and $u(\mathbf{x})$. We find

$$g^{(2)}(\mathbf{x},\mathbf{x}',t) = \sum_n \frac{(u_n(\mathbf{x}) - v_n(\mathbf{x}))\,(u_n(\mathbf{x}') - v_n(\mathbf{x}'))}{\sqrt{n_0(\mathbf{x})n_0(\mathbf{x}')}} \left\{1 + 2\left\langle\hat{b}_n^\dagger(t)\hat{b}_n(t)\right\rangle\right\}, \tag{7.73}$$

where $N_n(t) = \langle\hat{b}_n^\dagger(t)\hat{b}_n(t)\rangle$ is the number of excitations in a mode n at time t. The contribution of $g^{(2)}(\mathbf{x},\mathbf{x}',t)$ that is independent of $N_n(t)$ has an ultraviolet divergence that can be resolved by an appropriate subtraction [155]. However, generally this part is neglible compared to the contribution that depends on $N_n(t)$ as the photons are at room temperature. Thus, in the following we neglect this so-called quantum contribution.

To find the number of excitations $N_j(t)$, we solve the following coupled system of equations

$$\begin{aligned} &\frac{\partial N_\mathrm{s}(t)}{\partial t} + \sum_j \frac{\partial N_j(t)}{\partial t} = 0, \\ &\frac{\partial N_j(t)}{\partial t} = N_\mathrm{s}^2(t)\sum_{j'} W_{j,j'}(1 + N_{j'}(t))(1 + \delta_{j,j'} + N_j(t)), \end{aligned} \tag{7.74}$$

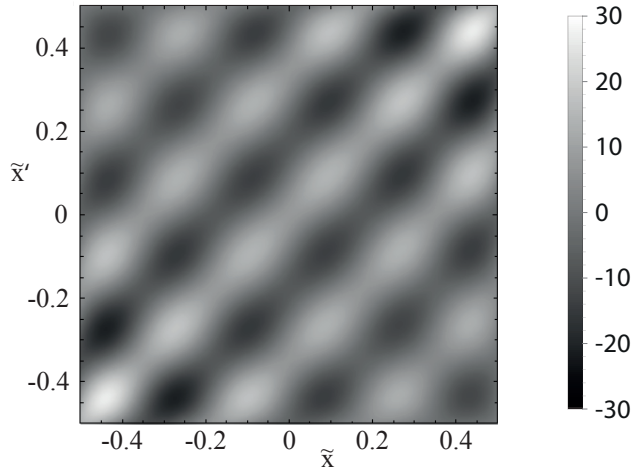

Figure 7.8: The density-density correlation function of the Bogoliubov excitations $8n_0\xi^2 g^{(2)}(\mathbf{x}, \mathbf{x}', t)$, where $n_0\xi^2 = \hbar^2/2mg$ with ξ the so-called coherence length and n_0 the condensate density in the center of the trap, in terms of $(\hbar\omega_x)^2\hbar\omega_y/\mu^3$ for $y = y' = 0$.

where $N_{\rm s}(t)$ denotes the number of scissors mode quanta and $W_{j,j'}$ is the decay rate that is defined in Eq. (7.70). As a lower limit we neglect the Bose stimulation factors in the rate equations and in this approximation we find

$$N_j(t) = \frac{N_{\rm s}^2(0)\sum_{j'} W_{j,j'}(1+\delta_{j,j'})t}{1 + N_{\rm s}(0)\sum_{j,j'} W_{j,j'}(1+\delta_{j,j'})t}. \tag{7.75}$$

Now we use the decay rates as displayed in Fig. 7.7 and as an illustration we consider a time t such that $N_j(t) = W_j/W_{\rm max}$. The corresponding contribution of the decay of the scissors modes to the density-density correlation function is displayed in Fig. 7.8. Note that in experiments there is always another contribution from the thermal background, which is given by replacing $\left\langle b_n^\dagger(t) b_n(t) \right\rangle$ by the Bose-Einstein distribution function at energy $\hbar\omega_n$. Therefore, to obtain the result of this figure experimentally, the contribution from the thermal background should be subtracted.

This is only possible when the contribution originating from this decay process is large enough compared to the background contribution. If we consider a time t such that $N_j(t) = W_j/W_{\rm max}$, for $x \simeq x'$ the value of the background contribution is at least two orders of magnitude larger and therefore we expect that in this region it is difficult to observe. However, for $|\tilde{x} - \tilde{x}'| \geq 0.2$ the largest value of the thermal background is maximally

a factor of ten larger than the scissors mode contribution. The exact time scale at which the number of excitations $N_i(t)$ takes this value depends on many parameters such as the number of scissors modes and the trapping frequencies. For an estimate we take values of the parameters from current experiments on Bose-Einstein condensation of photons and we obtain that this condition can be fulfilled within the nanosecond regime.

We calculated the number of excitations $N_n(t)$ while ignoring the Bose stimulation factors in the rate equations. To compare with experimental results, the incorporation of these additional terms can be important. In first approximation these factors can be incorporated by replacing the number of excitations by their expectation value. As this renormalization increases the decay rate, we obtain that within the nanosecond regime the signal of the decay of the scissors modes is comparable to the background for $|\tilde{x} - \tilde{x}'| \geq 0.2$. Hence, we expect that the effect of the decay of the scissors modes can be distinguished from the background and is observable in the density-density correlation function.

In the elongated configuration, as envisaged here, the Bogoliubov amplitudes are proportional to Legendre polynomials. Since these are approximately standing waves, the scissors mode decays predominently into a pair of excitations consisting of an excitation with a certain local momentum k and $-k$. This then also explains the correspondence with the dynamical Casimir effect as an external perturbation, in this case a sudden rotation of the trap, leads to the creation of phonon pairs from the vacuum. Therefore, a measurement of this density-density correlation function would give a demonstration of an analog of the dynamical Casimir effect in a Bose-Einstein condensate of light, which up to now only is considered in atomic and exciton-polariton condensates [178–180].

7.7 Discussion and conclusion

In this Chapter we discussed a model for a semiconductor that qualitatively contains the correct crossover physics. However, to obtain the correct quantitative result, several improvements have to be made. First, in our model we only take into account one conduction and valence band. In a realistic semiconductor there are multiple bands that all have to be included. Moreover, we have not taken into account the band-gap renormalization when self-consistently determining the chemical potential. However, for quantitative agreement it will be important to be more careful about this and include the effect of Coulomb screening on the renormalization of the band gap.

Another simplification is the use of the contact interaction for the interactions between the electrons and holes. Normally, these interactions are described by a Yukawa potential due to screening effects in the semiconductor. Although we use the scattering length for the Yukawa potential as input for the strength of the contact interaction, taking a contact interaction for the interactions between the electrons and holes is still a rough approximation at low carrier densities where screening is not very effective. However, we are primarily interested in large carrier densities and in this regime the Yukawa potential behaves more and more like a contact interaction. We verified that in this regime the susceptibility for Yukawa interactions and the contact interaction agree quite well. For a quantitative agreement at all carrier densities, the Yukawa potential has to be taken into account. Another extension of our model is to consider dynamical screening effects, which become important at very high carrier densities [181].

In conclusion, we have considered Bose-Einstein condensation of light in nano-fabricated semiconductor microcavities. We model the semiconductor as a two-band system consisting of electrons and holes that interact via a contact interaction. To incorporate screening effects, we use the scattering length for the Yukawa potential as input parameter for the strength of the contact interaction. We have demonstrated that this model contains a qualitative description of the regime with and without excitons. Moreover, we have shown that if we couple light to the semiconductor, for large carrier densities the finite-lifetime effects of the photons can be characterized by a single dimensionless parameter α, which is proportional to the slope of the imaginary part of the susceptibility at zero energy. Hereafter, we have proposed to probe the superfluidity of the light in the nano-fabricated semiconductor microcavities via the excitation that the scissors modes. By using Fermi's Golden Rule and a variational ansatz to calculate the Bogoliubov amplitudes, we determined the decay rates of the scissors modes into the non-condensed excitations. Finally, we have demonstrated that the density-density correlation function of the excited light fluid exhibits an analog of the dynamical Casimir effect.

Samenvatting

Door van jongs af aan goed om ons heen te kijken, hebben we een bepaalde intuïtie ontwikkeld waarmee we het gedrag van alledaagse dingen kunnen zien aankomen. Zo weten we dat een pen op de grond valt als deze van een tafel afrolt en een fiets uiteindelijk tot stilstand komt als je stopt met trappen. Het is echter belangrijk om onderscheid te maken tussen deze zogenaamde macroscopische processen en natuurkundige processen op microscopische schaal. Op dit allerkleinste niveau gedragen deeltjes zich namelijk anders dan dat wij gewend zijn. We kunnen dit al begrijpen aan de hand van de bouwsteen van alle materie op aarde: het atoom. Uit experimenten blijkt dat de fysische eigenschappen van een atoom, zoals bijvoorbeeld de lading, stapsgewijs toenemen. Zo is het voor een atoom dus alleen mogelijk om een elektrische lading te hebben die een veelvoud is van de elementaire ladingseenheid. Aangezien dit zo veel verschilt van het gedrag van voorwerpen waar we iedere dag mee te maken hebben, is het moeilijk om hiervan een voorstelling te maken.

Om het gedrag van atomen op microscopisch niveau te beschrijven is er een speciale theorie ontwikkeld, namelijk de kwantummechanica. Uit deze theorie volgt dat atomen zich niet alleen als deeltjes, maar ook als een golf kunnen gedragen. Hierbij worden de fysische eigenschappen van een deeltje, zoals bijvoorbeeld de plaats en snelheid, beschreven door een zogenaamde fysische toestand. Voor het gedrag van een atoom is het belangrijk om te kijken naar de waarde van zijn spin, een puur kwantummechanische eigenschap die op het macroscopische niveau doet denken aan de mate waarmee een tol rond zijn as draait. In de kwantummechanica wordt er onderscheid gemaakt tussen deeltjes met een heeltallige en halftallige spin. In het eerste geval spreken we over bosonen, terwijl fermionen deeltjes zijn met een halftallige spin. In een verzameling van identieke fermionen is het voor twee fermionen niet toegestaan om dezelfde fysische toestand te

bezetten. Daarentegen geldt voor identieke bosonen dat het aantal in dezelfde fysische toestand ongelimiteerd is. Het is zelfs zo dat het voor een boson waarschijnlijker is om een bepaalde toestand in te nemen, als deze al door meerdere bosonen wordt bezet. Bij extreem lage temperaturen of grote dichtheden van deeltjes, kunnen de bosonen zelfs in een bijzondere toestand komen. In dit zogenaamde Bose-Einstein condensaat hebben alle bosonen in het systeem de laagst mogelijke energie. Dit is voor fermionen onmogelijk, omdat identieke fermionen nooit in dezelfde fysische toestand kunnen zitten.

Bose-Einstein condensatie kunnen we het beste vergelijken met een alledaags voorbeeld zoals filevorming. Als er weinig auto's op de snelweg zijn, is het voor alle afzonderlijke auto's mogelijk om met een verschillende snelheid over de snelweg te rijden. Dit is echter niet meer het geval als het aantal auto's op de snelweg te groot wordt en er een file ontstaat. De auto's kunnen zich dan niet meer afzonderlijk voortbewegen en alleen een gezamenlijke verplaatsing is mogelijk. Ook weten we uit de praktijk dat de hoeveelheid auto's die nodig is om een file te laten ontstaan afhankelijk is van verschillende factoren. Zo weten we bijvoorbeeld dat het weer een grote invloed op files heeft. Bovendien zien we in deze vergelijking dat het niet zo vreemd is dat iets zich als een golf en deeltje tegelijk gedraagt. Als we de file namelijk als geheel bekijken, dan gedraagt deze zich als een golf, terwijl het geheel nog steeds uit afzonderlijke auto's bestaat.

In een experiment kunnen bosonen worden gevangen in een val, waardoor ze zich alleen nog in een klein gebied kunnen bewegen. Door het aantal deeltjes in dit gebied groot genoeg te maken, nemen de bosonen spontaan de laagst toegestane energie aan en vormen ze samen het Bose-Einstein condensaat. Net als bij filevorming, is het aantal benodigde bosonen om een condensaat te vormen afhankelijk van verschillende factoren, zoals de temperatuur in het experiment en de massa van de deeltjes. Verder wordt ook in dit geval het gezamenlijke gedrag van de deeltjes in het Bose-Einstein condensaat beschreven als een golf.

Vanuit een theoretisch oogpunt is het relatief eenvoudig om te bepalen wat de voorwaarde voor het optreden van Bose-Einstein condensatie is. Praktisch gezien is het maken van een Bose-Einstein condensaat daarentegen een grote technologische uitdaging. In de natuur komen namelijk alleen bosonische atomen voor met een relatieve grote massa, waardoor deze deeltjes alleen kunnen condenseren als het systeem wordt afgekoeld naar temperaturen die lager zijn dan een miljoenste graad boven het absolute nulpunt. Om deze temperaturen te bereiken, zijn zeer geavanceerde apparatuur en technieken vereist. Hierdoor heeft het tot 1995 geduurd om

een atomair gas tot deze temperatuur af te koelen en daarmee voor de eerste keer een Bose-Einstein condensaat waar te nemen.

Door de observatie van het eerste Bose-Einstein condensaat ontstond een heel nieuw onderzoeksgebied. Het systeem is zo interessant doordat de eigenschappen van de deeltjes in deze systemen sterk kunnen worden gemanipuleerd. Zo is het bijvoorbeeld mogelijk om de wisselwerking tussen de deeltjes aan te passen naar een willekeurige sterkte. Het is dus mogelijk om te veranderen tussen situaties waarbij atomen elkaar aantrekken of juist afstoten. Dit is met name cruciaal voor het onderzoeken van veeldeeltjesverschijnselen uit de kwantummechanica, omdat deze in grote mate afhankelijk zijn van de sterkte van de onderlinge interacties. Inmiddels zijn er meerdere veeldeeltjesverschijnselen geobserveerd. Het meest indrukwekkende fenomeen is waarschijnlijk supergeleiding, een toestand waarin atomen wrijvingsloos kunnen bewegen en er dus geen energieverlies optreedt.

Alhoewel we het tot nu toe alleen over bosonische atomen hebben gehad, is het in principe voor alle deeltjes met een bosonisch karakter mogelijk om een Bose-Einstein condensaat te vormen. Aangezien lichtdeeltjes ook bosonen zijn, zou het ook mogelijk moeten zijn om een Bose-Einstein condensaat van licht te maken. Het probleem is echter dat het foton geen massa heeft. Daardoor lijkt het onmogelijk om aan de conditie voor Bose-Einstein condensatie te voldoen. Een paar jaar geleden is er echter een oplossing voor dit probleem gevonden. Door het licht in een specifieke configuratie te vangen en te laten wisselwerken met een vloeistof, gedragen de lichtdeeltjes zich hetzelfde als bosonen met een bepaalde massa. Het grote voordeel is zelfs dat in vergelijking met bosonische atomen de massa heel klein blijkt te zijn, waardoor het mogelijk is om op kamertemperatuur een Bose-Einstein condensaat te vormen. In tegenstelling tot de experimenten met atomaire Bose-Einstein condensaten, is er een continue doorstroom van deeltjes. Hierdoor is het interessant om te bekijken in hoeverre deze verschillen de al geobserveerde veeldeeltjesverschijnselen veranderen. Ook zijn bepaalde experimenten, zoals een interferentie-experiment, makkelijker met licht uit te voeren dan met atomen. Daardoor zijn er nieuwe mogelijkheden om andere verschijnselen te onderzoeken, die moeilijk te bestuderen zijn in atomaire systemen.

In dit proefschrift onderzoeken we veeldeeltjesverschijnselen in een Bose-Einstein condensaat van licht. In de introductie beschrijven we meerdere veeldeeltjesverschijnselen in atomaire Bose-Einstein condensaten en behandelen we het experiment waar het eerste Bose-Einstein condensaat van licht werd waargenomen. Daarna construeren we in Hoofdstuk 2 een model

waarmee het volledige proces van Bose-Einstein condensatie van licht kan worden beschreven. Dit model gebruiken we in het vervolg van dit proefschrift om verschillende veeldeeltjesverschijnselen te onderzoeken.

In Hoofdstuk 3 bekijken we correlatiefuncties. Deze correlatiefuncties geven een beeld van de samenhang tussen de verschillende deeltjes in het systeem. Vervolgens onderzoeken we in Hoofdstuk 4 veranderingen in het aantal deeltjes van een Bose-Einstein condensaat. Aangezien fluctuaties in het aantal gecondenseerde deeltjes zijn waargenomen in het lichtcondensaat, maken we een directe vergelijking tussen de experimentele resultaten en ons model. Hierna bestuderen we in Hoofdstuk 5 de fase van de golffunctie van het Bose-Einstein condensaat. In het bijzonder beschrijven we een methode om de fase van Bose-Einstein condensaat van licht te onderzoeken. In Hoofdstuk 6 beschouwen we de situatie dat de fotonen zijn gevangen in een val met een periodieke structuur. In dit geval behandelen we de overgang tussen de twee verschillende fases waarin het licht zich kan bevinden. In de ene fase liggen de posities van alle fotonen vast en in het andere geval kunnen de deeltjes vrij rond bewegen. Tot slot verkennen we in Hoofdstuk 7 een ander systeem waarin licht zou kunnen condenseren. Ook bestuderen we een bijzondere collectieve beweging van fotonen die kan worden gebruikt om te bepalen of het licht supergeleidend is.

In de korte tijd na het ontdekken van het eerste Bose-Einstein condensaat van licht is al veel vooruitgang geboekt. Zo laten we in dit proefschrift zien dat we al een goed beeld hebben gekregen van verschillende veeldeeltjesverschijnselen in dit systeem. Ook zijn er inmiddels meerdere experimentele groepen die dit condensaat kunnen maken. Bovendien zijn er ideeën voor andere systemen waarin licht zou kunnen condenseren. Dit alles is een zeer bemoedigend vooruitzicht om uiteindelijk het volledige kwantumgedrag van gecondenseerd licht te begrijpen.

Curriculum Vitae

Ik ben geboren op 9 mei 1989 in Schoonrewoerd. Mijn VWO-opleiding heb ik gevolgd aan het Heerenlanden College in Leerdam van 2001 tot 2007. Hierna ben ik begonnen met de bacheloropleiding Natuur- en Sterrenkunde aan de Universiteit Utrecht. Na een overstap naar het dubbele bachelorprogramma Natuurkunde en Wiskunde ben ik in 2010 cum laude afgestudeerd in beide richtingen. Vervolgens heb ik de masteropleiding Theoretische Natuurkunde gevolgd. In 2012 behaalde ik mijn masterdiploma cum laude, waarna ik een promotieonderzoek heb gedaan onder begeleiding van Henk Stoof en Rembert Duine. De resultaten van dit onderzoek zijn terug te vinden in dit proefschrift.

Acknowledgments

First of all I would like to thank my supervisors Henk en Rembert for all the nice discussions and the many times you pointed me in the right direction. I am thankful I could benefit from your extensive knowledge and your enthusiasm about physics inspired me a lot. I have really enjoyed working together during the last four years!

Next, I want to thank the Master's students whom I supervised during my time as a PhD student. Oleksiy and Erik, the projects not only have led to publications that are part of this thesis, I also really liked working together with you. Thanks for all the hard work and I am pretty sure that both of you will write a nice PhD thesis within a few years. Moreover, I would like to thank Erik for reading parts of this thesis and helping me out with correcting misspellings.

There are also many people that did not directly contribute to the content of this thesis, but made my life the last four years more enjoyable. Especially, I would like to acknowledge all the people at the ITF for the nice breaks, conversations and the friendly atmosphere. I want to name a few people in particular. My office mates during the last four years: Benedetta, Jasper, Jeroen and Marco. Thanks for sharing the struggles with Mathematica and LaTeX, making me more familiar with the Italian culture and all the small talks. Jeffrey, I enjoyed working together during the Master and sharing the ups and downs of being a PhD student. Nick, thanks for the challenging Wordfeud matches. Joost, Olga, Riny and Wanda thanks for solving all kind of organizational problems and setting up the nice ITF coffee/tea get-togethers. And last but not least, I would like to acknowledge all members of the BEC group for the nice formal and more informal meetings.

Finally, but most importantly, I would like to mention the people closest to me. Hans, het was altijd leuk om samen te sporten of mee te doen

aan verschillende poules. Vittoria, buona fortuna per il tuo dottorato di ricerca. Hendrik en Ilona, ik heb erg genoten van de gezellige uitjes en etentjes. Sofie en Job, ook al zijn jullie nog klein, jullie zorgen altijd voor een glimlach op mijn gezicht. Marius en Joyce, het is altijd gezellig als jullie langskomen en we kunnen bijpraten over theoretische natuurkunde en andere dingen. Pa en moe, bedankt voor alle dingen die jullie voor mij hebben gedaan en dat jullie er altijd voor mij zijn geweest als het nodig was.

Bibliography

[1] S. Bose, Z. Phys. **26**, 178 (1924).

[2] A. Einstein, Sitz. ber. Preuss. Akad. Wiss. **1**, 3-14 (1925).

[3] M.H. Anderson, J.R. Ensher, M.R. Matthews, C.E. Wieman, and E.A. Cornell, Science **269**, 198 (1995).

[4] C.C. Bradley, C.A. Sackett, J.J. Tollett, and R.G. Hulet, Phys. Rev. Lett. **75**, 1687 (1995).

[5] K.B. Davis et al., Phys. Rev. Lett. **75**, 3969 (1995).

[6] M. Lewenstein and L. You, Phys. Rev. Lett. **77**, 3489-3493 (1996).

[7] C. Chin, R. Grimm, P. Julienne, and E. Tiesinga, Rev. Mod. Phys. **82**, 1225 (2010).

[8] L.D. Landau and E.M. Lifshitz, *Statistical Physics*, Pergamon Press (1958).

[9] A. Griffin, D.W. Snoke, and S. Stringari, *Bose-Einstein Condensation*, Cambridge University Press (1995).

[10] S. Stringari, Phys. Rev. Lett. **77**, 2360 (1996).

[11] D.S. Jin, J.R. Ensher, M.R. Matthews, C.E. Wieman, E.A. Cornell, Phys. Rev. Lett. **77**, 420 (1996).

[12] D.S. Jin, M.R. Matthews, J.R. Ensher, C.E. Wieman, E.A. Cornell, Phys. Rev. Lett. **78**, 764 (1997).

[13] M.O. Mewes et al., Phys. Rev. Lett. **77**, 988 (1996).

[14] M.R. Andrews et al., Phys. Rev. Lett. **79**, 553 (1997).

[15] L.V. Hau et al., Phys. Rev. A **58**, R54 (1998).

[16] J. R. Anglin and W. Ketterle, Nature **416**, 211 (2002).

[17] H.T.C. Stoof, Nature **415**, 25 (2002).

[18] D. Jaksch, C. Bruder, J.I. Cirac, C.W. Gardiner, and P. Zoller, Phys. Rev. Lett. **81**, 3108 (1998).

[19] M. Greiner, O. Mandel, T. Esslinger, T.W. Hänsch, and I. Bloch, Nature **415**, 39 (2002).

[20] M. Lewenstein, A. Sanpera, and V. Ahufinger, *Ultracold atomic gases in optical lattices: simulating quantum many-body systems*, Oxford University Press (2012).

[21] S. Sachdev, *Quantum phase transitions*, Cambridge University Press (2011).

[22] S. Jochim et al., Science **302**, 2101 (2003).

[23] M.W. Zwierlein et al., Phys. Rev. Lett. **91**, 250401 (2003).

[24] C.A. Regal, M. Greiner, and D.S. Jin, Phys. Rev. Lett. **92**, 040403 (2004).

[25] J. Kinnunen, M. Rodríguez, and P. Törmä, Phys. Rev. Lett. **92**, 040403 (2004).

[26] J. Kinast, S.L. Hemmer, M.E. Gehm, A. Turlapov, and J.E. Thomas, Phys. Rev. Lett. **92**, 150402 (2004).

[27] M. Bartenstein et al., Phys. Rev. Lett. **92**, 203201 (2004).

[28] T. Bourdel et al., Phys. Rev. Lett. **93**, 050401 (2004).

[29] S.O. Demokritov et al., Nature **443**, 430 (2006).

[30] J. Kasprzak et al., Nature **443**, 409 (2006).

[31] R. Balili et al., Science **316**, 1007 (2007).

[32] J. Klaers, J. Schmitt, F. Verwinger, and M. Weitz, Nature **468**, 545 (2010).

[33] J. Schmitt et al., Phys. Rev. A **92**, 011602 (2015).

[34] P. Kirton and J. Keeling Phys. Rev. Lett. **111**, 100404 (2013).

[35] P. Kirton and J. Keeling Phys. Rev. A **91**, 033826 (2015).

[36] J. Marelic and R.A. Nyman, Phys. Rev. A **91**, 033813 (2015).

[37] D. N. Sob'yanin, Phys. Rev. E **85**, 061120 (2012).

[38] A. Kruchkov and Y. Slyusarenko, Phys. Rev. A **88**, 013615 (2013).

[39] D. N. Sob'yanin, Phys. Rev. E **88**, 022132 (2013).

[40] R.A. Nyman and M.H. M.H. Szymańska, Phys. Rev. A **89**, 033844 (2014).

[41] A. Kruchkov, Phys. Rev. A **89**, 033862 (2014).

[42] A. Chiocchetta and I. Carusotto, Phys. Rev. A **90**, 023633 (2014).

[43] C.J. Pethick and H. Smith, *Bose-Einstein Condensation in Dilute Gases*, Cambridge University Press (2008).

[44] V. Bagnato and D. Kleppner, Phys. Rev. A **44**, 7439 (1991).

[45] W.J. Mullin, J. Low-Temp. Phys. **106**, 615 (1997).

[46] S.M. Rezende, Phys. Rev. B **79**, 174411 (2009).

[47] S.A. Bender, R.A. Duine, and Y. Tserkovnyak, Phys. Rev. Lett. **108**, 246601 (2012).

[48] I.G. Savenko, T.C.H. Liew, and I.A. Shelykh, Phys. Rev. Lett. **110**, 127402 (2013).

[49] A. Amo et al., Nature (London) **457**, 291 (2009).

[50] R.T. Brierley, P.B. Littlewood, and P.R. Eastham, Phys. Rev. Lett. **107**, 040401 (2011).

[51] M. Wouters, I. Carusotto, and C. Ciuti, Phys. Rev. B **77**, 115340 (2008).

[52] D. Read, T.C.H. Liew, Y.G. Rubo and A.V. Kavokin, Phys. Rev. B **80**, 195309 (2009).

[53] J. Klaers, J. Schmitt, T. Damm, F. Verwinger, and M. Weitz, Phys. Rev. Lett. **108**, 160403 (2012).

[54] W. Fun, M. Yin, and Z. Cheng, arXiv:1301.7136.

[55] E.G. Dalla Torre et al., Phys. Rev. A **87**, 023831 (2013).

[56] H.T.C. Stoof, J. Low Temp. Phys **114**, 11 (1999).

[57] R.R. Birge, *Kodak Laser Dyes*, Kodak publication JJ-169.

[58] J.R. Lakowicz, *Principles of fluorescence spectroscopy*, Springer (2006).

[59] H.T.C. Stoof, K.B. Gubbels, D.B.M. Dickerscheid, *Ultracold Quantum Fields*, Springer, Dordrecht (2009).

[60] M. Wouters and I. Carusotto, Phys. Rev. Lett. **99**, 140402 (2007).

[61] A. Görlitz et al., Phys. Rev. Lett. **87**, 130402 (2001).

[62] F. Schreck et al., Phys. Rev. Lett. **87**, 080403 (2001).

[63] H. Ott, J. Fortagh, G. Schlotterbeck, A. Grossmann, and C. Zimmermann, Phys. Rev. Lett. **87**, 230401 (2001).

[64] W. Hänsel, P. Hommelhoff, T.W. Hänsch, and J. Reichel, Nature **413**, 501 (2001).

[65] N.D. Mermin and H. Wagner, Phys. Rev. Lett. **22**, 1133 (1966).

[66] P.C. Hohenberg, Phys. Rev. **158**, 383 (1967).

[67] W. Ketterle and N.J. van Druten, Phys. Rev. A **54**, 656 (1996).

[68] J.M. Kosterlitz and D.J. Thouless, J.Phys. C **6**, 1181 (1973).

[69] V.N. Popov, *Functional Integral in Quantum Field Theory and Statistical Physics* Riedel, Dordrecht (1983).

[70] M.H. Szymańska, J. Keeling, and P.B. Littlewood, Phys. Rev. Lett. **96**, 230602 (2006).

[71] M.H. Szymańska, J. Keeling, and P.B. Littlewood, Phys. Rev. B **75**, 195331 (2007).

[72] A. Chiocchetta and I. Carusotto, Europhysics Lett. **102**, 67007 (2013).

[73] M. Wouters and I. Carusotto, Phys. Rev. B **74**, 245316 (2006).

[74] V.N. Gladilin, K. Ji, and M. Wouters, Phys. Rev. A **90**, 023615 (2014).

[75] A.-W. de Leeuw, H.T.C. Stoof, and R.A. Duine, Phys. Rev. A **88**, 033829 (2013).

[76] U. Al Khawaja, J.O. Andersen, N.P. Proukakis, and H.T.C. Stoof, Phys. Rev. A **66**, 013615 (2002).

[77] T.L. Ho and M. Ma, J. Low-Temp. Phys. **115**, 61 (1999).

[78] D.S. Petrov, M.Holzmann, and G.V. Shlyapnikov, Phys. Rev. Lett. **84**, 2551 (2000).

[79] D.S. Petrov, G.V. Shlyapnikov, and J.T.M. Walraven, Phys. Rev. Lett. **85**, 3745 (2000).

[80] Z. Hadzibabic and J. Dalibard, Rivista del Nuovo Cimento **34**, 389 (2011).

[81] G. Roumpos et al., Proc. Nat. Acad. Sci **109**, 6467 (2012).

[82] E. Altman, L.M. Sieberer, L. Chen, S. Diehl, and J. Toner, Phys. Rev. X **5**, 011017 (2015).

[83] J.Schmitt et al., Phys. Rev. Lett. **112**, 030401 (2014).

[84] C. Beenakker and C. Schönenberger, Phys. Today **56**, 37 (2003).

[85] W. Schottky, Ann. Phys. **57**, 541 (1918).

[86] F. Lefloch, C. Hoffmann, M. Sanquer and D. Quirion, Phys. Rev. Lett. **90**, 067002 (2003).

[87] R. de Picciotto, M. Reznikov, M. Heiblum, V. Umansky, G. Bunin and D. Mahalu, Nature **389**, 162 (1997).

[88] H. Nyquist, Phys. Rev. **32**, 110 (1928).

[89] J. Johnson, Phys. Rev. **32**, 97 (1928).

[90] H.B. Callen and T.A. Welton Phys. Rev. **83**, 34 (1951).

[91] R. Kubo, Rep. Prog. Phys. **29**, 255 (1966).

[92] E. Altman, E. Demler and M. Lukin, Phys. Rev. A **70**, 013603 (2004).

[93] N. Cherroret and S.E. Skipetrov, Phys. Rev. Lett. **101**, 190406 (2008).

[94] J. Klaers, J. Schmitt, T. Damm, F. Vewinger and M. Weitz, Appl. Phys. B **105**, 17 (2011).

[95] G. Baym and C. J. Pethick, Phys. Rev. Lett. **76**, 6 (1996).

[96] C.C. Gerry and P.L. Knight, *Introductory Quantum Optics*, Cambridge University Press (2005).

[97] S. Yaltkaya and R. Aydin, Turk. J. Phys. **22**, 41 (2002).

[98] *Handbook of Chemistry and Physics*, CRC Press, 91st Edition (2009).

[99] J. Bardeen, L.N. Cooper, and J.R. Schrieffer, Phys. Rev., **108**, 1175 (1957).

[100] D.A. Kirzhnits and A.D. Linde, Phys. Lett. B **42** 471 (1972).

[101] Y. Aoki, Z. Fodor, S.D. Katz, and K.K. Szabó, Phys. Lett. B **643** 46 (2006).

[102] F. Karsch and the RBC-Bielefeld Collaboration, J. Phys. G **34** S627 (2007).

[103] L. Landau, Zh. Eksp. Teor. Fiz **7**, 19-32 (1937).

[104] Y. Nambu and G. Jona-Lasinio, Phys. Rev. **122**, 345-358 (1961).

[105] J. Goldstone, Nuovo Cim. **19**, 154-164 (1961).

[106] W. Heisenberg, Zeits. f. Physik **49**, 619 (1928).

[107] A. Imamoglu, M. Lewenstein and L. You, Phys. Rev. Lett. **78**, 2511-2514 (1997).

[108] E.M. Wright, D.F. Walls and J.C. Garrison, Phys. Rev. Lett. **77**, 2158-2161 (1996).

[109] J. Javanainen and M. Wilkens, Phys. Rev. Lett. **78**, 4675-4678 (1997).

[110] K. Mølmer, Phys. Rev. A **58**, 566-575 (1998).

[111] R. Graham, Phys. Rev. Lett. **81**, 5262-5265 (1998).

[112] S.Yi, Ö.E. Müstecaplioğlu, and L. You, Phys. Rev. Lett. **90**, 140404 (2003).

[113] H. Xiong, S. Liu, G. Huang and L. Wang, J. Phys. B **36**, 3315-3324 (2003).

[114] H.-J. Miesner and W. Ketterle, Solid State Comm., **107**, 629 (1998).

[115] D.S. Hall, M.R. Matthews, C.E. Wieman, and E.A. Cornell, Phys. Rev. Lett. **81**, 1543-1546 (1998).

[116] M. Greiner, O. Mandel, T.W. Hänsch, and I.Bloch, Nature **419**, 51-54 (2002).

[117] A. Altland and B. Simons, *Condensed Matter Field Theory*, Cambridge University Press (2010).

[118] R.A. Duine and H.T.C. Stoof, Phys. Rev. A **65**, 013603 (2001).

[119] K.G. Lagoudakis, B. Pietka, M. Wouters, R. André, and B. Deveaud-Plédran, Phys. Rev. Lett. **105**, 120403 (2010).

[120] M. Abbarchi et al., Nature Physics **9**, 275 (2013).

[121] B.P. Anderson and M.A. Kasevich, Science **282**, 1686 (1998).

[122] W. K. Hensinger et al., Nature **412**, 52 (2001).

[123] S. Burger et al., Phys. Rev. Lett. **86**, 4447 (2001).

[124] F.S. Cataliotti et al., Science **293**, 843 (2001).

[125] O. Morsch, J.H. Muller, M. Cristiani, D. Ciampini, and E. Arimondo, Phys. Rev. Lett. **87**, 140402 (2001).

[126] M. Greiner, I. Bloch, O. Mandel, T.W. Hänsch, and T. Esslinger, Phys. Rev. Lett. **87**, 160405 (2001).

[127] F. Ferlaino et al., Phys. Rev. A **66**, 011604 (2002).

[128] O. Morsch, M. Cristiani, J.H. Muller, D. Ciampini, and E. Arimondo, Phys. Rev. A **66**, 021601 (2002).

[129] J.H. Denschlag et al., J. Phys. B **35**, 3095 (2002).

[130] P.W. Anderson, Science **235**, 1196 (1987).

[131] W. Hofstetter, J.I. Cirac, P. Zoller, E. Demler, and M.D. Lukin, Phys. Rev. Lett. **89**, 220407 (2002).

[132] P.W. Anderson et al., J. Phys. Cond. Mat. **16**, R755 (2004).

[133] E. Roddick and D. Stroud, Phys. Rev. B **48**, 16600 (1993).

[134] K. Sheshadri, H.R. Krishnamurthy, R. Pandit, and T. Ramakrishnan, Europhys. Lett. **22**, 257 (1993).

[135] A. van Otterlo and K.H. Wagenblast, Phys. Rev. Lett. **72**, 3598 (1994).

[136] T. Stöferle, H. Moritz, C. Schori, M. Köhl, and T. Esslinger, Phys. Rev. Lett. **92**, 130403 (2004).

[137] C. Schori, T. Stöferle, H. Moritz, M. Köhl, and T. Esslinger, Phys. Rev. Lett. **93**, 240402 (2004).

[138] K. Xu et al., Phys. Rev. A **72**, 043604 (2005).

[139] F. Gerbier, S. Fölling, A. Widera, O.Mandel, and I. Bloch, Phys. Rev. Lett. **96**, 090401 (2006).

[140] J. Larson, B. Damski, G. Morigi, and M. Lewenstein, Phys. Rev. Lett. **100**, 050401 (2008).

[141] M.J. Hartmann, F.G.S.L. Brandão, and M.B. Plenio, Nature Physics **2**, 849 (2006).

[142] A.D. Greentree, C. Tahan, J.H. Cole, and L.C.L. Hollenberg, Nature Physics **2**, 856 (2006).

[143] D.G. Angelakis, M.F. Santos, and S. Bose, Phys. Rev. A **76**, 031805(R) (2007).

[144] J. Koch and K. Le Hur, Phys. Rev. A **80**, 023811 (2009).

[145] S. Schmidt and G. Blatter, Phys. Rev. Lett. **103**, 086403 (2009).

[146] T. Byrnes, P. Recher, and Y. Yamamoto, Phys. Rev. B. **81**, 205312 (2010).

[147] A.A. Houck, H.E. Türeci, and J. Koch, Nature Physics **8**, 292 (2012).

[148] M.J. Hartmann and M.B. Plenio, Phys. Rev. Lett. **99**, 103601 (2007).

[149] A. Tomadin et al., Phys. Rev. A **81**, 061801 (2010).

[150] H. Zheng and Y. Takada, Phys. Rev. A **84**, 043819 (2011).

[151] K. Kamide, M. Yamaguchi, T. Kimura, and T. Ogawa, Phys. Rev. A **87**, 053842 (2013).

[152] J. Klaers et al., Proc. SPIE **8600**, 86000L (2013).

[153] D. van Oosten, P. van der Straten, and H.T.C. Stoof, Phys. Rev. A **63**, 053601 (2001).

[154] W. Zwerger, J. Opt. B **5**, s9 (2003).

[155] A.-W. de Leeuw, H.T.C. Stoof, and R.A. Duine, Phys. Rev. A **89**, 053627 (2014).

[156] V. Zapf, M. Jaime, and C.D. Batista, Rev. of Mod. Phys. **86**, 563 (2014).

[157] M.R. Matthews, B.P. Anderson, P.C. Haljan, D.S. Hall, C.E. Wieman, and E.A. Cornell, Phys. Rev. Lett. **83**, 2498 (1999).

[158] K.W. Madison, F. Chevy, W. Wohlleben, and J. Dalibard, Phys. Rev. Lett. **84**, 806 (2000).

[159] J.R. Abo-Shaeer, C. Raman, J.M. Vogels, and W. Ketterle, Science **292**, 476-479 (2001).

[160] E.C.I. van der Wurff, A.-W. de Leeuw, R.A. Duine, and H.T.C. Stoof, Phys. Rev. Lett. **113**, 135301 (2014).

[161] M.C.F. Dobbelaar, S. Greveling, and D. van Oosten, Opt. Express **23**, 7481 (2015).

[162] J.I. Pankove, *Optical processes in Semiconductors*, Dover Publications, Inc, New York (1971).

[163] P.J. Harding et al., arXiv:0901.3855 (2009).

[164] J. Keeling, Phys. Rev. Lett. **107**, 080402 (2011).

[165] V. Hakim, Phys. Rev. E **55**, 2835 (1997).

[166] R.Y. Chiao and J. Boyce, Phys. Rev. A **60**, 4114 (1999).

[167] P. Leboeuf and S. Moulieras, Phys. Rev. Lett. **105**, 163904 (2010).

[168] P.-É. Larré and I. Carusotto, Phys. Rev. A **91**, 053809 (2015).

[169] D. Guéry-Odelin and S. Stringari, Phys. Rev. Lett. **83**, 4452 (1999).

[170] O.M. Maragò et al., Phys. Rev. Lett. **84**, 2056 (2000).

[171] E. Hodby, O. M. Maragò, G. Hechenblaikner, and C.J. Foot, Phys. Rev. Lett. **86**, 2196 (2001).

[172] E. Cancellieri, F.M. Marchetti, M.H. Szymańska and C. Tejedor, Phys. Rev. B **82**, 224512 (2010).

[173] S. Pigeon, I. Carusotto, and C. Ciuti, Phys. Rev. B **83**, 144513 (2011).

[174] M.A.M. Versteegh, T. Kruis, H.T.C. Stoof, and J.I. Dijkhuis, Phys. Rev. B **84**, 035207 (2011).

[175] P. Nozières and S. Schmitt-Rink, J. Low Temp. Phys. **59**, 195 (1985).

[176] G.E. Astrakharchik, J. Boronat, J. Casulleras, and S. Giorgini, Phys. Rev. Lett. **95**, 230405 (2005).

[177] G.M. Falco and H.T.C. Stoof, Phys. Rev. A **75**, 023612 (2007).

[178] I. Carusotto, R. Balbinot, A. Fabbri, and A. Recati, Eur. Phys. J. D **56**, 391-404 (2010).

[179] J.-C. Jaskula, G.B. Partridge, M. Bonneau, R. Lopes, J. Ruaudel, D. Boiron, and C.I. Westbrook, Phys. Rev. Lett **109**, 220401 (2012).

[180] S. Koghee, and M. Wouters, Phys. Rev. Lett **112**, 036406 (2014).

[181] H. Haug and S. W. Koch, *Quantum Theory of the Optical and Electronic Properties of Semiconductors*, World Scientific, Singapore, 4th edition (2004).